ESCUELA TÉCNICA SUPERIOR DE INGENIERÍA (ICAI)

GRADO EN INGENIERÍA ELECTROMECÁNICA

Especialidad Electrónica

ROTATING COIL SYSTEM FOR MEASURING PMQS

Autor: Mariano Colmenar Cascón

Director: Julio Lucas Torralba

Madrid

Mayo 2019

AUTORIZACIÓN PARA LA DIGITALIZACIÓN, DEPÓSITO Y DIVULGACIÓN EN RED DE PROYECTOS FIN DE GRADO, FIN DE MÁSTER, TESINAS O MEMORIAS DE BACHILLERATO

1º. Declaración de la autoría y acreditación de la misma.

El autor D. Mariano Colmenar Corcón

DECLARA ser el titular de los derechos de propiedad intelectual de la obra: ROTATING COIL SYSTEM FOR MEASURING PMQS, que ésta es una obra original, y que ostenta la condición de autor en el sentido que otorga la Ley de Propiedad Intelectual.

2º. Objeto y fines de la cesión.

Con el fin de dar la máxima difusión a la obra citada a través del Repositorio institucional de la Universidad, el autor **CEDE** a la Universidad Pontificia Comillas, de forma gratuita y no exclusiva, por el máximo plazo legal y con ámbito universal, los derechos de digitalización, de archivo, de reproducción, de distribución y de comunicación pública, incluido el derecho de puesta a disposición electrónica, tal y como se describen en la Ley de Propiedad Intelectual. El derecho de transformación se cede a los únicos efectos de lo dispuesto en la letra a) del apartado siguiente.

3º. Condiciones de la cesión y acceso

Sin perjuicio de la titularidad de la obra, que sigue correspondiendo a su autor, la cesión de derechos contemplada en esta licencia habilita para:

a) Transformarla con el fin de adaptarla a cualquier tecnología que permita incorporarla a internet y hacerla accesible; incorporar metadatos para realizar el registro de la obra e incorporar "marcas de agua" o cualquier otro sistema de seguridad o de protección.
b) Reproducirla en un soporte digital para su incorporación a una base de datos electrónica, incluyendo el derecho de reproducir y almacenar la obra en servidores, a los efectos de garantizar su seguridad, conservación y preservar el formato.
c) Comunicarla, por defecto, a través de un archivo institucional abierto, accesible de modo libre y gratuito a través de internet.
d) Cualquier otra forma de acceso (restringido, embargado, cerrado) deberá solicitarse expresamente y obedecer a causas justificadas.
e) Asignar por defecto a estos trabajos una licencia Creative Commons.
f) Asignar por defecto a estos trabajos un HANDLE (URL *persistente)*.

4º. Derechos del autor.

El autor, en tanto que titular de una obra tiene derecho a:

a) Que la Universidad identifique claramente su nombre como autor de la misma
b) Comunicar y dar publicidad a la obra en la versión que ceda y en otras posteriores a través de cualquier medio.
c) Solicitar la retirada de la obra del repositorio por causa justificada.
d) Recibir notificación fehaciente de cualquier reclamación que puedan formular terceras personas en relación con la obra y, en particular, de reclamaciones relativas a los derechos de propiedad intelectual sobre ella.

5º. Deberes del autor.

El autor se compromete a:

a) Garantizar que el compromiso que adquiere mediante el presente escrito no infringe ningún derecho de terceros, ya sean de propiedad industrial, intelectual o cualquier otro.
b) Garantizar que el contenido de las obras no atenta contra los derechos al honor, a la intimidad y a la imagen de terceros.
c) Asumir toda reclamación o responsabilidad, incluyendo las indemnizaciones por daños, que pudieran ejercitarse contra la Universidad por terceros que vieran infringidos sus derechos e

intereses a causa de la cesión.

d) Asumir la responsabilidad en el caso de que las instituciones fueran condenadas por infracción de derechos derivada de las obras objeto de la cesión.

6º. Fines y funcionamiento del Repositorio Institucional.

La obra se pondrá a disposición de los usuarios para que hagan de ella un uso justo y respetuoso con los derechos del autor, según lo permitido por la legislación aplicable, y con fines de estudio, investigación, o cualquier otro fin lícito. Con dicha finalidad, la Universidad asume los siguientes deberes y se reserva las siguientes facultades:

- La Universidad informará a los usuarios del archivo sobre los usos permitidos, y no garantiza ni asume responsabilidad alguna por otras formas en que los usuarios hagan un uso posterior de las obras no conforme con la legislación vigente. El uso posterior, más allá de la copia privada, requerirá que se cite la fuente y se reconozca la autoría, que no se obtenga beneficio comercial, y que no se realicen obras derivadas.
- La Universidad no revisará el contenido de las obras, que en todo caso permanecerá bajo la responsabilidad exclusive del autor y no estará obligada a ejercitar acciones legales en nombre del autor en el supuesto de infracciones a derechos de propiedad intelectual derivados del depósito y archivo de las obras. El autor renuncia a cualquier reclamación frente a la Universidad por las formas no ajustadas a la legislación vigente en que los usuarios hagan uso de las obras.
- La Universidad adoptará las medidas necesarias para la preservación de la obra en un futuro.
- La Universidad se reserva la facultad de retirar la obra, previa notificación al autor, en supuestos suficientemente justificados, o en caso de reclamaciones de terceros.

Madrid, a ..29..... de ....Mayo.............. de .2019

ACEPTA

Fdo..

Motivos para solicitar el acceso restringido, cerrado o embargado del trabajo en el Repositorio Institucional:

Declaro, bajo mi responsabilidad, que el Proyecto presentado con el título ROTATING COIL SYSTEM FOR MEASURING PMQS

en la ETS de Ingeniería - ICAI de la Universidad Pontificia Comillas en el curso académico 2018/2019 es de mi autoría, original e inédito y no ha sido presentado con anterioridad a otros efectos. El Proyecto no es plagio de otro, ni total ni parcialmente y la información que ha sido tomada de otros documentos está debidamente referenciada.

Fdo.: Mariano Colmenar Cascón Fecha: 29/05/2019

Autorizada la entrega del proyecto

EL DIRECTOR DEL PROYECTO

Fdo.: Julio Lucas Torralba Fecha: 5/VI/2019

ESCUELA TÉCNICA SUPERIOR DE INGENIERÍA (ICAI)

GRADO EN INGENIERÍA ELECTROMECÁNICA

Especialidad Electrónica

ROTATING COIL SYSTEM FOR MEASURING PMQS

Autor: Mariano Colmenar Cascón

Director: Julio Lucas Torralba

Madrid

Mayo 2019

SISTEMA DE MEDIDA DE PMQS POR BOBINA ROTATORIA

Autor: Colmenar Cascón, Mariano.
Director: Lucas Torralba, Julio.
Entidad colaboradora: Elytt Energy.

RESUMEN DEL PROYECTO

1. <u>INTRODUCCIÓN</u>

Este proyecto consiste en un sistema de bobina rotatoria que será usado para medir el campo magnético de PMQs (Cuadrupolo de Imán Permanente).

La idea general de la máquina es una mesa rotatoria que sostiene una bobina plana impresa en un PCB (Placa de Circuito Impreso) en posición vertical *(Figura 1)*. La bobina estará colocada en el centro del PMQ, y tan pronto como esta empiece a girar, la variación del flujo magnético inducirá una tensión en la bobina rotatoria.

El PCB contiene dos bobinas independientes y opuestas. Las señales de tensión inducidas en cada bobina serán amplificadas directamente a través de un circuito en el PCB. Cuando las señales de estas dos bobinas se sumen, los términos de los harmónicos dipolares y cuadrupolares se anularán. Esta señal compensada también será amplificada a través de un circuito en el PCB y se obtendrá como una señal independiente con el sistema de adquisición de datos.

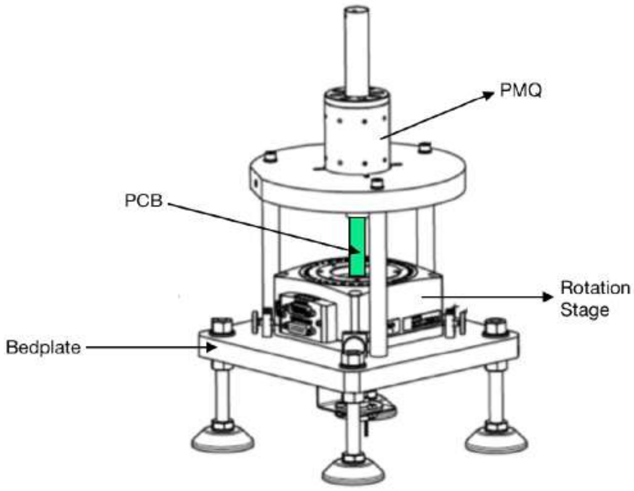

Figura 1: Partes principals del Sistema de bobina rotatoria

El gradiente integrado, error de los ejes y el roll serán calculados a partir de la señal de una de las dos bobinas independientes, mientras que el contenido harmónico será calculado a partir de la señal compensada.

Después de ser procesadas por medio de un análisis de Fourier, la señal de tensión será utilizada, junto con la posición angular de la mesa rotatoria, para calcular los harmónicos del campo magnético del PMQ.

La memoria de este proyecto está estructurada de la siguiente forma: primero, se introducirá el concepto de PMQ. A continuación, se explicará el proyecto LINAC 4 del CERN, y cómo estos PMQs se utilizarán en él. Después, se realizará un estudio sobre las tecnologías existentes para la medida de PMQs, además de la motivación para llevar a cabo este proyecto.

A continuación, se explicará con detalle el desarrollo completo de la máquina, que incluirá: diseño inicial de la máquina, diseño de la bobina, circuito de amplificación y filtrado, encargo del PCB y soldadura de componentes, prototipado rápido con LEGO EV3, configuración de la mesa rotatoria y del sistema de adquisición de datos, diseño de la bancada y ensamblaje, y finalmnte, procesamiento de datos, calibración, pruebas y resultados.

La idea general de un PMQ (Cuadrupolo de Imán Permanente) *(Figura 2)* es un tipo de disposición de imanes en el que estos están colocados de tal forma que, cuando mirando a expansión planar del campo magnético, los términos significativos más bajos de las ecuaciones de campo son cuadrupolares, ya que los términos dipolares se cancelan.

Figura 2: Vista superior de un PMQ

2. ESTADO DEL ARTE Y MOTIVACIÓN DEL PROYECTO

Con respecto a la tecnología existente para la medida de PMQs, la sonda Hall es la alternativa más común al sistema de bobina rotatoria. Es además la tecnología que *Elytt Energy* utilizaba para la medida de PMQs hasta que este sistema de bobina rotatoria fue desarrollado.
La sonda Hall caracteriza el campo magnético a partir de la medida de tensión a través del cristal de la sonda Hall, esta tensión está provocada por el efecto Hall. *(Figura 3)*

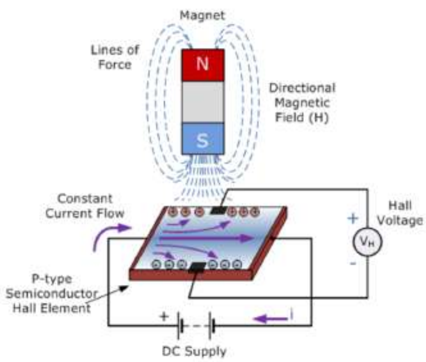

Figura 3: Medida del efecto Hall por medio de sonda Hall [F3]

La sonda Hall, junto con un sistema de desplazamiento controlado por ordenador, proporciona un detallado mapa del campo del imán. Sin embargo, la principal desventaja de usar la sonda

Hall para medir PMQs es el largo tiempo requerido, que está comprendido entre 30 y 60 minutos para medir un único PMQ, sin ser capaz si quiera de extraer los harmónicos.

En conclusión, la principal razón por la que este proyecto se ha llevado a cabo es tener un sistema de medida rápido y preciso que permita identificar los harmónicos del campo de un PMQ, ya que la sonda Hall es muy lenta en comparación y no permite medir los harmónicos.

3. DESARROLLO DEL SISTEMA

En el proceso de diseñar el sistema podemos distinguir varias fases, que serán explicadas detalladamente en los apartados a continuación:

3.1. Diseño de la bobina plana

La "antena" del sistema está formada por dos bobinas planas, una interior y otra exterior, impresas en las cuatro capas de un PCB *(Figura 4).* La función de usar dos bobinas es medir la tensión individual inducida en cada bobina para obtener el harmónico principal del cuadrupolo (harmónico de segundo orden). Adicionalmente, para obtener los harmónicos de orden superior, se medirá la tensión total de las dos bobinas conectadas en anti-serie, que corresponde a la tensión resultante de la resta de las tensiones inducidas en cada bobina).

Figura 4: Capa de la bobina interior (Coil 1) y bobina exterior (Coil 2)

3.2. Diseño del circuito de amplificación y filtrado

Se necesitará utilizar un circuito de amplificación y filtrado antes de procesar la medida de la señal de tensión. El circuito estará formado por cuatro etapas: las dos primeras etapas *(A1 y A2)* serán filtros paso bajo idénticos aplicados directamente a las señales de tensión medidas individualmente de la bobina interior *(Coil 1)* y exterior *(Coil 2)*, la tercera etapa *(A_3)* y la cuarta etapa *(A_4)* serán aplicadas a la señal de tensión compensada de las dos bobinas en anti-serie. Se deberá determinar la frecuencia de corte y ganancia estática para las cuatro etapas.

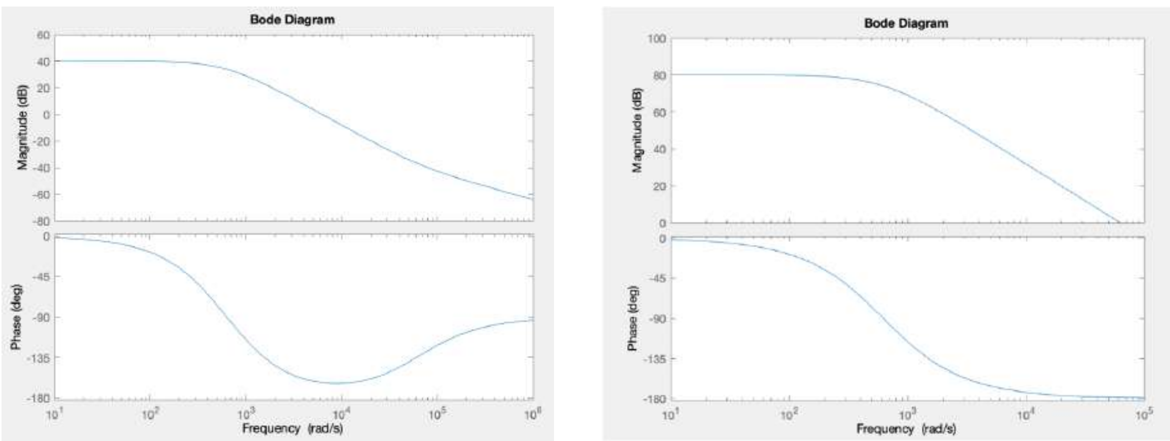

Figura 5: Diagrama de Bode de A_1 y A_2 (izquierda) y diagrama de Bode de A_3 x A_4 (derecha)

3.3. Diseño del PCB y soldadura de componentes

El siguiente paso fue diseñar el PCB (Placa de Circuito Impreso) por medio de una herramienta informática llamada *KiCad*. Una vez diseñado, se realizó el pedido del PCB y de los componentes. A continuación, los componentes fueron soldados en el PCB.

Figura 6: Vista general del diseño de PCB en KiCad

3.4. Prototipado rápido con LEGO EV3

Antes de continuar y comprar la mesa rotatoria, el sistema de adquisición de datos, fabricar las piezas y ensamblar la estructura completa, que supone un gran coste, se decidió montar un prototipo del sistema de bobina rotatoria usando piezas de *LEGO (Figura 7)* y realizar algunos experimentos midiendo señales de tensión. Se utilizó un servomotor *LEGO EV3.*

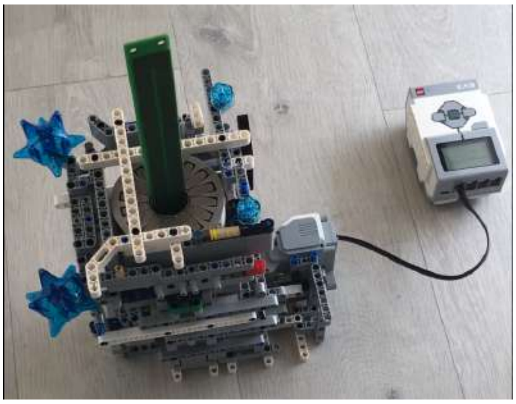

Figura 7: Prototipo del sistema con LEGO EV3

3.5. Configuración de la mesa rotatoria y del sistema de adquisición de datos:

Una vez puesto a prueba el prototipo, el siguiente paso fue configurar la mesa rotatoria, el controlador de movimiento, y el *encoder*. Se utilizó una mesa rotatoria *Newport RGV100-BLS*, y un controlador de movimiento *Newport XPS-RL.*

3.6. Diseño de la bancada

Diseñar una buena bancada *(Figura 1)* es crucial para la calidad del sistema de medida. Es imprescindible tener una estructura rígida y estable para minimizar el ruido en las señales medidas y para garantizar que el movimiento de la mesa rotatoria no causará vibraciones en la estructura que afecten a las mediciones.

3.7. Procesamiento de datos

Una vez recopiladas las medidas de la tensión inducida $\in$, la velocidad angular ω y la posición angular θ, se calcularán por medio de análisis de Fourier los coeficientes a_n, b_n, c_n, y el IG (Gradiente Integrado). Todos estos cálculos se realizarán utilizando *Matlab.*

4. PRUEBAS, RESULTADOS, Y CALIBRACIÓN

Se hicieron muchas pruebas con el fin de asegurar el mínimo error a la hora de realizar las medidas. La calibración del sistema de bobina rotatoria se realizó midiendo 15 PMQs con este nuevo sistema y comparando las medidas con las anteriores realizadas con sonda Hall.

Una vez calibrado el sistema, la máxima diferencia en el IG (Gradiente Integrado) entre las medidas por bobina rotatoria y por sonda Hall fue inferior al 0.15% *(Figura 8)*, para cada uno de los 15 PMQs, cumpliendo satisfactoriamente los requisitos.

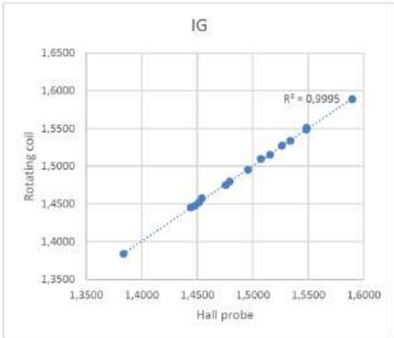

Figura 8: Calibración del IG

En cuanto a los errores en los ejes *x* e *y*, la *Figura 9* muestra la correlación entre las medidas por bobina rotatoria y por sonda Hall. Se puede apreciar una mayor dispersión en las medidas realizadas por bobina rotatoria, que es significativamente mayor en la dirección horizontal *x*.

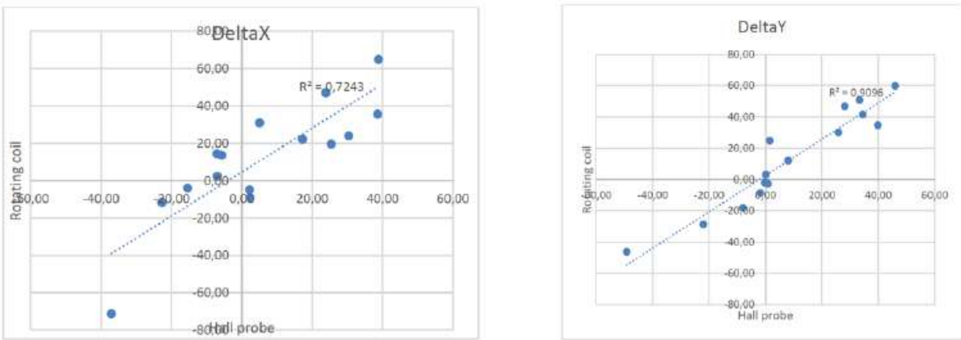

Figura 9: Calibración del eje X (izquierda) y calibración del eje Y (derecha)

Con respecto al *roll*, los resultados de las medidas por bobina rotatoria concuerdan bastante en el roll con las medidas por sonda Hall.

5. CONCLUSIÓN

El funcionamiento de este sistema de medida de PMQs por bobina rotatoria cumple con todos los requisitos y objetivos, haciendo posible identificar los harmónicos del campo de un PMQ en menos de un minuto.

6. REFERENCIAS

[F3] https://www.electronics-tutorials.ws/electromagnetism/hall-effect.html

ROTATING COIL SYSTEM FOR MEASURING PMQS

Author: Colmenar Cascón, Mariano.
Director: Lucas Torralba, Julio.
Collaborating entity: Elytt Energy.

ABSTRACT

1. <u>INTRODUCTION</u>

This project is a rotating coil system which will be used for measuring the magnetic field of Permanent Magnet Quadrupoles (PMQs).

The general idea of the machine is a rotation stage which holds a flat coil printed on a PCB (printed circuit board) in a vertical position *(Figure 1)*. The coil is placed in the center of the PMQ, and as soon as the coil starts turning, the variation of magnetic flux will induce a voltage in the rotating coil.

The PCB has two independent opposite coils. The voltage signals induced in each coil are pre-amplified directly in the PCB. When the signals of these two coils are added, the dipolar and quadrupolar harmonic terms cancel out. This compensated signal is also amplified in the PCB circuit and is obtained as an independent signal with the data acquisition device.

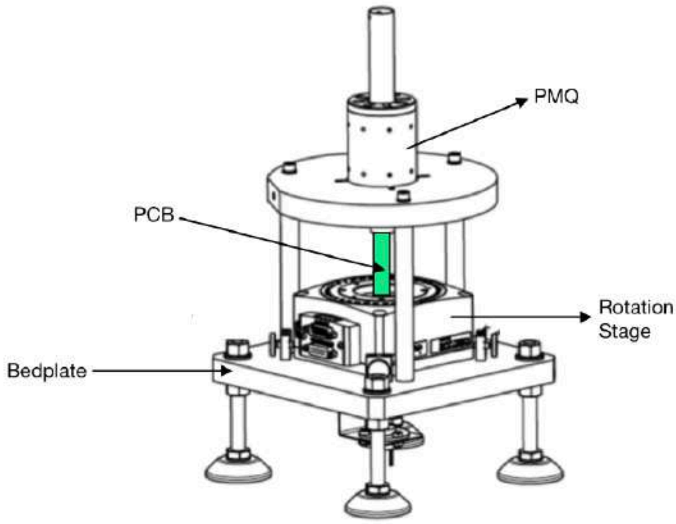

Figure 1: Main parts of the rotating coil system

The integrated gradient, axis error and roll can be obtained from the signal of one of the coils. The harmonic content can be obtained from the compensated signal.

After being processed with Fourier analysis, the signal will be used, together with the angle position of the rotation stage, to calculate the harmonics of the PMQ's magnetic field.

The memory for this project is structured in the following way: firstly, the concept of PMQ will be introduced (magnetic field and flux description, equations derivation and specific applications). Then, CERN's project LINAC 4 will be explained, as well as how these PMQs will be used in it. After that, a research on the already existing technologies for measuring PMQs will be illustrated, along with the motivation for carrying out this project.

Consecutively, the development of the entire machine will be explained in detail, this involves: initial design of the machine, coil design, filtering and amplification circuit, ordering the PCB and component soldering, LEGO EV3 rapid prototyping, rotation stage configuration and data acquisition, design of the bedplate and assembly, and finally, data processing, calibration, tests, and results.

Finally, some concluding remarks will be presented in the last section of the memory.

The general idea of a PMQ (Permanent Magnet Quadrupole) *(Figure 2)* is a type of magnet layout in which the magnets are placed in such way that, when looking at the planar expansion of the magnetic field, the lowest significant terms of the field equations are quadrupole, since the dipole terms cancel out.

Figure 1:Top view of a PMQ

2. STATE OF THE ART AND PROJECT MOTIVATION

Regarding already existing technologies, the Hall probe is the most commonly used alternative to the rotating coil system for measuring PMQs. It is also the technology that *Elytt Energy* used for measuring PMQs until this rotating coil system was developed.
The Hall probe measures the magnetic field by measuring the voltage across the crystal in the Hall probe, this voltage is caused by the *Hall effect (Figure 3)*.

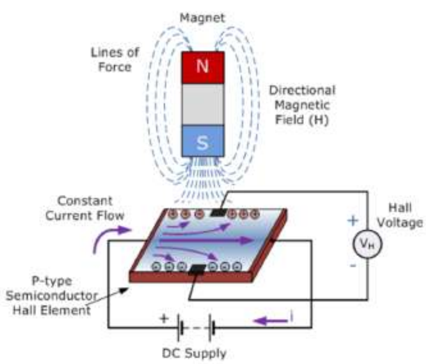

Figure 3: Measuring the Hall effect voltage with a Hall sensor [F3]

The Hall probe, combined with a computer-controlled displacement system, provides a detailed field map of the magnet. However, the main drawback of using the Hall probe to measure PMQs is the long time required, taking from 30 to 60 minutes to measure a single PMQ, not being able to analyze all harmonics. Whereas this rotating coil system only takes 1 minute to measure each PMQ, making it possible to save an enormous amount of time and fully analyze field harmonics.

In conclusion, the main reason for carrying out this project is to have a fast, accurate system that can identify all field harmonics of a PMQ, given that the Hall probe is comparatively slow and does not allow to measure field harmonics.

3. DEVELOPMENT OF THE SYSTEM

In the process of designing the system different phases can be distinguished, which are explained with detail in the following sections:

3.1. Flat coil design

The "antenna" of the system is formed by two flat coils, an internal coil and an external coil, printed in four layers of a PCB *(Figure 4)*. The purpose of using two coils is to measure the individual voltage induced in each coil to acquire the main harmonic of the quadrupole (the second order harmonic). Additionally, in order to acquire the higher order harmonics, the overall voltage of both coils connected in anti-series is measured (the resulting subtraction of the voltages induced in each coil).

Figure 4: A layer of Coil 1 and Coil 2

3.2. Design of the filter and amplifier circuit

The use of an amplifier and filter circuit is required before processing the measured voltage signal. The circuit is formed by four stages: the first two stages (A_1 and A_2) are two identical low pass filters applied directly to the voltage signals measured individually from *Coil 1 and Coil 2,* stage 3 *(A_3)* and stage 4 *(A_4)* are applied to the compensated anti-series voltage signal. For all four stages a cutoff frequency and a static gain is determined.

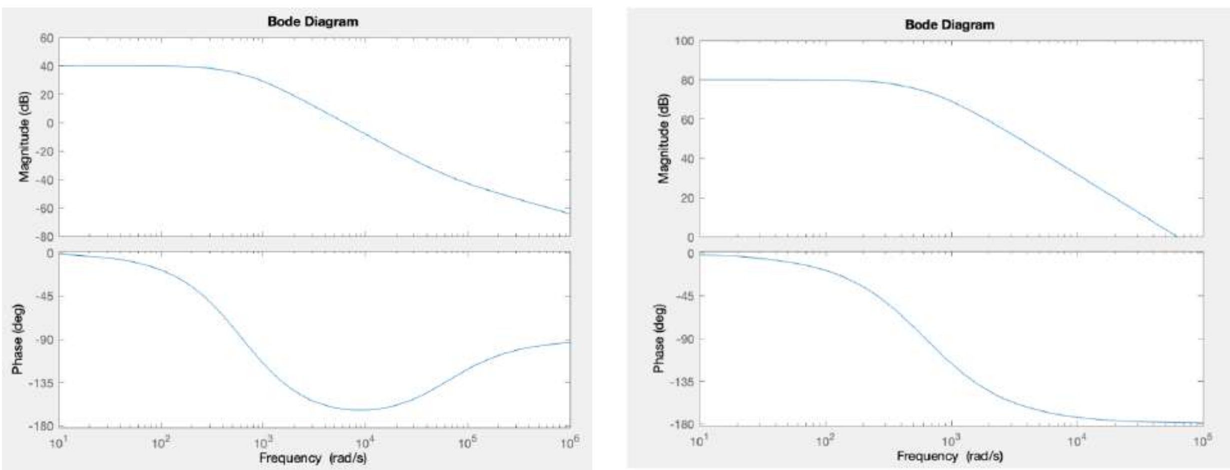

Figure 5: Bode plot of stages A_1 and A_2 (left) and Bode plot of stage A_3 x A_4 (right)

3.3. PCB design and component soldering

The next step was to design the PCB (Printed Circuit Board) and do the layout using a CAD tool called *KiCad.* Once it had been designed, the PCB and components were ordered. Then, the components were soldered onto the PCB.

Figure 6: Overall view of the PCB KiCad design

3.4. Rapid prototyping with LEGO EV3

Before proceeding to buy the rotation stage, the data acquisition, manufacture and assemble the entire structure, given the very high price, a decision was made concluding that it would be best to do a *LEGO* prototype of the rotating coil system *(Figure 7)* and run some experiments by measuring voltage signals. A *LEGO EV3* servomotor was used.

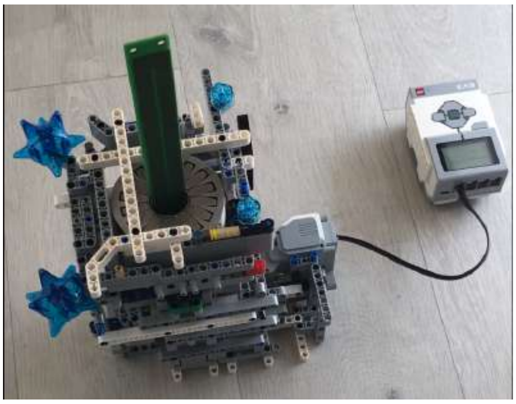

Figure 7: Prototype of the system with LEGO EV3

3.5. Rotation stage and data acquisition setup:

Once the prototype had been tested, the next step was to set up the rotation stage, the motion controller and encoder. A *Newport RGV100-BLS* rotation stage was used, and a *Newport XPS-RL* motion controller.

3.6. Bedplate design

Designing a good bedplate *(Figure 1)* was crucial for the quality of the measuring system. A highly stiff and stable structure is desired in order to minimize the noise in the measured signals and to assure that the motion of the rotation stage will not cause undesired vibrations in the structure and will not affect the measurements.

3.7. Data processing

After gathering the measurements of the induced voltage $\in$, the rotating speed ω and the angle θ, coefficients a_n, b_n, c_n, and IG (Integrated Gradient) are calculated through Fourier analysis. All of these calculations are made using *Matlab.*

4. TESTS, RESULTS, AND CALIBRATION

Many tests and experiments needed to be done to ensure the minimum error when measuring. Calibration of the rotating coil system was made by measuring 15 PMQs with this new system and comparing the measurements with the previous Hall probe measurements.

Once the rotating coil system was calibrated, the maximum difference in IG (Integrated Gradient) between the rotating coil measurements and Hall probe measurements was successfully less than 0.15%, for all 15 PMQs *(Figure 8)*.

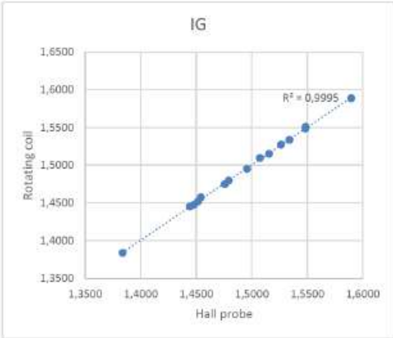

Figure 8: IG calibration

Regarding the x and *y* axis errors, *Figure 9* shows that the rotating coil measurements are correlated to the Hall probe measurements, although the results obtained using the rotating coil have a larger dispersion, which is significantly higher in the horizontal direction *x*.

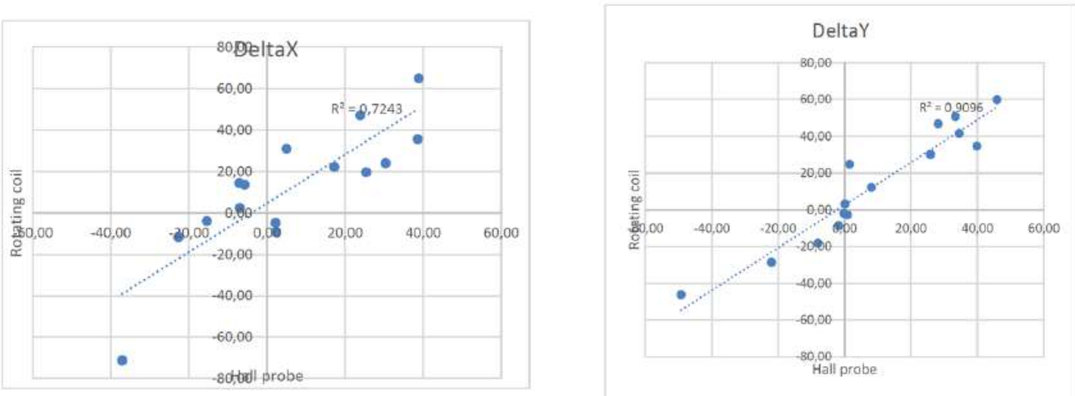

Figure 9: X axis calibration (left) and Y axis calibration (right)

Finally, regarding the roll, the results of the rotating coil measurements show a good roll agreement with the Hall probe measurements.

5. CONCLUSION

The operation of this rotating coil system for measuring PMQs has successfully met all of the requirements and accomplished the main objectives. And made it possible to identify the field harmonics of a PMQ in less than one minute.

6. REFERENCES

[F3] https://www.electronics-tutorials.ws/electromagnetism/hall-effect.html

DOCUMENT 1

MEMORY

TABLE OF CONTENTS

TABLE OF TABLES

TABLE OF FIGURES

PART I: MEMORY

1. INTRODUCTION

This project is a rotating coil system which will be used for measuring the magnetic field of Permanent Magnet Quadrupoles (PMQs).

The general idea of the machine is a rotation stage which holds a flat coil printed on a PCB (printed circuit board) in a vertical position *(Figure 1)*. The coil is placed in the center of the PMQ, and as soon as the coil starts turning, the variation of magnetic flux will induce a voltage in the rotating coil.
The PCB has two independent opposite coils. The voltage signals induced in each coil are pre-amplified directly in the PCB. When the signals of these two coils are added, the dipolar and quadrupolar harmonic terms cancel out. This compensated signal is also amplified in the PCB circuit and is obtained as an independent signal with the data acquisition device.

The integrated gradient, axis error and roll can be obtained from the signal of one of the coils. The harmonic content can be obtained from the compensated signal.

After being processed with Fourier analysis, the signal will be used, together with the angle position of the rotation stage, to calculate the harmonics of the PMQ's magnetic field.

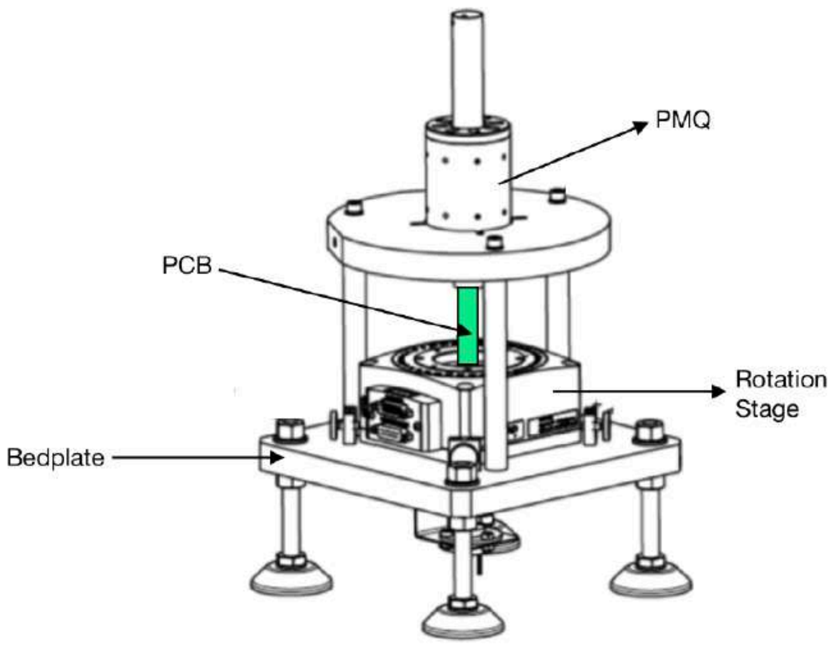

Figure 1: Main parts of the rotating coil system

This memory is structured in the following way: firstly, the concept of PMQ will be introduced (magnetic field and flux description, equations derivation and specific applications). Then, CERN's project LINAC 4 will be explained, as well as how these PMQs will be used in it. After that, a research on the already existing technologies for measuring PMQs will be illustrated, along with the motivation for carrying out this project.

Consecutively, the development of the entire machine will be explained in detail, this involves: initial design of the machine, coil design, filtering and amplification circuit, ordering the PCB and component soldering, LEGO EV3 rapid prototyping, rotation stage configuration and data acquisition, design of the bedplate and assembly, and finally, data processing, calibration, tests, and results.

Finally, some concluding remarks will be presented in the last section of this memory.

1.1. PERMANENT MAGNET QUADRUPOLES

1.1.1. INTRODUCTION TO PMQS

A PMQ (Permanent Magnet Quadrupole) is a type of magnet layout in which the magnets are placed in such way that, when looking at the planar expansion of the magnetic field, the lowest significant terms of the field equations are quadrupole, since the dipole terms cancel out. [WIKI01]

Figure 2:Top view of a PMQ

PMQs are widely used to focus beams of charged particles in particle accelerators, given the rapid growth of its magnetic field's magnitude with the radial distance from the central axis.

1.1.2. MAGNETIC FIELD OF A QUADRUPOLE

In order to illustrate the magnetic field of a quadrupole, an electromagnetic quadrupole will be used as shown in the figure bellow.

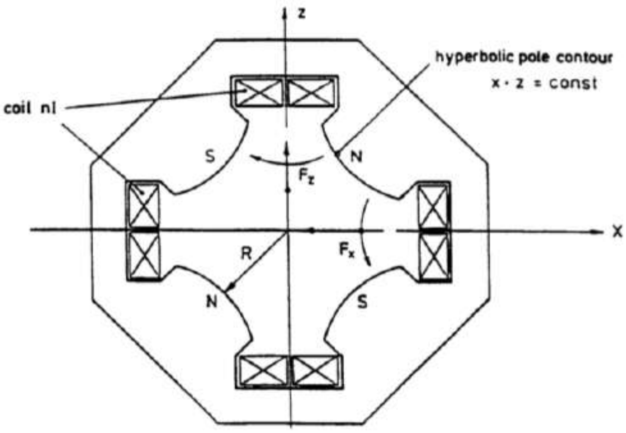

Figure 3: Cross-section of a quadrupole magnet [F3]

Given the polarity in the figure above, the horizontal component of the Lorentz force applied to a positively charged particle, moving into the plane of the drawing, will be directed towards the axis, whereas the vertical component will be directed away from it. Hence, the magnet shown will focus along the horizontal direction, and will defocus along the vertical direction. In case the direction of motion of the particle, the particle's charge, or the current direction were to be reversed, the exact opposite phenomenon will take place [TURN94].

The magnetic field is linear as it deviates from the axis:

$$B_z = -gx, \;\; B_x = -gz \tag{1.1}$$

In the air space of the magnet the Maxwell equation applies:

$$\nabla \times B = 0 \tag{1.2}$$

The field can be expressed as the gradient of a potential:

$$B = -\nabla V \; , \; s.t \; V(x,z) = gxz \tag{1.3}$$

In a quadrupole, equipotential lines have the shape of hyperbolas such that *xz=constant*, being the field lines perpendicular to these hyperbolas [TURN94].

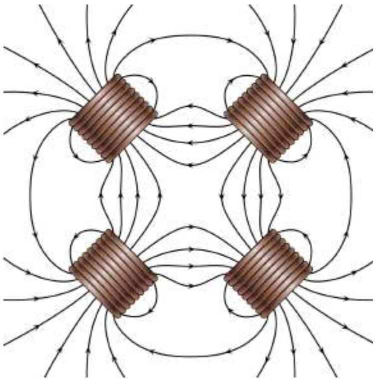

Figure 4: Magnetic field lines of an ideal quadrupole [F4]

1.1.3. LORENTZ FORCES

The following theorem relates the gradient *g* and the current *I* that flows through the coils [TURN94]:

$$\oint H \cdot ds = nI \tag{1.4}$$

Given the following path of integration:

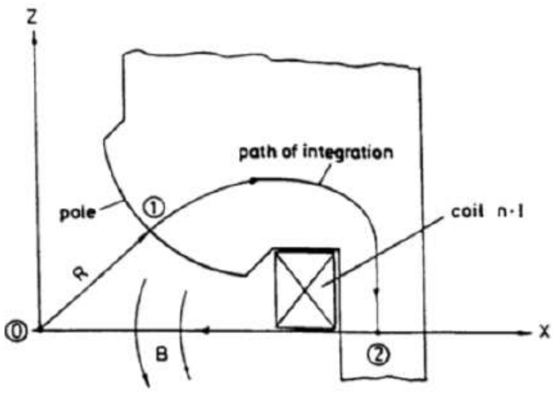

Figure 5: Path of integration used to relate g and I [F5]

Using equation *(1.4)* and the path of integration in *Figure 5*:

$$nI = \oint H \cdot ds = \int_0^R H(r)\, dr + \int_1^2 H_E \cdot ds + \int_2^0 H \cdot ds \tag{1.5}$$

In equation *(1.5)*, the second integral is very small for $\mu_r \gg 1$, and since H is perpendicular to ds, the third integral also disappears, leaving the first integral as the only path $H(r) = gr/\mu_o$. This leaves us with the following:

$$nI = \frac{1}{\mu_o}\int_0^R g\, r\, dr \qquad\qquad r = \sqrt{x^2 + z^2}$$

$$g = \frac{2\mu_o nI}{R^2} \tag{1.6}$$

The next step is to relate the field strength to its optical effect. In order to do this, the field gradient g must be normalized to the particle momentum p by using equation *(1.7)*, in which e denotes the particle charge. This way the quadrupole strength is defined:

$$k[m^{-2}] = \frac{eg}{p} \tag{1.7}$$

The focal length f of the quadrupole is given by the following equation *(1.8)*, with l being the length of the quadrupole.

$$\frac{1}{l} = k \cdot f \tag{1.8}$$

The horizontal and vertical Lorentz forces result:

$$F_x = evB_z(x,z) = -evgx$$

$$F_z = -evB_x(x,z) = evgz \tag{1.9}$$

Equation *(1.9)* reflects that both vertical and horizontal components of the Lorentz force are independent. The vertical Lorentz force component only depends on the vertical position, whereas the horizontal Lorentz force component only depends on the horizontal position [TURN94].

1.1.4. GENERAL MULTIPOLE EXPANSION

Firstly, note that what had been called coordinate *z* in sections *1.1.2* and *1.1.3* will now be called coordinate *y*, in order to keep the conventional notation $z = x + yi$ for complex numbers [TURN94].

Modern accelerator magnets usually have a much larger length than their bore radius. It is a fair approximation to ignore the end field contribution and take into account only transverse components.

The theory of analytic functions can be applied for two-dimensional fields such that:

$$div\ B = 0$$

Then a vector potential A exists such that:

$$B = rot\ A \qquad (1.10)$$

Since only the transverse components of the field are considered, as explained before, the vector potential only has a component A_s in the longitudinal direction *s*. Additionally, in vacuum, as present in the inside of a particle accelerator beam pipe, the following equation applies:

$$rot\ B = 0$$

This way *B* can also be expressed as the gradient of a scalar potential *V*:

$$B = -grad\ V \qquad (1.11)$$

Combining *(1.10)* and *(1.11)*:

$$B_x = -\frac{\partial V}{\partial x} = \frac{\partial A_s}{\partial y} \qquad B_y = -\frac{\partial V}{\partial y} = -\frac{\partial A_s}{\partial x} \qquad (1.12)$$

Equations *(1.12)* are the Cauchy-Riemann conditions for the real and imaginary part of an analytic function.

Next, a complex potential function $\tilde{A}$ of the form $z = x + iy$ is defined:

$$\tilde{A}(z) = A_s(x,y) + iV(x,y) \qquad (1.13)$$

In conclusion, the complex potential is an analytic function and so it can be expanded as the following series

$$\tilde{A}(z) = \sum_{n=0}^{\infty} k_n z^n \qquad k_n = \lambda_n + i\mu_n \qquad (1.14)$$

in which λ_n and μ_n are real constants [TURN94].

1.1.5. CYLINDRICAL COORDINATES REPRESENTATION

In the following chapters of this report, a large majority of the equations will be expressed in cylindrical coordinates *(r, φ, s)* for practical purposes [TURN94].

$$x = r\,cos\varphi \qquad y = r\,sin\varphi \qquad z^n = r^n \cdot e^{in\varphi} = r^n(cos\,n\varphi + i\sin n\varphi) \qquad (1.15)$$

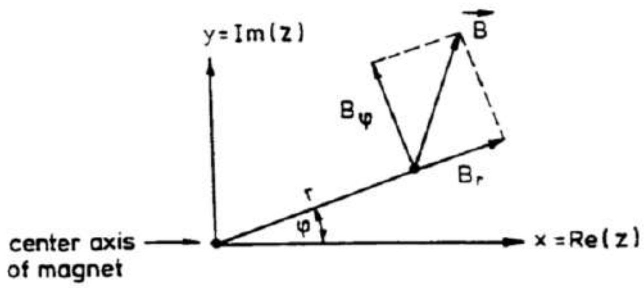

Figure 6: Cylindrical coordinate system used for multipole expansion [F6]

The scalar potential *V* is given by:

$$V(r,\varphi) = \sum_{n=0}^{\infty}(\mu_n \cos n\varphi + \lambda_n \sin n\varphi)\, r^n \qquad (1.16)$$

The longitudinal component A_s of the vector potential is given by:

$$A_s(r,\varphi) = \sum_{n=0}^{\infty}(\lambda_n \cos n\varphi - \mu_n \sin n\varphi)\, r^n \qquad (1.17)$$

The gradient of -*V(r, φ)* leads to the multipole expansion of the radial and azimuthal field components:

$$B_r = -\frac{\partial V}{\partial r} = -\sum_{n=1}^{\infty} n(\mu_n \cos n\varphi + \lambda_n \sin n\varphi)\, r^{n-1} \qquad (1.18)$$

$$B_\varphi = -\frac{1}{r}\frac{\partial V}{\partial \varphi} = -\sum_{n=1}^{\infty} n(\lambda_n \cos n\varphi - \mu_n \sin n\varphi)\, r^{n-1} \qquad (1.19)$$

B_{main} is now defined as the magnitude of the main field component of the magnet. Additionally, a reference radius r_o is defined for the multipole expansion.

In the following equations the *normal* multipole coefficients b_n and the *skew* coefficients a_n are introduced:

$$b_n = -\frac{n\lambda_n}{B_{main}} r_o^{n-1} \qquad a_n = +\frac{n\mu_n}{B_{main}} r_o^{n-1} \qquad (1.20)$$

The multiple expansions result in the following expressions:

$$V(r,\varphi) = -B_{main} r_o \sum_{n=1}^{\infty}\left(-\frac{a_n}{n}\cos n\varphi + \frac{b_n}{n}\sin n\varphi\right)\left(\frac{r}{r_o}\right)^n \qquad (1.21)$$

$$A_s(r,\varphi) = -B_{main} r_o \sum_{n=1}^{\infty}\left(\frac{b_n}{n}\cos n\varphi + \frac{a_n}{n}\sin n\varphi\right)\left(\frac{r}{r_o}\right)^n \qquad (1.22)$$

$$B_\varphi(r,\varphi) = B_{main} \sum_{n=1}^{\infty}(b_n \cos n\varphi + a_n \sin n\varphi)\left(\frac{r}{r_o}\right)^{n-1} \qquad (1.23)$$

$$B_r(r,\varphi) = B_{main} \sum_{n=1}^{\infty}(-a_n \cos n\varphi + b_n \sin n\varphi)\left(\frac{r}{r_o}\right)^{n-1} \qquad (1.24)$$

In the equations shown above, V denotes the scalar potential, A_s denotes the longitudinal component of the vector potential, B_φ denotes the azimuthal component of the magnetic field, and B_r denotes the radial component of the magnetic field.

Also note that b_o and a_o are set to zero since they do not contribute to the magnetic field.

For all equations derived in this section, the value of n determines the *2n-pole*. More specifically, for an ideal *2n-pole* magnet: $b_n = 1$, being all other a_n, $b_n = 0$.

The names given to magnets and their corresponding n values are:

n = 1 Dipole
n = 2 Quadrupole
n = 3 Sextupole
n = 4 Octupole
n = 5 Decapole
n = 6 Dodecapole

This means that for the particular case of a quadrupole, $n = 2$ in all equations.

Expressing the magnetic field B in a standard complex number form $B_\varphi + iB_r$ [TURN94]:

$$B_\varphi + iB_r = B_{main} \sum_{n=1}^{\infty} \left(\frac{r}{r_o}\right)^{n-1} [b_n(\cos n\varphi + i \sin n\varphi) - ia_n(\cos n\varphi + i \sin n\varphi)] \quad (1.25)$$

$$B_\varphi + iB_r = B_{main} \sum_{n=1}^{\infty} \left(\frac{r}{r_o}\right)^{n-1} (b_n - ia_n)e^{in\varphi} \quad (1.26)$$

Hence:

$$(|B|)_n = \left(\sqrt{B_r^2 + B_\varphi^2}\right)_n = B_{main} \left(\frac{r}{r_o}\right)^{n-1} \sqrt{a_n^2 + b_n^2} \quad (1.27)$$

1.1.6. INTRODUCTION TO ACCELERATOR OPTICS

[TURN94] In any accelerator, it is desired that all particles move along one specific path, this path is called the design orbit (*Figure 7).* This design orbit may be curved for various purposes, in which case *bending forces* are required to keep the particles moving along the desired design orbit.

Of course, this is the ideal case, in reality most particles in the beam will always be deviated from the design orbit to some degree. These deviations must be kept small along the whole orbit, which could reach 10^{10} km in a storage ring. In order to achieve this, *focusing forces* are required.

The way of accomplishing both *bending* and *focusing* forces is using electromagnetic fields, given the definition of the Lorentz force:

$$F = e\,(E + v \times B) \qquad (1.28)$$

Due to the large velocities v ≈ c, only transverse magnetic fields are considered, given that a moderately strong magnetic field of 1 Tesla would correspond to a very strong electric field of $3x10^8$ V/m.

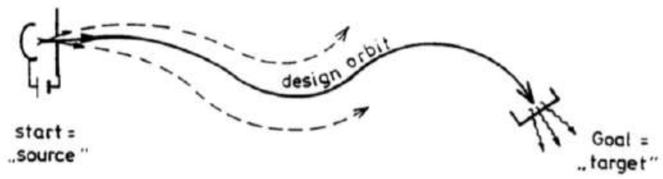

Figure 7: Guidance of particles along a curved design orbit [F7]

Depending on the magnitude of the focusing forces, a distinction can be made between *strong focusing* and *weak focusing.*

Weak focusing, also called geometrical focusing, is achieved by exposing the particles to uniform magnetic fields that make them move in circular paths due to the Lorentz force *(1.28).* This means that in a homogenous magnetic field all plane orbits are circles, so particles diverging from one point will meet again after 180º of revolution, as seen in *Figure 8*.

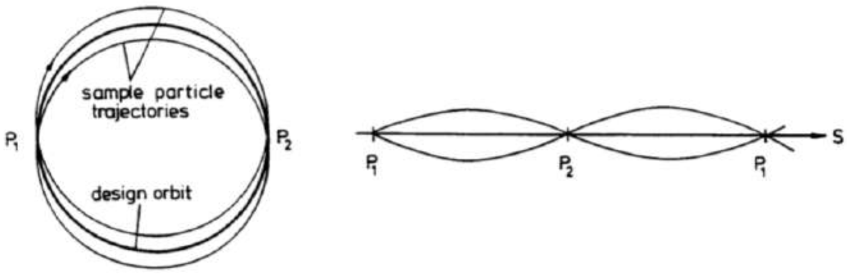

Figure 8: Geometrical focusing in a homogenous magnetic field [F8]

Nevertheless, deviations exist between these orbits. If the motion is stable, restoring forces will arise for small deviations in the particles from the design orbit. These restoring forces lead to oscillations around the design orbit, which are called betatron oscillations.

However, there is one major drawback when applying weak focusing: the circumference of the particle accelerator is smaller than the betatron oscillation wavelength, which means that for a large circumference, large deviations from the design orbit will take place.

Figure 9: Illustrating the circular shape of a particle accelerator [F9]

Strong focusing is used in most modern particle accelerators. The purpose of strong focusing is to make the particle beam converge by making the particles pass through a series of alternating field gradients, as can be seen in *Figure 10.* This process is also called alternating-gradient focusing.

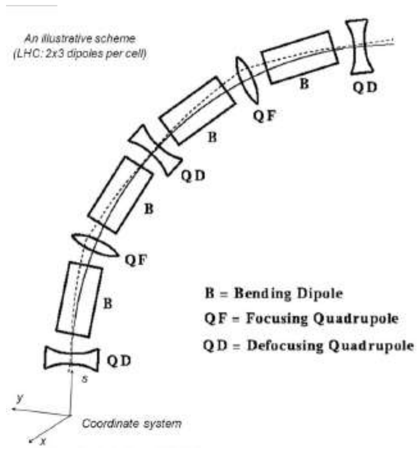

Figure 10: Alternating gradient focusing [F10]

Figure 10 reveals an arrangement of quadrupole magnets that provides a net focusing in both planes (strong focusing). Dipoles are used for keeping the particles on the circular orbit. Alternating focusing quadrupoles and defocusing quadrupoles ends up focusing in both planes [TURN94].

1.1.7. QUADRUPOLES IN PARTICLE ACCELERATORS

In this section an explanation on how quadrupoles contribute to *strong focusing* will be given, a concept that was introduced in the previous section.
Figure 11 illustrates an electron exposed to a quadrupole magnetic field on the positive *y* axis. According to the Lorentz force, the electron bends towards the z axis (which represents the desired path or design orbit), resulting in a focusing effect. [HOCK10]

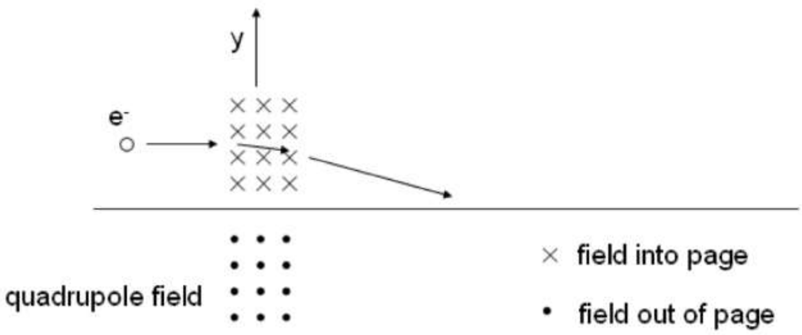

Figure 11: Focusing field in the y axis [F11]

On the other hand, when looking at the effect of this quadrupole's field along the *x* axis *(Figure 12)*, the Lorentz force makes the electron move away from the desired path (*z* axis), resulting in a defocusing effect.

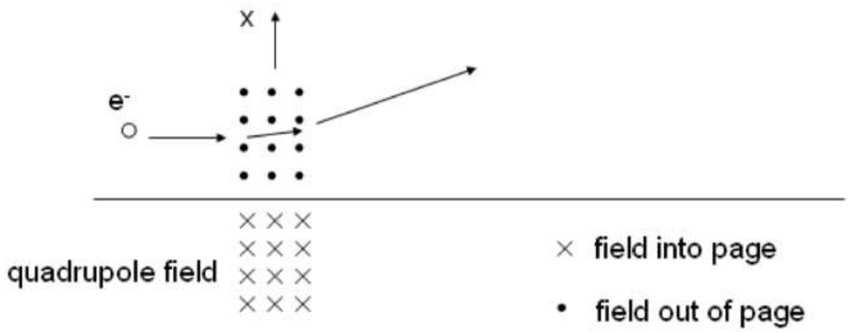

Figure 12: Defocusing field in the x axis [F12]

In conclusion, this quadrupole is focusing along the *y* direction, and defocusing along the *x* direction.

A new quadrupole is now placed separated from the previous one [HOCK10]. This quadrupole's magnetic field behaves the opposite to the first one, so it focuses the electrons along the *x* axis, and defocuses along the *y* axis. If the magnitude of both quadrupole's fields is the same, the total resulting effect on an electron will be focusing, along both axes *x* and *y (Figure 13)*.

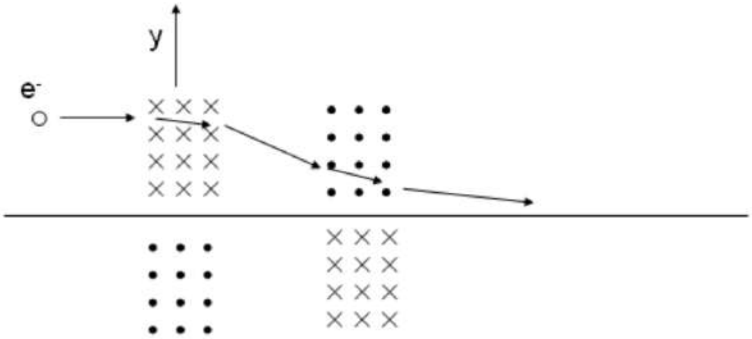

Figure 13: Net focusing effect of two equally strong but opposite quadrupoles [F13]

The names give to these two types of quadrupoles are: *F quadrupoles* (which are focusing along the *x* direction and defocusing along the *y* direction), and *D quadrupoles* (which are focusing along the *y* direction and defocusing along the *x* direction).

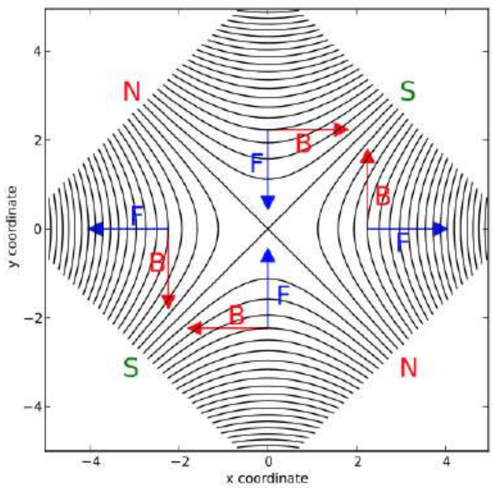

Figure 14: Quadrupole field and Lorentz forces [F14]

Figure 14 illustrates the effect of a quadrupole on a positively charged particle moving into the image. Thus, this quadrupole is focusing in the *y* direction and defocusing on the *x* direction and hence, a *D quadrupole [WIKI01]*

1.2. CERN: THE CLIENT

The European Organization for nuclear research, known as CERN, is the world's largest particle physics laboratory. Founded in 1954, it is located next to the Franco-Swiss border, close to Geneva. [WIKI02]

CERN's ultimate goal is to study the basic constituents of matter: fundamental particles. To achieve this, subatomic particles are made to collide with each other at high velocities close to the speed of light. By studying the interaction of these subatomic colliding particles, much knowledge can be acquired about the fundamental laws of the Universe. [CERN01]

The main instruments used in CERN are particle accelerators and detectors. The mission of particle accelerators is to boost beams of particles to high energies before making them collide. Whereas the purpose of detectors is to record and analyze collisions.

CERN Specifications	*Family 1*	*Family 2*
Integrated Gradient, Max	3,6 Tesla	4,0 Tesla
Integrated Gradient, Min	2,0 Tesla	2,0 Tesla
Length	45 mm	80 mm
Inner diameter	22 mm	22mm
Outer diameter before final machining	61 mm	61 mm
Final outer diameter	60 mm	60 mm
Gradient integral error (rms)	±0,5%	±0,5%
Magnetic versus geometric axis	<0,1 mm	<0,1 mm
Harmonic content at 7.5 mm radius: Bn/B2 for n=3,4,...	<0.01	<0.01
Yaw/pitch/roll:	1 mrad	1 mrad

Table 1: CERN specifications for Permanent Magnet Quadrupoles [T1]

Permanent Magnet Quadrupoles (PMQs) are used in CERN's particle accelerators (specifications shown in *Table 1*) for strong focusing.

1.2.1. LINAC 4

LINAC 4 is a linear accelerator developed by CERN with the mission of boosting negative hydrogen ions to high energies, and will become the source of proton beams for the Large Hadron Collider (LHC). LINAC 4 is 86 meters long and it's located 12 meters below ground.
LINAC 4 accelerates negative hydrogen ions (H^-, formed by adding one additional electron to a hydrogen atom) up to 160 MeV, this way it prepares the ions to enter the Proton Synchrotron Booster, which is part of the LHC injection chain. The pulse of these Negative hydrogen ions as they pass through the accelerator is as low as 400 microseconds at a time.

The linear accelerator is formed by cylindrical conductors. The hydrogen ions pass through these conductors, which are alternately charged positive and negative (the accelerator charges these conductors by using radiofrequency cavities). The ions are accelerated when they get pushed by the conductors behind them and pulled by the conductors ahead of them. [CERN02]

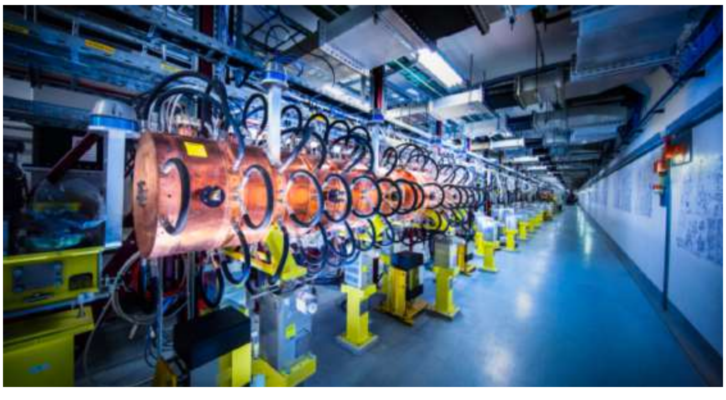

Figure 15: Linear accelerator LINAC 4 [F15]

The role played by quadrupole magnets (*Elytt Energy's* manufactured PMQs) is to ensure that the hydrogen ions remain in a tight beam at all times.

2. STATE OF THE ART AND PROJECT MOTIVATION

2.1. STATE OF THE ART

Regarding already existing technologies, the Hall probe is the most commonly used alternative to the rotating coil system for measuring PMQs. It is also the technology that *Elytt Energy* used for measuring PMQs until this rotating coil system was developed.

A Hall probe is formed by a semiconductor crystal used as a sensor, which is built onto an aluminum plate. The probe is designed in such a way that the semiconductor crystal is placed perpendicularly to the handle. All connections from the crystal to the circuit go through the handle. This handle does not cause any disturbance on the measurements and field, since it is made of a non-ferrous material. [ELEC01]

The Hall probe measures the magnetic field by measuring the voltage across the crystal caused by the *Hall effect*. The Hall effect takes place when a conductor (the crystal) passes through a homogenous magnetic field. In this scenario, a Lorentz force is applied the charge carriers in the conductor, due to the natural electron drift of these charge carriers. This Lorentz force results in a separation or charges, with an accumulation of positive or negative charges on the top or the bottom of the plate, resulting in what is known as *Hall effect voltage.* [HYPE01]

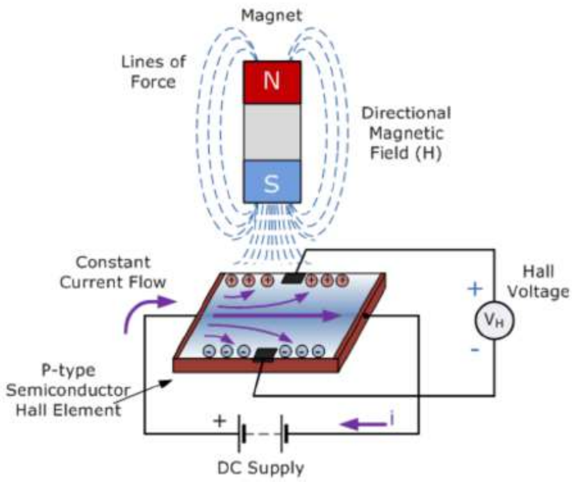

Figure 16: Measuring the Hall effect voltage with a Hall sensor [F16]

Going back to the Hall probe, the crystal is exposed to a magnet's uniform field, additionally, a current is made pass through the crystal. This results in a *Hall effect voltage* across the crystal, which is proportional and leads to the magnetic field strength. Whenever the field lines pass at a 90º angle through the sensor (crystal) of the probe, the probe measures the value of the magnetic flux density (B).

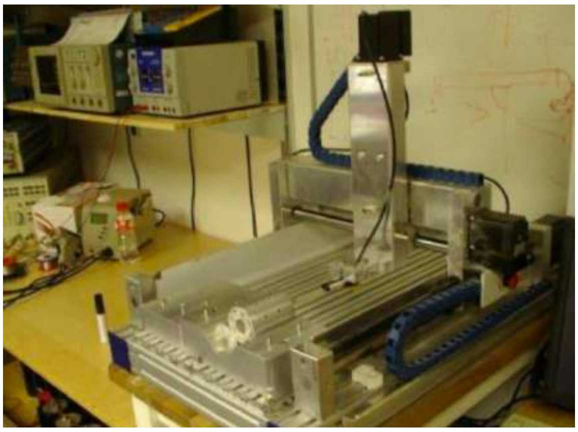

Figure 17: Measurement of PMQ with Hall probe at Elytt Energy [F17]

The Hall probe, combined with a computer-controlled displacement system, provides a detailed field map of the magnet. However, the main drawback of using the Hall probe to measure PMQs is the long time required, taking from 30 to 60 minutes to measure a single PMQ, not being able to analyze all harmonics. Whereas this rotating coil system only takes 1 minute to measure each PMQ, making it possible to save an enormous amount of time and fully analyze field harmonics.

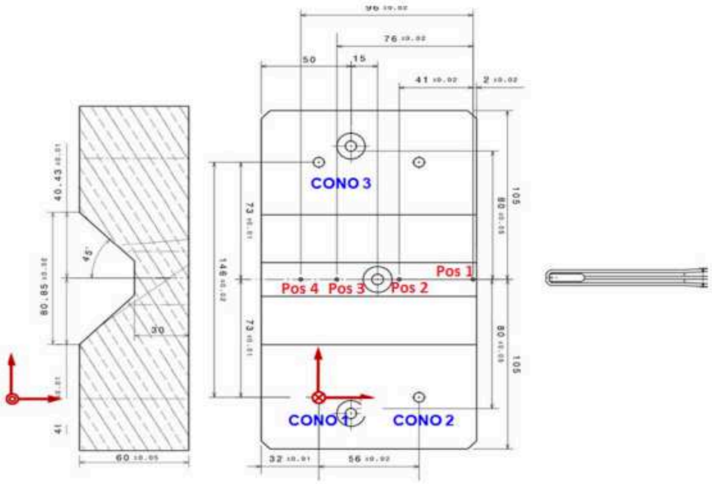

Figure 18: Hall probe bench for measuring PMQ at Elytt Energy [F18]

2.2. MOTIVATION AND OBJECTIVES

The main reason for carrying out this project is to have a fast, accurate system that can identify all field harmonics of a PMQ, given that the Hall probe is comparatively slow and does not allow to measure field harmonics.

Elytt Energy designs and manufactures PMQ’s, therefore strict requirements demanded by clients must be met. It is essential to provide the most accurate information to clients, including the field harmonics. For measuring these harmonics, an accurate rotating coil system is required. The objectives pursued for this rotating coil system are the following:

- To save time and money by measuring our PMQs at *Elytt Energy’s* own facilities with a rotating coil system, instead of having them measured elsewhere. Having another company measure the PMQ’s field harmonics is both slow and expensive.

- To be able to fully map the field harmonics of a PMQ with the smallest possible error.

- To be able to measure as many PMQs in the least possible amount of time: the goal is 1 PMQ per minute.

- To increase *Elytt Energy's* client's trust by having an own rotating coil system and not having to rely on another company.

- To make a completely embedded rotating coil system, so it can be easily transported.

3. DEVELOPMENT OF THE SYSTEM

The main goal of this new machine was to fully measure the field harmonics of a PMQ as fast as possible and with the maximum precision.

In the process of designing the system different phases can be distinguished, which are explained with detail in the following sections.

3.1. FLAT COIL DESIGN

The "antenna" of the system is formed by two flat coils, an internal coil and an external coil, printed in four layers of a PCB. The purpose of using two coils is to measure the individual voltage induced in each coil to acquire the main harmonic of the quadrupole (the second order harmonic). Additionally, in order to acquire the higher order harmonics, the overall voltage of both coils connected in anti-series is measured (the resulting subtraction of the voltages induced in each coil).

It is convenient that the second order voltage harmonics are equal in both coils, so that they cancel out when measuring the overall voltage of both coils connected in anti-series. Therefore, both coils must be equally centered. Additionally, the highest possible sensibility is desired for measuring each of the second order harmonics individually. Additionally, the maximum sensibility is desired when measuring the overall anti-series voltage to acquire the higher order harmonics. To accomplish all of these specifications, some parameters are to be calculated, such as the width of the central gap of the inner coil, the number of spires in each coil, and the displacement of the coil center from the rotating axis.

These parameters must provide maximum sensibility for the individual measurement of the main harmonic, as well as the overall anti-series measurement of the higher order harmonics. For calculations, an Octave code was written (*Annex I)*, which is based on the following equation derivations.

When rotating inside the PMQ's magnetic field, a voltage is induced in each thread of the coil. For the following coordinate system:

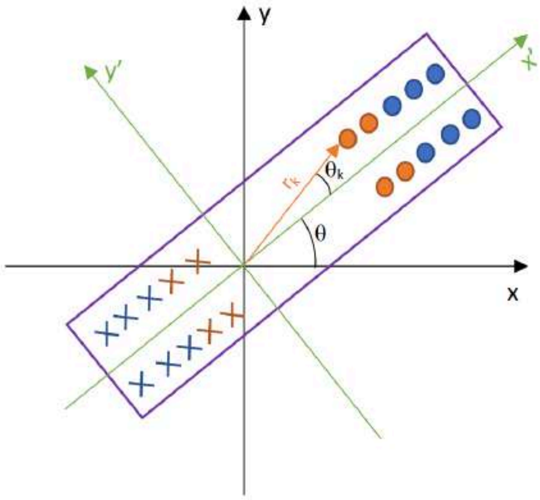

Figure 19: Coordinate system referred to the rotating coil

In *Figure 19* a simplified version of the rotating coil is shown for better understanding. This example is formed by two coils. The inner coil is *Coil 1* (in orange), and it has only 2 spires. The outer coil is *Coil 2* (in blue), and it has 3 spires. Both coils are distributed in two layers of a PCB. The real coil will have many more spires and will be printed in 4 PCB layers. The circles represent the filaments of the upstream spires and the crosses represent the downstream filaments of spires located on the opposite side of the coil center. A coordinate system *x', y'* is conveniently defined, and it is solidary to the coil at all times, in which *x'* is the center of the coil, and *y'* is a perpendicular axis that passes through the origin. Each filament of each spire is located at a radius r_k from the origin and at an azimuthal angle θ_k from the coil central axis *x'*. Furthermore, the coil central axis is located at an azimuthal angle θ from the original x axis. In other words, angle θ_k is solidary to the coil and does not change with rotation, whereas θ constantly changes with the coil rotation.

Using vector potential A:

$$B = \nabla \times A \tag{3.1}$$

Applying Stokes theorem:

$$\phi = \iint B \cdot dS = \iint \nabla \times A \cdot dS = \oint A \cdot dl \tag{3.2}$$

Lenz law:

$$\epsilon = \frac{d\phi}{dt} = \frac{d\phi}{d\theta} \cdot \frac{d\theta}{dt} \Rightarrow \frac{d\phi}{d\theta} = \frac{\epsilon}{\omega} \tag{3.3}$$

Deriving this expression is highly convenient since the data acquisition device will be able to obtain the induced voltage $\in$, the rotating speed ω, and the angle θ.

[LUCA17] Going back to the *normal* multipole coefficients b_n and the *skew* coefficients a_n defined in equation *1.20*, defining $c_n = a_n + b_n \cdot i$:

$$\phi = \oint A \cdot dl = -B_m \cdot r_{ref} \cdot \sum_{n=1}^{\infty} \left(\left(\frac{b_n}{n} \cdot \cos(n \cdot \theta) + \frac{a_n}{n} \cdot \sin(n \cdot \theta) \right) \cdot \left(\frac{r}{r_{ref}} \right)^n \right) \tag{3.4}$$

Using the information shown in *Figure 19*, and defining a parameter *w* that indicates whether the spire's filament goes upstream or downstream, along with the reference radius r_{ref} which is a parameter of each PMQ, the following expression is derived:

$$\phi = -\sum_{(k=1)}^{total\ spires}\left(sign(w_k)\cdot B_m\cdot r_{ref}\cdot\sum_{(n=1)}^{\infty}\left(\left(\frac{b_n}{n}\cdot\cos\big(n\cdot(\theta+\theta_k)\big)+\frac{a_n}{n}\cdot\sin\big(n\cdot(\theta+\theta_k)\big)\cdot\left(\frac{r_k}{r_{ref}}\right)^n\right)\right)\right) \quad (3.5)$$

And using equation *3.3*:

$$\frac{\epsilon}{\omega}=\frac{d\phi}{d\theta}=-\sum_{(k=1)}^{(total\ spires)}\left(sign(w_k)\cdot B_m\cdot r_{ref}\cdot\sum_{(n=1)}^{\infty}\left(\left(-b_n\cdot\sin\big(n\cdot(\theta+\theta_k)\big)+a_n\cdot\cos(n\cdot(\theta+\theta_k))\right)\cdot\left(\frac{r_k}{r_{ref}}\right)^n\right)\right) \quad (3.6)$$

Which leads to:

$$\frac{\epsilon}{\omega}=\frac{d\phi}{d\theta}=-\sum_{k=1}^{total\ spires}\left(sign(w_k)\cdot B_m\cdot r_{ref}\cdot\sum_{n=1}^{\infty}\left(\left(-b_n\cdot(\sin(n\cdot\theta)\cdot\cos(n\cdot\theta_k)+\sin(n\cdot\theta_k)\cdot\cos(n\cdot\theta))+a_n\cdot(\cos(n\cdot\theta)\cdot\cos(n\cdot\theta_k)-\sin(n\cdot\theta_k)\cdot\sin(n\cdot\theta))\right)\cdot\left(\frac{r_k}{r_{ref}}\right)^n\right)\right) \quad (3.7)$$

Since both coils will be symmetrical with respect to axis *y*, all terms $sin(n\theta_k)$ cancel out, leading to the following equation:

$$\frac{\epsilon}{\omega}=B_m\cdot\sum_{n=1}^{\infty}(S_n\cdot b_n\cdot\sin(n\cdot\theta)+S_n\cdot a_n\cdot\cos(n\cdot\theta)) \quad (3.8)$$

S_n refers to the sensibility of order n:

$$S_n=\frac{1}{r_{ref}^{n-1}}\sum_{k=1}^{total\ spires}sign(w_k)\cdot r_k^n\cdot\cos(n\cdot\theta_k) \quad (3.9)$$

For the design, the first specification that must be accomplished is a maximum individual sensibility for the main harmonic S_2, which must be equal in both coils, as explained previously. An Octave code (*Annex I)* was written to determine the design variables for both coils in order to achieve the highest S_2. Given the following parameters:

- Maximum width of PCB: 20 mm

- Minimum width of inner coil gap: 2 mm

- Step between spires: 0.3 mm

- Number of layers: 4

- Distance between layers: 0.5 mm

- PMQ magnetic reference radius: 7.5 mm

- PMQ inner diameter: 26 mm

- PMQ length: 80 mm

Obtaining the following results:

- Gap width of inner coil: 2.1 mm

- Coil center displacement from rotating axis: 3.34 mm

- Number of spires in Coil 1 (inner coil): 12 (per layer)

- Number of spires in Coil 2 (outer coil): 6 (per layer)

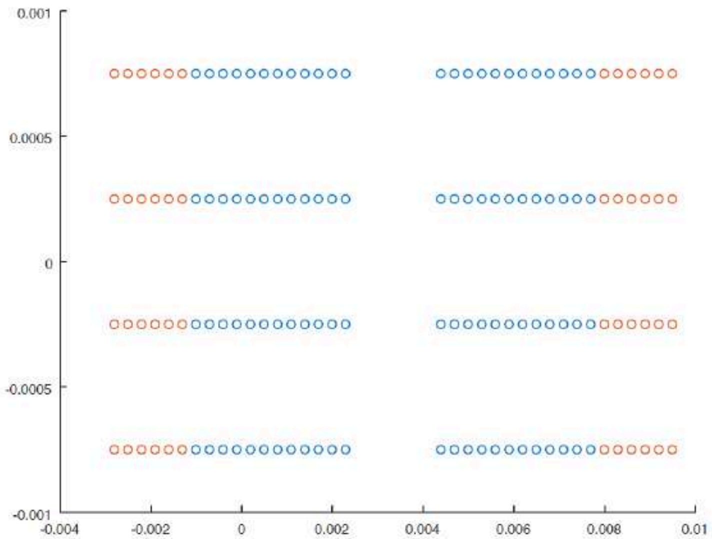

Figure 20: Section of the coil. Coil 1 in blue and Coil 2 in red

In *Figure 20* the filaments of both coils can be clearly seen, as well as the distance between them, distance between all four layers, displacement of the coil center from the rotating axis, and the gap width of *Coil 1*.

The *Octave* code *(Annex I)* also calculates all sensibilities S_n for harmonics of any order. One relevant observation of these calculations is that for the individual sensibilities of each coil, the second order harmonic S_2 had the largest sensibility, as desired. The higher the order, the lower the sensibility for each coil measured separately. On the other hand, for the overall sensibility of both coils connected in anti-series ($|S_{Coil\ 2} - S_{Coil\ 1}|$), the sensibility for the main harmonic S_2 was zero, as desired, and it increased with the order of the harmonics.

For this reason, the system will take two different measurements. The first measurement would be the voltage induced in *Coil 2*, which is used to calculate the main harmonic (second order). The second measurement is the overall compensated voltage of the two coils connected in anti-series, which will be used to obtain the higher order harmonics. These two voltage signals need to be amplified and filtered, as seen in section *3.2*.

Figure 21: Coil 1 and Coil 2 front copper layer

Figure 22: Coil 1 and Coil 2 inner copper layer 1

Figure 23: Coil 1 and Coil 2 inner copper layer 2

Figure 24: Coil 1 and Coil 2 back copper layer

Figure 25: Coil 1 and Coil 2 with a closer look

The total dimensions of *Coil 1* are 190.75 x 8.89 mm and the dimensions of *Coil 2* are 201.93 x 12.45 mm, in each of the 4 layers.

3.2. DESIGN OF THE FILTER AND AMPLIFIER CIRCUIT

(All of the components used in this section can be found in the Bill of Materials in *Annex III)*

The use of an amplifier and filter circuit is required before processing the measured voltage signal. The circuit is formed by four stages: the first two stages (A_1 and A_2) are two identical low pass filters applied directly to the voltage signals measured individually from *Coil 1 and Coil 2,* stage 3 *(A_3)* and stage 4 *(A_4)* are applied to the compensated anti-series voltage signal. For all four stages a cutoff frequency and a static gain is determined. The four operational amplifiers used in these stages are put together in one single component: *Texas Instrument OPA4209 (Annex III)*

-Stages A_1 and A_2:

The first step is to determine the desired static gain. The goal is to obtain a voltage with an amplitude of at least 1V for the main harmonic at the output of both A_1 and A_2. Stages A_1 and A_2 are identical, this way the voltage main harmonic is still the same at the output of both stages.

Knowing that:

$$\frac{V_n}{\omega} = B_n[T \cdot m] \cdot S_n = B_n[T] \cdot r_{ref} \cdot S_n \tag{3.10}$$

It is also known that: r_{ref} = *7.5 mm*, S_2*=0.2446 (calculated in Octave Annex I),* B_{2min}*=0.88 T (looking at the PMQ specifications)*, assuming that $\omega = 2\pi$ *rad/s*.

Then $V_2 = 0.88 \cdot 0.0075 \cdot 0.2445 \cdot 2 \cdot \pi = 0.01\ V$

Given that an output voltage of 1 V is desired: $Gain = A_1(0) = A_2(0) = \frac{1}{0.01} = 100$

The circuit schematic for stages A_1 and A_2 are shown in the figure below:

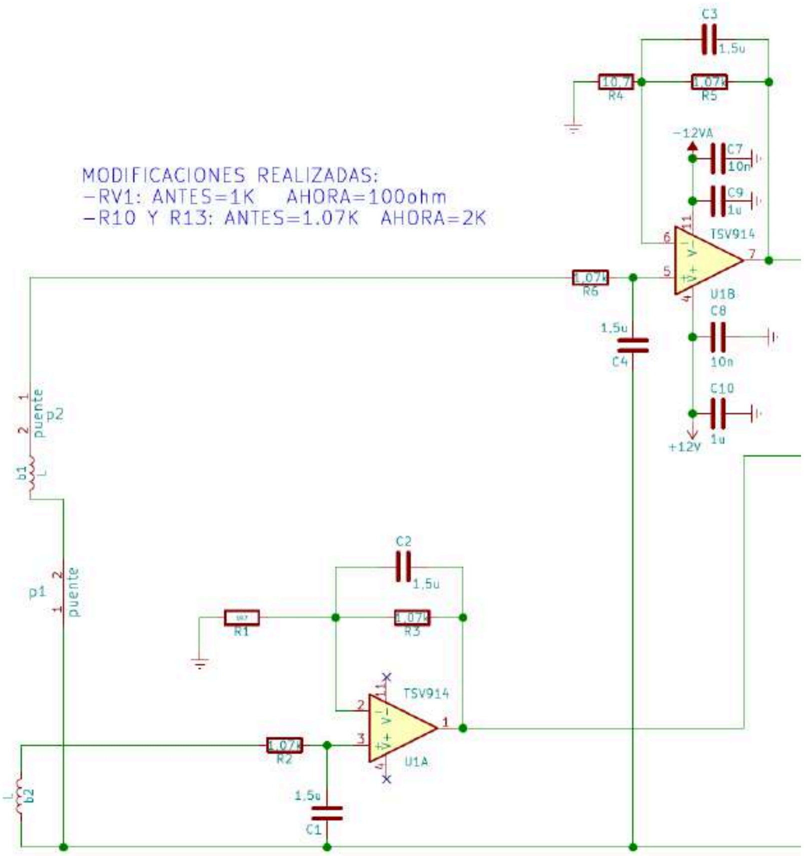

Figure 26: Circuit schematic for stages A_1 and A_2

From the circuit shown in *Figure 26* the transfer functions for A_1 and A_2 are obtained, respectively:

$$A_1(s) = \frac{R_4 \cdot R_5 \cdot C_3 \cdot s + R_4 + R_5}{R_4 \cdot R_5 \cdot C_3 \cdot R_6 \cdot C_4 \cdot s^2 + (R_4 \cdot R_6 \cdot C_4 + R_4 \cdot R_5 \cdot C_3) \cdot s + R_4} \tag{3.11}$$

$$A_2(s) = \frac{R_1 \cdot R_3 \cdot C_2 \cdot s + R_1 + R_3}{R_1 \cdot R_3 \cdot C_2 \cdot R_2 \cdot C_1 \cdot s^2 + (R_1 \cdot R_2 \cdot C_1 + R_1 \cdot R_3 \cdot C_2) \cdot s + R_1} \tag{3.12}$$

Given the desired gains $A_1(0) = 100$ and $A_2(0) = 100$:

$$A_1(0) = \frac{R_4+R_5}{R_4} = 100 \tag{3.13}$$

$$A_2(0) = \frac{R_1+R_3}{R_1} = 100 \tag{3.14}$$

From equations *3.13* and *3.14* two constraints are obtained for R_5, R_4 and R_3, R_1, respectively.

The desired cutoff frequency is now used to obtain some additional constraints.

It is desired for this system to determine the first 25 harmonics, therefore it seems reasonable to place the cutoff frequency at 25 Hz = 50π rad/s. However, if the cutoff frequency is placed at 25 Hz, the harmonic at 25 Hz will be reduced by 3 dB, therefore the cutoff frequency ω_o is finally placed at 100 Hz= 200π rad/s. Given that each of the two stages is formed by two first order low-pass RC filters put together, and the transfer function of a low pass filter is of the following form:

$$F(s) = \frac{1}{1+\frac{1}{\omega_O}\cdot s} = \frac{1}{1+C_4\cdot R_6\cdot s} = \frac{1}{1+C_3\cdot R_5\cdot s} = \frac{1}{1+C_1\cdot R_2\cdot s} = \frac{1}{1+C_2\cdot R_3\cdot s} \tag{3.15}$$

The following constraints are obtained:

$$\omega_o = 200\pi = \frac{1}{C_4\cdot R_6} = \frac{1}{C_3\cdot R_5} = \frac{1}{C_1\cdot R_2} = \frac{1}{C_2\cdot R_3} \tag{3.16}$$

The following component values are chosen to satisfy the constraints in equation *3.16*:

$$R_6 = R_5 = R_2 = R_3 = 1.07\ k\Omega$$

$$C_4 = C_3 = C_1 = C_2 = 1.5\ \mu F$$

Using equations *3.13* and *3.14*:

$$\frac{R_4 + R_5}{R_4} = \frac{R_4 + 1070}{R_4} = 100 \rightarrow R_4 = 10.7\ \Omega$$

$$\frac{R_1 + R_3}{R_1} = \frac{R_1 + 1070}{R_1} = 100 \rightarrow R_1 = 10.7\ \Omega$$

It is required to verify that the maximum voltage at the output of stages A_1 and A_2 is less than 10V so that the operational amplifiers will not saturate.

$$V_{2\max} = B_{2\max} \cdot r_{ref} \cdot S_2 \cdot \omega$$

It is known that: r_{ref} = *7.5 mm*, S_2*=0.2446 (calculated in Octave Annex I),* B_{2max}*=3.07T (looking at the PMQ specifications)*, assuming $\omega = 2\pi\ rad/s$.

$$V_{2\max} = 3.07 \cdot 0.0075 \cdot 0.2446 \cdot 2 \cdot \pi = 0.035\ V$$

Multiplying by the static gain $A_1(0) = A_2(0) = 100$:

$$V_{2\max} = 100 \cdot 0.035 = 3.5\ V$$

The maximum possible voltage at the output of these stages is 3.5 V, which is considerably less than 10 V. This assures that for the chosen component values, the operational amplifiers will not saturate.

A Bode plot of the frequency response of A_1 and A_2 is shown in the following figure:

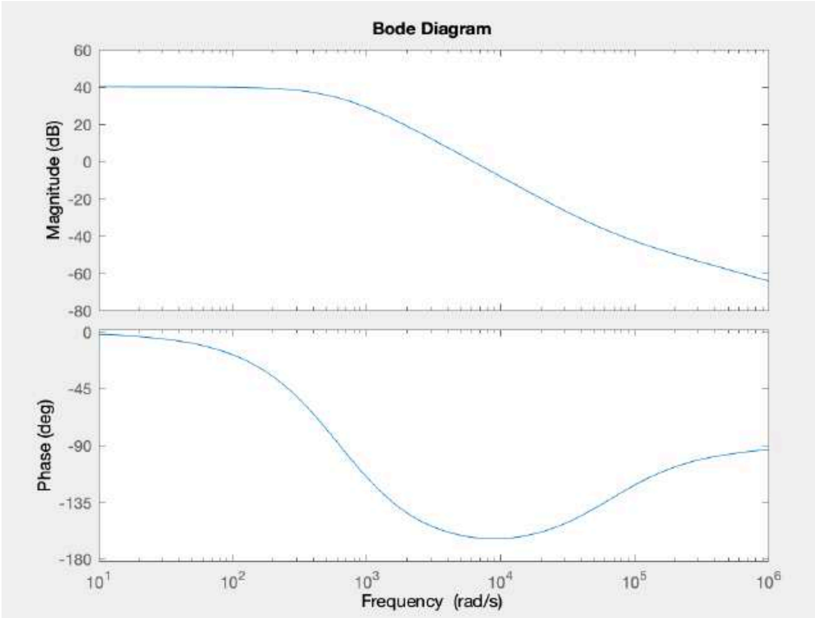

Figure 27: Bode plot of stages A_1 and A_2

-Stages A_3 and A_4:

The purpose of stages A_3 and A_4 is to amplify and filter the compensated voltage signal of *Coil 1* and *Coil 2* connected in anti-series, in order to calculate the higher order harmonics. It is desired that the main voltage harmonics of the two coils cancel out, therefore an adding configuration is needed before stage A_3, since the main harmonics of the two voltage signals will be of equal magnitude but opposite. This adding configuration is achieved with resistors R_7 and R_8, then, a potentiometer R_{POT} is connected, which will be used if any small adjustment is required for the two voltages to be exactly equal and cancel out. Additionally, $R_7'=R_7 + R_{POT}$ and $R_8'=R_8 + R_{POT}$.

By looking at the circuit shown in *Figure 28*, the following transfer function can be calculated for A_3, where V_{i1} and V_{i2} are the output voltages of stages A_1 and A_2, respectively, and V_{o3} is the output of stage A_3:

$$V_{o3} = \left(\frac{V_{i1}}{R_7'} + \frac{V_{i2}}{R_8'}\right) \cdot \left(\frac{1}{\frac{1}{R_{10}} + C_5 \cdot s}\right) \quad (3.17)$$

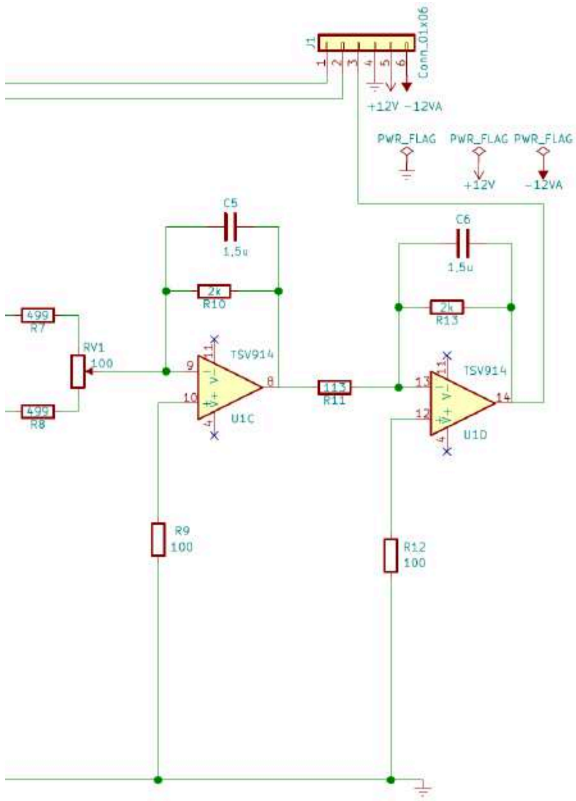

Figure 28: Circuit schematic for stages A_3 and A_4

The addition of main harmonics of the two voltages must be the zero. Therefore, R_7' must be equal to R_8'. This is the first design constraint.

$$R_7' = R_8' \tag{3.18}$$

If V_{o3} is the output of stage A_3, and V_{o4} is the output of stage A_4, the transfer function for the final stage A_4 is:

$$A_4(s) = \frac{V_{o4}}{V_{o3}} = \frac{1}{R_{11}} \cdot \left(\frac{1}{\frac{1}{R_{13}} + C_6 \cdot s}\right) \tag{3.19}$$

The final overall output of stages A_3 and A_4 is given by:

$$V_{o4} = \left(\frac{V_{i1}}{R_7'} + \frac{V_{i2}}{R_8'}\right) \cdot \left(\frac{1}{\frac{1}{R_{10}} + C_5 \cdot s}\right) \cdot \frac{1}{R_{11}} \cdot \left(\frac{1}{\frac{1}{R_{13}} + C_6 \cdot s}\right) \tag{3.20}$$

Equation *3.18* reveals that $R_7' = R_8'$, therefore:

$$V_{o4} = (V_{i1} + V_{i2}) \cdot \frac{R_{13} \cdot R_{10}}{R_{7'} \cdot R_{11}} \cdot \left(\frac{1}{1 + R_{10} \cdot C_5 \cdot s}\right) \cdot \left(\frac{1}{1 + R_{13} \cdot C_6 \cdot s}\right) \tag{3.21}$$

The static gain k_o of the system is:

$$k_o = \frac{R_{13} \cdot R_{10}}{R_{7'} \cdot R_{11}} \tag{3.22}$$

The first step is to determine the cutoff frequency of the system. The desired cutoff frequency for stages A_1 and A_2 is 100 Hz, then $\omega_o = 200\pi$ rad/s, hence:

$$\omega_o = \frac{1}{R_{10} \cdot C_5} = \frac{1}{R_{13} \cdot C_6} = 200 \cdot \pi \tag{3.23}$$

Therefore:

$$R_{10} = R_{13} = 1.07\ k\Omega$$

$$C_5 = C_6 = 1.5\ \mu F$$

The next step is to determine the desired static gain k_o, the goal is to obtain the maximum possible gain without saturating any operational amplifier. Hence, the maximum possible output voltage is calculated for each harmonic.

First, the maximum voltage for each harmonic n is calculated at the output of stages A_1 and A_2, these are V_{i1max} and V_{i2max}.

$$V_{i1\max}(n) = B_{nmax} \cdot r_{ref} \cdot S_1(n) \cdot 2 \cdot \pi \cdot |A_1(2\pi \cdot n)| \tag{3.24}$$

$$V_{i2\max}(n) = B_{nmax} \cdot r_{ref} \cdot S_2(n) \cdot 2 \cdot \pi \cdot |A_2(2\pi \cdot n)| \tag{3.25}$$

The final output for each harmonic V_{o4n} must satisfy the following condition, in order to maintain the operational amplifiers unsaturated for the first 25 harmonics:

$$\sqrt{\sum_{n=1}^{25} V_{o4n}^2} \leq 8\ V \tag{3.26}$$

The Octave code shown in *Figure 29* leads to:

$$\sqrt{\sum_{n=1}^{25} V_{o4nmax}^2} = 0.8 \cdot k_o \text{, which means that } k_o = \frac{8}{0.8} = 10\ V/V \tag{3.27}$$

```
%CALCULAMOS LOS VALORES DE LAS TENSIONES DESPUES DE CADA ETAPA PARA CADA ARMONICO DE FRECUENCIA t
i=sqrt(-1);
for t=1:1:30
  if(t<=2)
  v1min(t)=0.88*0.0075*S1_tot(t)*2*pi*1*abs((0.034/2*t*2*pi*10^(-3)*i+1.072)/(0.1084/4*(t*2*pi*10^(-3)*i)^2+0.068/2*(t*2*pi*10^(-3)*i)+0.0107));
  v2min(t)=-0.88*0.0075*S2_tot(t)*2*pi*1*abs((0.034/2*t*2*pi*10^(-3)*i+1.072)/(0.1084/4*(t*2*pi*10^(-3)*i)^2+0.068/2*(t*2*pi*10^(-3)*i)+0.0107));
  v1max(t)=3.07*0.0075*S1_tot(t)*2*pi*abs((0.034/2*t*2*pi*10^(-3)*i+1.072)/(0.1084/4*(t*2*pi*10^(-3)*i)^2+0.068/2*(t*2*pi*10^(-3)*i)+0.0107));
  v2max(t)=-3.07*0.0075*S2_tot(t)*2*pi*abs((0.034/2*t*2*pi*10^(-3)*i+1.072)/(0.1084/4*(t*2*pi*10^(-3)*i)^2+0.068/2*(t*2*pi*10^(-3)*i)+0.0107));
  else
   v1min(t)=0.88*0.01*0.0075*S1_tot(t)*2*pi*1*abs((0.034/2*t*2*pi*10^(-3)*i+1.072)/(0.1084/4*(t*2*pi*10^(-3)*i)^2+0.068/2*(t*2*pi*10^(-3)*i)+0.0107));
  v2min(t)=-0.88*0.01*0.0075*S2_tot(t)*2*pi*1*abs((0.034/2*t*2*pi*10^(-3)*i+1.072)/(0.1084/4*(t*2*pi*10^(-3)*i)^2+0.068/2*(t*2*pi*10^(-3)*i)+0.0107));
  v1max(t)=3.07*0.01*0.0075*S1_tot(t)*2*pi*abs((0.034/2*t*2*pi*10^(-3)*i+1.072)/(0.1084/4*(t*2*pi*10^(-3)*i)^2+0.068/2*(t*2*pi*10^(-3)*i)+0.0107));
  v2max(t)=-3.07*0.01*0.0075*S2_tot(t)*2*pi*abs((0.034/2*t*2*pi*10^(-3)*i+1.072)/(0.1084/4*(t*2*pi*10^(-3)*i)^2+0.068/2*(t*2*pi*10^(-3)*i)+0.0107));
  end
  vomax(t)=(v1max(t)+v2max(t))*abs(10/((1+3.183/2*2*pi*t*10^(-3)*i)^2));
  vomin(t)=(v1min(t)+v2min(t))*abs(10/((1+3.183/2*2*pi*t*10^(-3)*i)^2));
 end
resmax=0;
resmin=0;
%la suma cuadrática de los 20 primeros armónicos no debe exceder los 8V para que no sature el operacional
 for t=1:1:20
  resmax=vomax(t)^2+resmax;
  resmin=vomin(t)^2+resmin;
  end
  resmax=sqrt(resmax);
  resmin=sqrt(resmin);
```

Figure 29: Octave code for calculating the maximum overall output voltage

Using equations *3.22* and *3.27* the following constraint is obtained:

$$k_o = 10 = \frac{R_{13} \cdot R_{10}}{R_{7'} \cdot R_{11}} \tag{3.28}$$

Since $R_{13} = R_{10} = 1.07\ k\Omega$, the following component values can be used for R_7' and R_{11}:

$$R_{11} = 112.6\ \Omega$$

$$R_7' = R_8' = 1\ k\Omega = \mathrm{R}_7 + R_{POT} = R_8 + R_{POT} \rightarrow$$

$$\rightarrow R_7 = R_8 = 0.5\ k\Omega$$

$$\rightarrow R_{POT} = 0.5\ k\Omega$$

To accomplish the conditions above, a potentiometer of 1 kΩ is chosen.

Due to expense reasons, resistors $R_{13} = R_{10} = 1.07\ k\Omega$ were used, and a potentiometer of 100 Ω. However, these changes were not significant and all objectives were accomplished.

The following figures show the Bode plots of the transfer functions $A_3(s) = \frac{V_{o3}}{V_{i1}+V_{i2}}$, $A_4(s) = \frac{V_{o4}}{V_{o3}}$, and finally the transfer function $A_t(s) = A_3(s) \cdot A_4(s)$

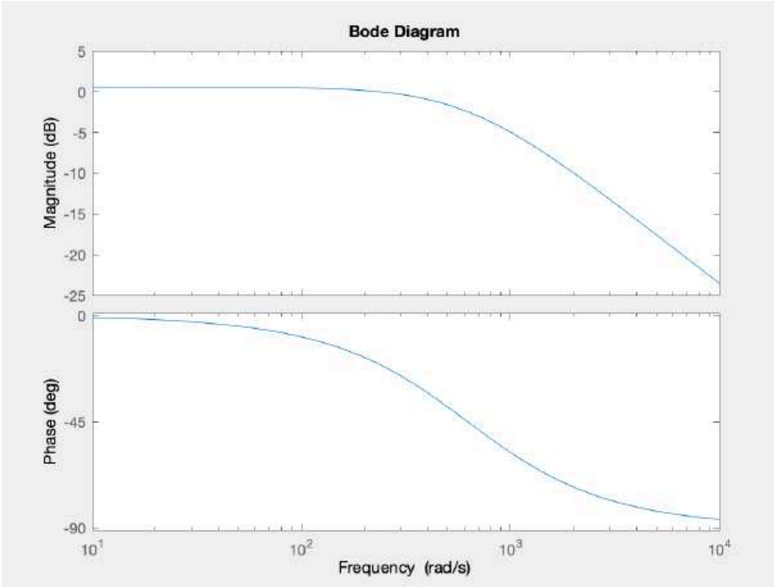

Figure 30: Bode plot of stage A_3

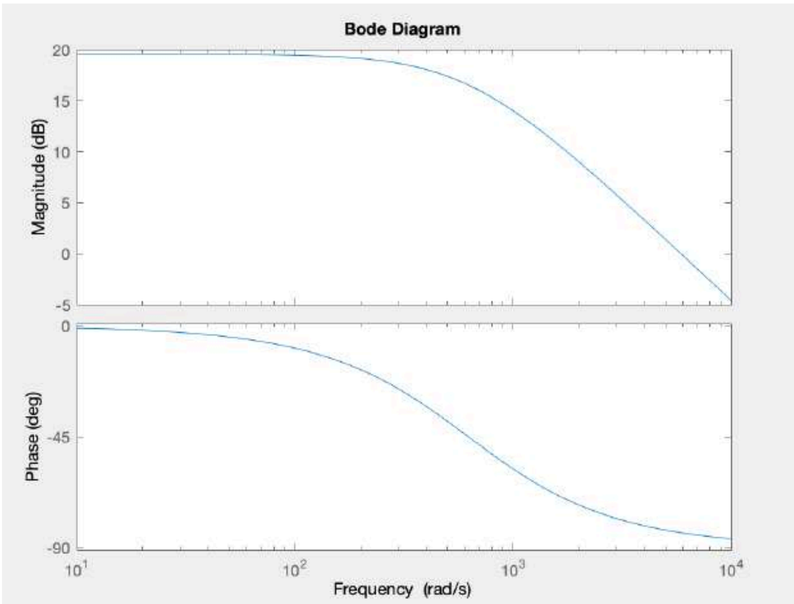

Figure 31: Bode plot of stage A_4

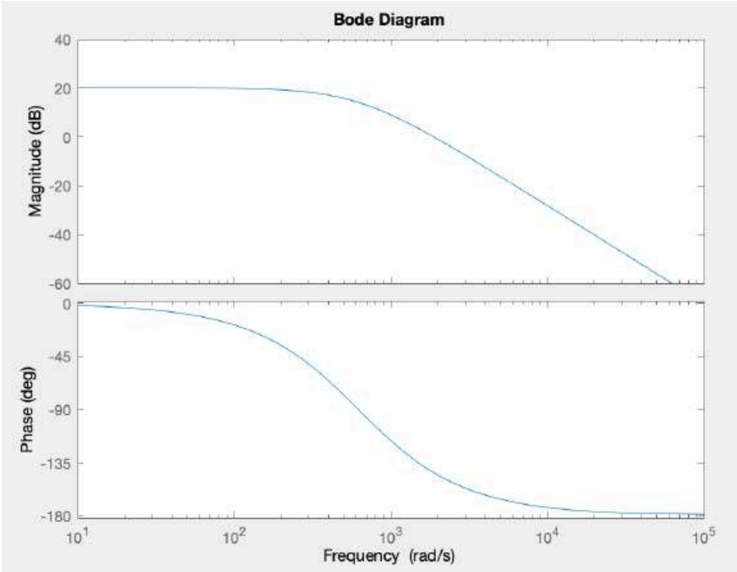

Figure 32: Bode plot of stage $A_t = A_3 * A_4$

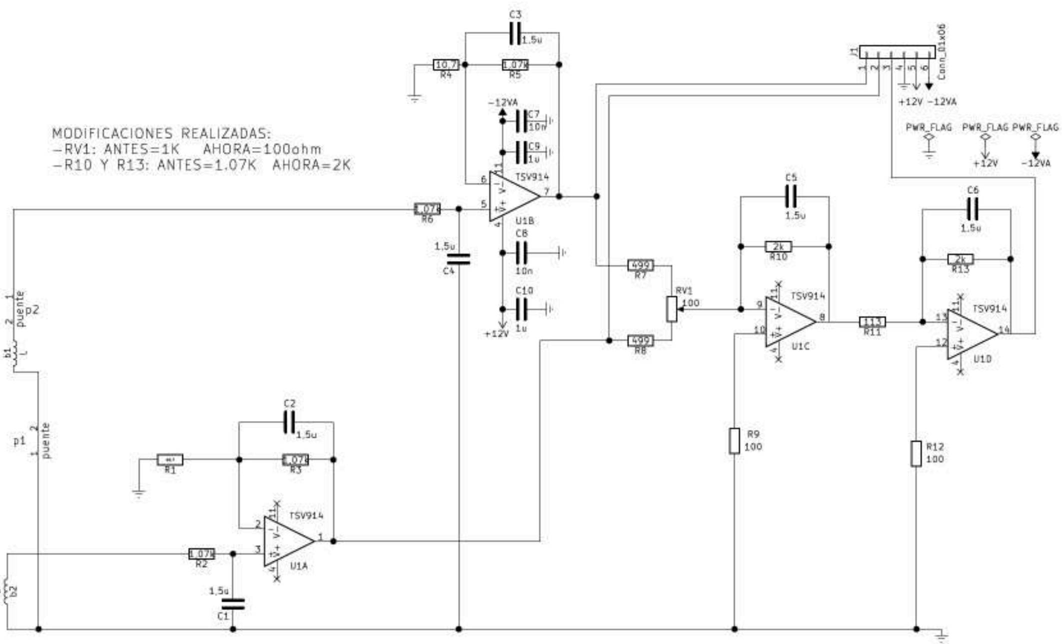

Figure 33: Schematic of the entire circuit

3.3. PCB DESIGN AND COMPONENT SOLDERING

The next step was to design the PCB and do the layout using a CAD tool. For this purpose, a program called *KiCad* was used.

The first task was to draw the footprint of both coils on *KiCad.* To achieve this, some research was done on the code format for drawing footprints on *KiCad*. A program was written in *Octave*, using loops to generate the code text needed for drawing the coil on *KiCad* (*Figure 34).* This helped to save a lot of time by not drawing it "manually" on *KiCad.*

```
 printf( '\n \n b1_capa1: \n');
 for i=1:1:length(b1i)-1
   fprintf('(fp_line (start %f %f) (end %f %f) (layer F.Cu) (width 0.15))\n',b1i(i,1),b1i(i,2),b1i(i+1,1),b1i(i+1,2));
 end
% printf( '\n \n b2_capa1: \n');
%  for i=1:1:length(b2i)-1
%   fprintf('(fp_line (start %f %f) (end %f %f) (layer F.Cu) (width 0.15))\n',b2i(i,1),b2i(i,2),b2i(i+1,1),b2i(i+1,2));
% end
 %printf( '\n \n b1_capa2: \n');
 for i=1:1:length(b1p)-1
   fprintf('(fp_line (start %f %f) (end %f %f) (layer In1.Cu) (width 0.15))\n',b1p(i,1),b1p(i,2),b1p(i+1,1),b1p(i+1,2));
 end
   %printf( '\n \n b2_capa2: \n');
%  for i=1:1:length(b2p)-1
%   fprintf('(fp_line (start %f %f) (end %f %f) (layer In1.Cu) (width 0.15))\n',b2p(i,1),b2p(i,2),b2p(i+1,1),b2p(i+1,2));
%  end
 printf( '\n \n b1_capa3: \n');
for i=1:1:length(b1i)-1
   fprintf('(fp_line (start %f %f) (end %f %f) (layer In2.Cu) (width 0.15))\n',b1i(i,3),b1i(i,4),b1i(i+1,3),b1i(i+1,4));
 end
% printf( '\n \n b2_capa3: \n');
%  for i=1:1:length(b2i)-1
%    fprintf('(fp_line (start %f %f) (end %f %f) (layer In2.Cu) (width 0.15))\n',b2i(i,3),b2i(i,4),b2i(i+1,3),b2i(i+1,4));
%  end
     printf( '\n \n b1_capa4: \n');
 for i=1:1:length(b1p)-1
   fprintf('(fp_line (start %f %f) (end %f %f) (layer B.Cu) (width 0.15))\n',b1p(i,3),b1p(i,4),b1p(i+1,3),b1p(i+1,4));
 end
% % printf( '\n \n b2_capa4: \n');
% for i=1:1:length(b2p)-1
%   fprintf('(fp_line (start %f %f) (end %f %f) (layer B.Cu) (width 0.15))\n',b2p(i,3),b2p(i,4),b2p(i+1,3),b2p(i+1,4));
% end
%

%% %filename=fopen('b1_imp.txt','w');
%   printf( '\n \n b1_capa1: \n');
%   for i=length(b1i):-1:2
%    fprintf('(segment (start %f %f) (end %f %f) (width 0.15) (layer F.Cu) (net 0)) \n',b1i(i,1),b1i(i,2),b1i(i-1,1),b1i(i-1,2));
%   end
%%    %printf( '\n \n b2_capa1: \n');
%%   %for i=length(b2i):-1:2
%%    %fprintf('(segment (start %f %f) (end %f %f) (width 0.15) (layer F.Cu) (net 0)) \n',b2i(i,1),b2i(i,2),b2i(i-1,1),b2i(i-1,2));
%%   %end
%    printf( '\n \n b1_capa2: \n');
%   for i=length(b1p):-1:2
%    fprintf('(segment (start %f %f) (end %f %f) (width 0.15) (layer In1.Cu) (net 0)) \n',b1p(i,1),b1p(i,2),b1p(i-1,1),b1p(i-1,2));
%   end
%%   % printf( '\n \n b2_capa2: \n');
%%   %for i=length(b2p):-1:2
%%    %fprintf('(segment (start %f %f) (end %f %f) (width 0.15) (layer In1.Cu) (net 0)) \n',b2p(i,1),b2p(i,2),b2p(i-1,1),b2p(i-1,2));
%%   %end
%   printf( '\n \n b1_capa3: \n');
%   for i=length(b1i):-1:2
%    fprintf('(segment (start %f %f) (end %f %f) (width 0.15) (layer In2.Cu) (net 0)) \n',b1i(i,3),b1i(i,4),b1i(i-1,3),b1i(i-1,4));
%   end
%%    %printf( '\n \n b2_capa3: \n');
%%   %for i=length(b2i):-1:2
%%    %fprintf('(segment (start %f %f) (end %f %f) (width 0.15) (layer In2.Cu) (net 0)) \n',b2i(i,3),b2i(i,4),b2i(i-1,3),b2i(i-1,4));
%%   %end
%   printf( '\n \n b1_capa4: \n');
%   for i=length(b1p):-1:2
%    fprintf('(segment (start %f %f) (end %f %f) (width 0.15) (layer B.Cu) (net 0)) \n',b1p(i,3),b1p(i,4),b1p(i-1,3),b1p(i-1,4));
%   end
%%   % printf( '\n \n b2_capa4: \n');
%%   %for i=length(b2p):-1:2
%%    %fprintf('(segment (start %f %f) (end %f %f) (width 0.15) (layer B.Cu) (net 0)) \n',b2p(i,3),b2p(i,4),b2p(i-1,3),b2p(i-1,4));
%  % end
```

Figure 34: Octave code used for drawing the coil footprints on KiCad

After drawing the coil, it was necessary to include all components in the PCB and doing the layout. Firstly, the circuit schematic was drawn and all components were added on *KiCad*. Then, the desired footprint for each component was included on the schematic. Most of the components used are SMD (Surface Mount Device) of size 0603, which is the second smallest size existent for SMD (1.6 mm wide x 0.4 mm high). Although these small dimensions made the soldering part very challenging, they were necessary in order to fit the PCB in the rotation stage.

Finally, the layout was done, and after enrouting all components, the design of the PCB was complete.

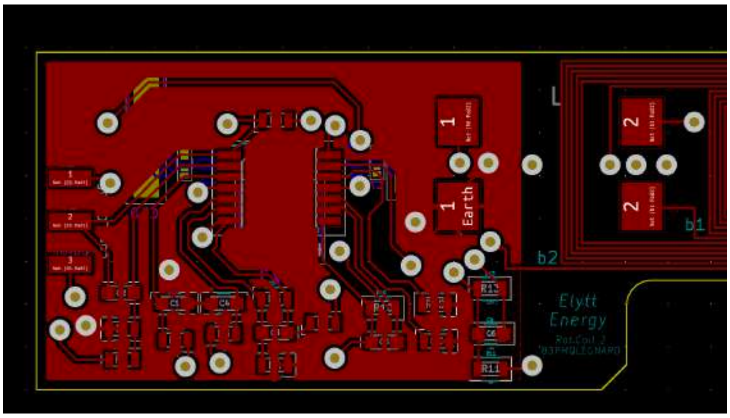

Figure 35: Final PCB layout with all component footprints

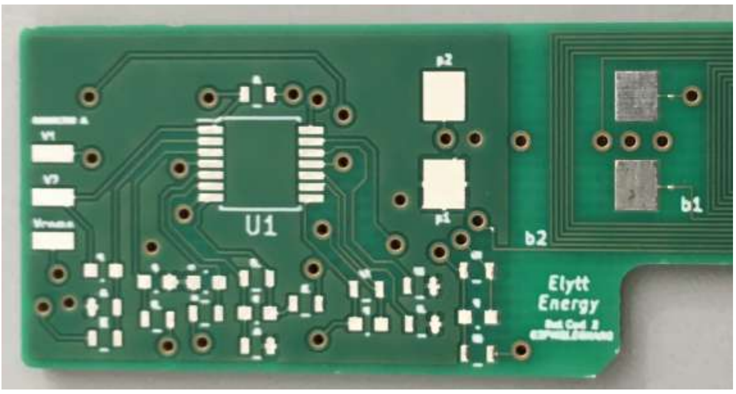

Figure 36: Real picture of the PCB component layout

Figure 37: Overall view of the PCB KiCad design

Figure 38: Real picture of the overall final PCB

The next step was to order the PCB using a website called https://www.eurocircuits.com. This website allowed to upload the *KiCad* design directly, making the job conveniently simple. Additionally, a bill of materials (BOM) was made and components were ordered through a distributor called *Farnell.*

Finally, all of the components were soldered, a significantly challenging task given the small dimensions of the components.

3.4. RAPID PROTOTYPING WITH LEGO EV3

Before proceeding to buy the rotation stage, the data acquisition, manufacture and assemble the entire structure, given the very high price, a decision was made concluding that it would be best to do a *LEGO* prototype of the rotating coil system and run some experiments by measuring voltage signals.

One week was spent building the structure out of *LEGO*, additionally, a prototype of the rotation stage was built with a *LEGO EV3* servomotor, which came with its own encoder. The experiments were run by making the coil rotate and measuring the induced voltage signal with an oscilloscope.

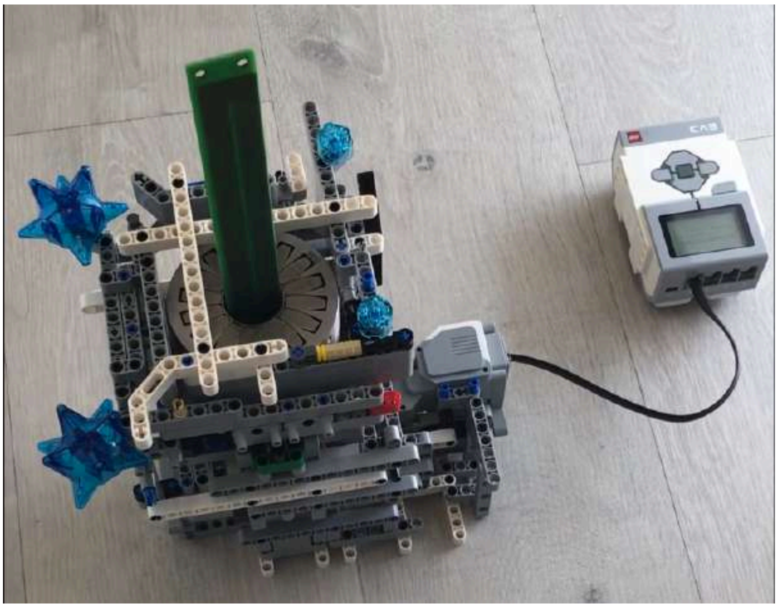

Figure 39: Prototype of the system with LEGO EV3

The results of the experiments were not as successful as expected, unfortunately. The structure was not stiff enough, given the undesired elasticity of the *LEGO* pieces. Therefore, the motion was more quivery and unsteady than desired, which resulted in a lot of noise in the voltage signal. However, the sine wave was clearly visible and the amplitude laid within the desired range.

3.5. *ROTATION STAGE AND DATA ACQUISITION SETUP*

Once the prototype had been tested, the next step was to set up the rotation stage, the motion controller and encoder. A *Newport RGV100-BLS* rotation stage was used, and a *Newport XPS-RL* motion controller.

After doing some research on *TCL* coding, a *TCL* script was written to make the rotation stage turn and gather the angle, speed, and both values of the individual voltage induced in *Coil 2*, and of the overall compensated voltage of both coils connected in anti-series. This code is shown in *Annex II.*

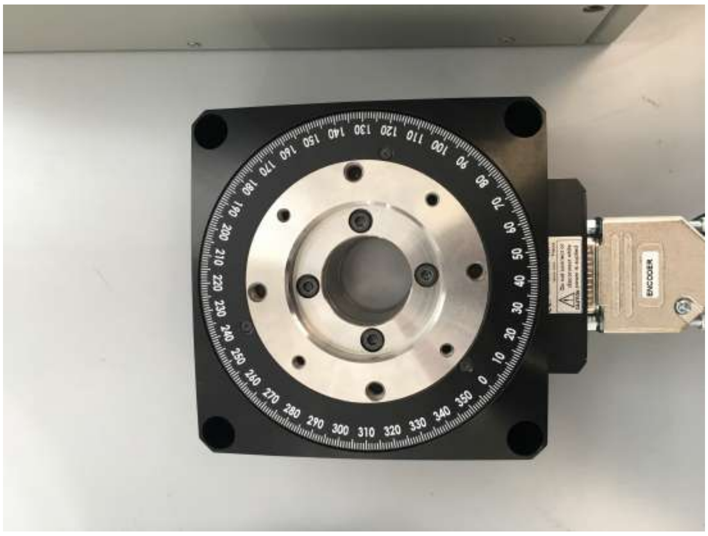

Figure 40: Newport RGV100-BLS rotation stage

The rotation stage would turn at 2Hz, first anticlockwise for 8 laps, and then clockwise for 22 laps, the trigger is set to start measuring at the beginning of the 8^{th} clockwise lap, proceeding by analyzing exclusively data gathered from the 8^{th} clockwise lap to the 18^{th} clockwise lap, to ensure that neither the initial acceleration nor the final deceleration would affect the calculations.

The measurements are taken at a frequency of 1 kHz, and a total of 40000 data points. These measurements will include position (angle) and velocity, measured through the encoder, and the two aforementioned voltages, which will be measured through the two *GPIO's* in the motion controller.

Figure 41: Newport XPS-RL motion controller

3.6. BEDPLATE DESIGN

Designing a good bedplate was crucial for the quality of the measuring system. A highly stiff and stable structure is desired in order to minimize the noise in the measured signals and to assure that the motion of the rotation stage will not cause unwanted vibrations in the structure and will not affect the measurements.

Each part of the bedplate was designed with *CATIA* then they were ordered to be manufactured. Finally, the bedplate was assembled manually.

Some key parts in this design were the mole for the PCB and the slip rings. In order to couple the PCB to the rotation stage, a mole (*Figure 42)* was needed, it would be screwed to the rotation stage, additionally, the PCB would be glued to this mole.

The mole had to be made of a plastic non-conducting material to avoid parasitic capacitances and any other effect on the measurements.

Additionally, a slip rings mechanism was needed to avoid the wires getting tangled while the coil rotates.

Figure 42: Mole used to couple the PCB to the rotation stage

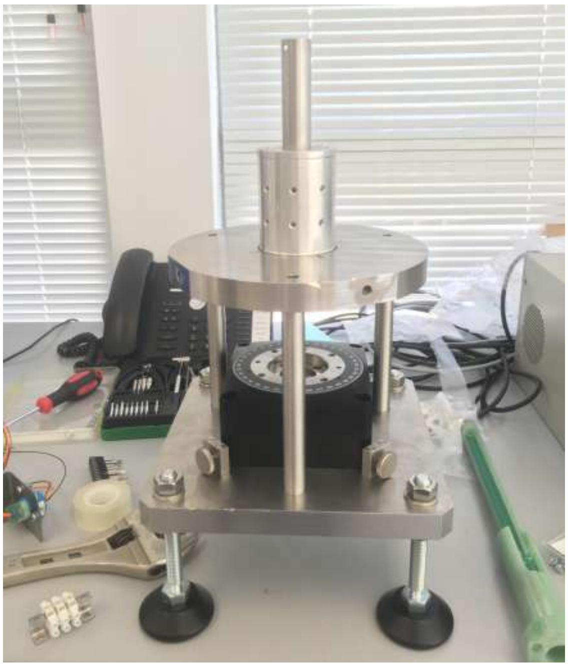

Figure 43: Picture of the bedplate

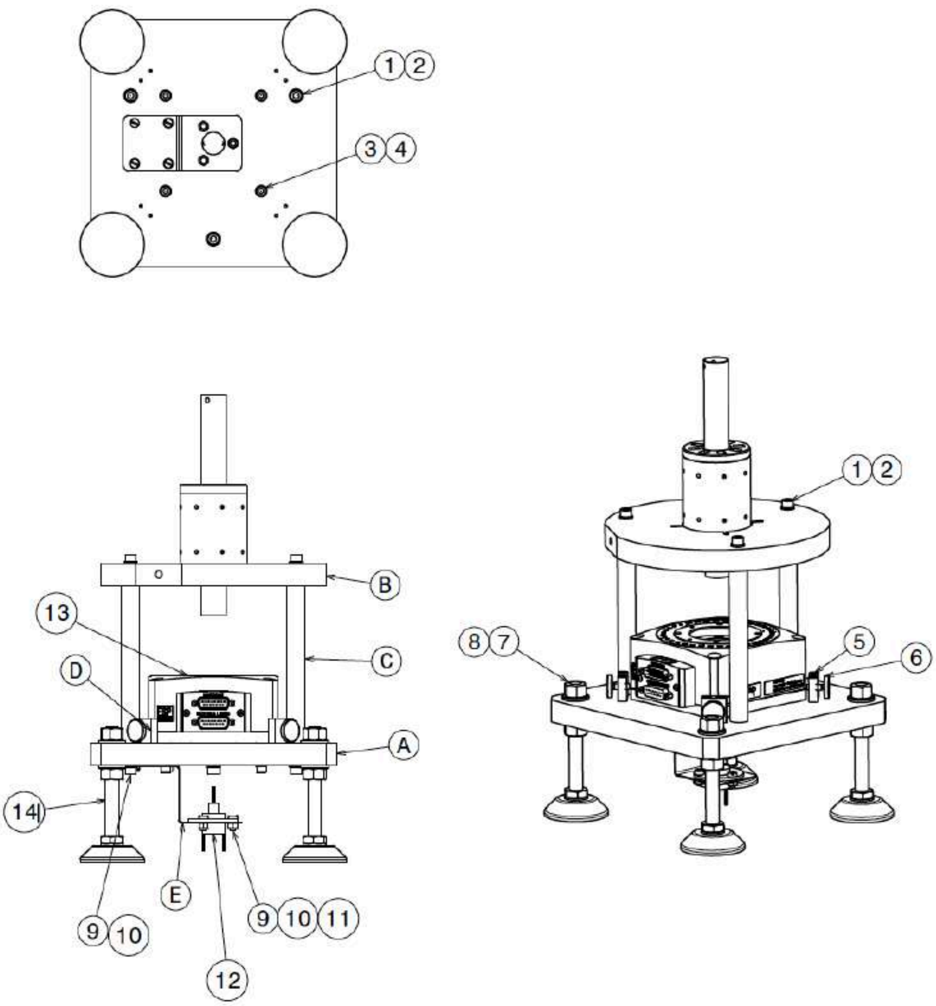

1.	Socket screw	8.	Feet fixation washer
2.	Washers	9.	Screw for slip rings
3.	Washers	10.	Nut for slip rings
4.	Socket screw	11.	Washer for slip rings
5.	Conical screw	12.	Slip rings
6.	Knurled screw	13.	Rotation stage
7.	Feet fixation nut	14.	Feet

Figure 44: Overview of the bedplate

3.7. DATA PROCESSING

All calculations used for data processing are done through the *Matlab* script shown in *Annex IV*.

Using the following nomenclature for sensibilities:

$$COS_n = \sum_{k=1}^{\substack{total\\spires}} \left(sign(w_k) \cdot \cos(n \cdot \theta_k) \cdot \left(\frac{r_k}{r_{ref}}\right)^n \right) \tag{3.29}$$

$$SIN_n = \sum_{k=1}^{\substack{total\\spires}} \left(sign(w_k) \cdot \sin(n \cdot \theta_k) \cdot \left(\frac{r_k}{r_{ref}}\right)^n \right) \tag{3.30}$$

Equation *(3.7)* leads to:

$$\frac{\epsilon}{\omega} = \frac{d\phi}{d\theta} = B_m \cdot r_{ref} \cdot \sum_{n=1}^{\infty}((b_n \cdot COS_n + a_n \cdot SIN_n) \cdot \sin(n \cdot \theta) + (b_n \cdot SIN_n - a_n \cdot COS_n) \cdot \cos(n \cdot \theta)) \tag{3.31}$$

By doing a Fourier analysis of ϵ/ω :

$$\frac{\epsilon}{\omega} = \sum_{n=1}^{\infty} \tau_n \cdot \sin(n \cdot \theta) + \rho_n \cdot \cos(n \cdot \theta) \tag{3.32}$$

The following system of equations is obtained:

$$B_m \cdot r_{ref} \cdot \begin{bmatrix} \mathrm{COS_n} & SIN_n \\ SIN_n & -COS_n \end{bmatrix} \cdot \begin{bmatrix} b_n \\ a_n \end{bmatrix} = \begin{bmatrix} \tau_n \\ \rho_n \end{bmatrix} \tag{3.33}$$

There is a matrix M_n for each harmonic containing the sensibilities:

$$M_n = \begin{bmatrix} \mathrm{COS_n} & SIN_n \\ SIN_n & -COS_n \end{bmatrix} \tag{3.34}$$

Shall the rotating coil be symmetrical respect to its mid plane (in the thickness direction), then the terms $SINn$ will be zero, however, these terms are maintained to study the possibility of a misalignment in the rotating coil.

A Discrete Fourier Transform of the discrete data is now applied $F_k = \epsilon_k / \omega_k$. If N points are obtained, considering that $\theta \rightarrow \theta_k = \frac{2\pi k}{N}$ then:

$$DFT(F_k) = \gamma_n + i \cdot \delta_n \text{ with } k = \left(-\frac{N-1}{2}\right) \dots \left(+\frac{N-1}{2}\right) \text{ if } N \text{ is odd} \tag{3.35}$$

$$DFT(F_k) = \gamma_n + i \cdot \delta_n \text{ with } k = -\left(\frac{N}{2} - 1\right) \dots \left(+\frac{N}{2}\right) \text{ if } N \text{ is even} \tag{3.36}$$

$$F_k = \frac{1}{N} \cdot \sum_{-\frac{N-1}{2} or -\left(\frac{N}{2}-1\right)}^{\frac{N-1}{2} or \frac{N}{2}} (\gamma_n + i \cdot \delta_n) \cdot e^{i \cdot \frac{2\pi k}{N} \cdot n} \tag{3.37}$$

Since F_k is real, the following must happen:

$$\gamma_n = \gamma_{-n} \tag{3.38}$$

$$\delta_n = -\delta_{-n} \tag{3.39}$$

This implies:

$$\begin{bmatrix} \tau_n \\ \rho_n \end{bmatrix} = \begin{bmatrix} -2 \cdot \frac{\delta_n}{N} \\ 2 \cdot \frac{\gamma_n}{N} \end{bmatrix} \tag{3.40}$$

Applying *Matlab's "fft"* command to sampled points $\in_k/\omega_k$, γ_n and δ_n are obtained for each harmonic:

- To obtain γ_n and δ_n with n ≤ 2 → *DFT* of sampled points $\in_k/\omega_k$ from *Coil 2* individually

- To obtain γ_n and δ_n with n > 2 → *DFT* of sampled points $\in_k/\omega_k$ from the overall compensated signal

Once γ_n and δ_n are calculated with *Matlab's "fft"* command , and N is the total number of sampled points, then:

$$\begin{bmatrix} b_n \\ a_n \end{bmatrix} = \frac{1}{B_m \cdot r_{ref}} \cdot M_n^{-1} \cdot \begin{bmatrix} -2 \cdot \frac{\delta_n}{N} \\ 2 \cdot \frac{\gamma_n}{N} \end{bmatrix} \text{for } n = 1 \dots \frac{N}{2} \text{ (if even) or } \frac{N-1}{2} \text{ (if odd)} \tag{3.41}$$

Knowing that:

$$B_n = b_n \times B_{main} \qquad A_n = a_n \times B_{main} \tag{3.42}$$

Equations *3.41* and *3.42* lead to:

$$\begin{bmatrix} B_n \\ A_n \end{bmatrix} = \frac{1}{r_{ref}} \cdot M_n^{-1} \cdot \begin{bmatrix} -2 \cdot \frac{\delta_n}{N} \\ 2 \cdot \frac{\gamma_n}{N} \end{bmatrix} for\ n = 1 \ldots \frac{N}{2}\ (if\ even)\ or\ \frac{N-1}{2}\ (if\ odd) \tag{3.43}$$

Coefficients B_n and A_n are calculated from equation *3.43*.

It is also known that:

$$C_n = \sqrt{A_n^2 + B_n^2} \rightarrow\ C_2 = \sqrt{A_2^2 + B_2^2} \tag{3.44}$$

Going back to equation *1.27*:

$$(|B|)_n = \left(\sqrt{B_r^2 + B_\varphi^2}\right)_n = B_{main}\left(\frac{r}{r_o}\right)^{n-1}\sqrt{a_n^2 + b_n^2} \rightarrow$$

$$\rightarrow (|B|)_n = \left(\frac{r}{r_o}\right)^{n-1}\sqrt{A_n^2 + B_n^2} \tag{3.45}$$

If $n = 2$ (for the main harmonic), then:

$$(|B|)_2 = B_{main} = \left(\frac{r}{r_o}\right)^{1}\sqrt{A_2^2 + B_2^2} \tag{3.46}$$

Assuming $r \approx r_o$ and using equations *3.44* and *3.46*:

$$B_{main} \approx \sqrt{A_2^2 + B_2^2} \approx C_2 \tag{3.47}$$

B_{main} is easily calculated using equation *3.47*

The next step is to calculate the IG (integrated gradient), axis errors, and roll.

<u>IG calculation:</u>

The IG is measured in Tesla [T], and it is calculated in the following way:

$$IG\ [T] = \frac{B_{main}}{r_{ref}} \tag{3.48}$$

Axis errors:

To calculate the axis errors, the PMQ must be initially measured in *Position 1*. Using the calculated parameters A_n, B_n and C_n in this position, axis errors are:

$$-Horizontal\ axis\ error\ in\ Position\ 1: \Delta x_1 = -\frac{B_1 \cdot r_{ref}}{C_2} \quad (3.49)$$

$$-Vertical\ axis\ error\ in\ Position\ 1: \Delta y_1 = \frac{A_1 \cdot r_{ref}}{C_2} \quad (3.50)$$

Consequently, the PMQ must be measured in *Position 2*, in which it is rotated 180º from *Position 1*. Again, using the calculated parameters A_n, B_n and C_n in this new position, axis errors are:

$$-Horizontal\ axis\ error\ in\ Position\ 2: \Delta x_2 = -\frac{B_1 \cdot r_{ref}}{C_2} \quad (3.51)$$

$$-Vertical\ axis\ error\ in\ Position\ 2: \Delta y_2 = \frac{A_1 \cdot r_{ref}}{C_2} \quad (3.52)$$

Using the errors in *Position 1* and *Position 2*, the overall axis errors are:

$$-Overall\ horizontal\ axis\ error: \Delta x = \frac{\Delta x_1 - \Delta x_2}{2} \quad (3.53)$$

$$-Overall\ vertical\ axis\ error: \Delta y = \frac{\Delta y_1 - \Delta y_2}{2} \quad (3.54)$$

Roll:

To calculate *Roll 1* ($\Delta\theta_1$), the PMQ must be measured in *Position 1*. Using the calculated parameters A_n, B_n and C_n in this position, $\Delta\theta_1$ is determined:

$$\Delta\theta_1 = -\frac{A_2}{2C_2} \quad (3.55)$$

The same applies to calculate *Roll 2* ($\Delta\theta_2$), for which the PMQ must me measured in *Position 2*, rotated 90º from *Position 1*, then $\Delta\theta_2$ is determined:

$$\Delta\theta_2 = -\frac{A_2}{2C_2} \quad (3.56)$$

4. TESTS, RESULTS, AND CALIBRATION

Many tests and experiments needed to be done to ensure the minimum error when measuring. The results of the measurements of *Tank 3 [1]* are shown in *Annex V*, and the results of the measurements of *Tank 4 [2]* are shown in *Annex VI.*

The calibration of the rotating coil was made using the Hall probe measurements. *PMQ 413 [3]* was measured by *CERN*, obtaining a good agreement with the Hall probe machine at *Elytt Energy* (less than 0.15% error). Since *PMQ 413* had already been delivered to *INFN*, it could not be used to calibrate the rotating coil system. However, all *Tank 4* and *Tank 3* PMQs were measured in the Hall probe using the same procedure. Therefore, it seemed reasonable to calibrate the rotating coil using all of the *Tank 3* PMQs, making the new rotating coil measurements match the Hall probe measurements.

All calculations used for calibrating the system where done using the *Matlab* script shown in *Annex IV.*

[1] Set of 15 PMQs manufactured by *Elytt Energy*

[2] Ser of 13 PMQs manufactured by *Elytt Energy*

[3] PMQ that belongs to *Tank 4*

4.1. IG (INTEGRATED GRADIENT) CALIBRATION

Once the rotating coil system was calibrated, the maximum difference in IG between the rotating coil measurements and Hall probe measurements was less than 0.15%, for all 15 PMQs in *Tank 3*.

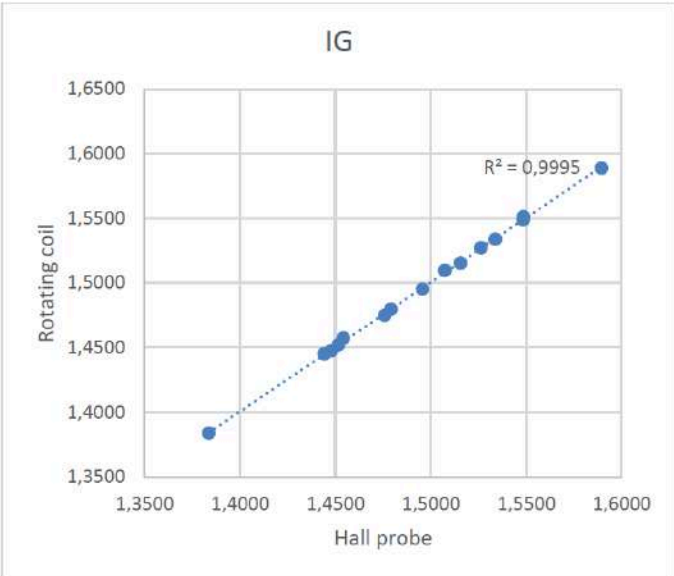

Figure 45: Rotating coil IG calibration

4.2. AXIS

A comparison of the X-Y axis errors between the Hall probe measurements and the rotating coil measurements is shown in *Figure 47* and *Figure 48*.

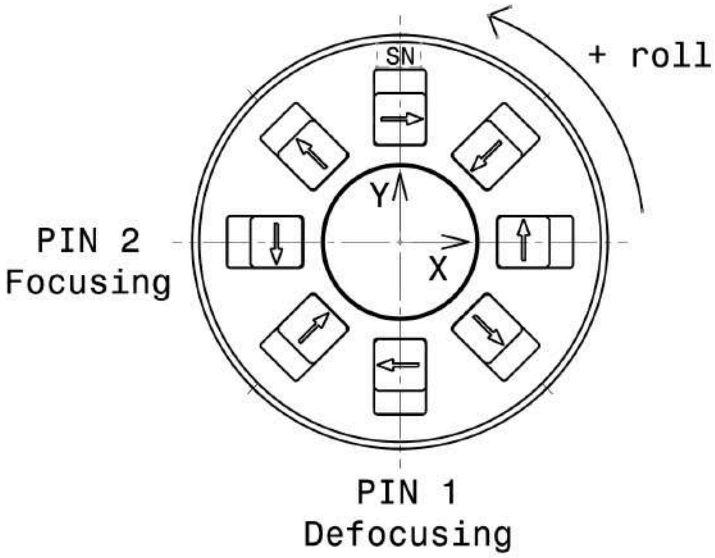

Figure 46: Coordinate system used for measuring PMQs [F46]

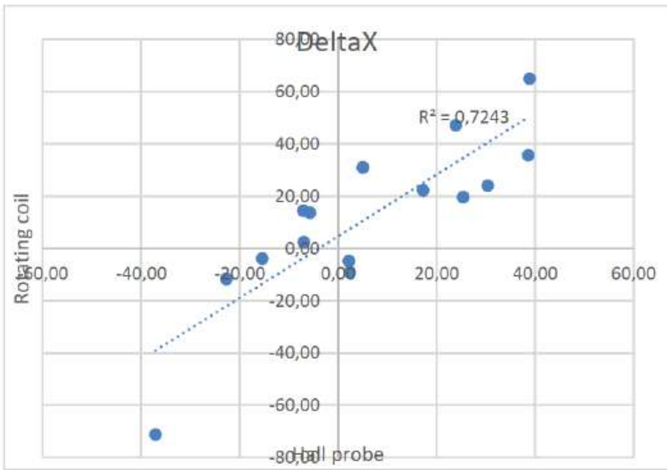

Figure 47: X axis error comparison

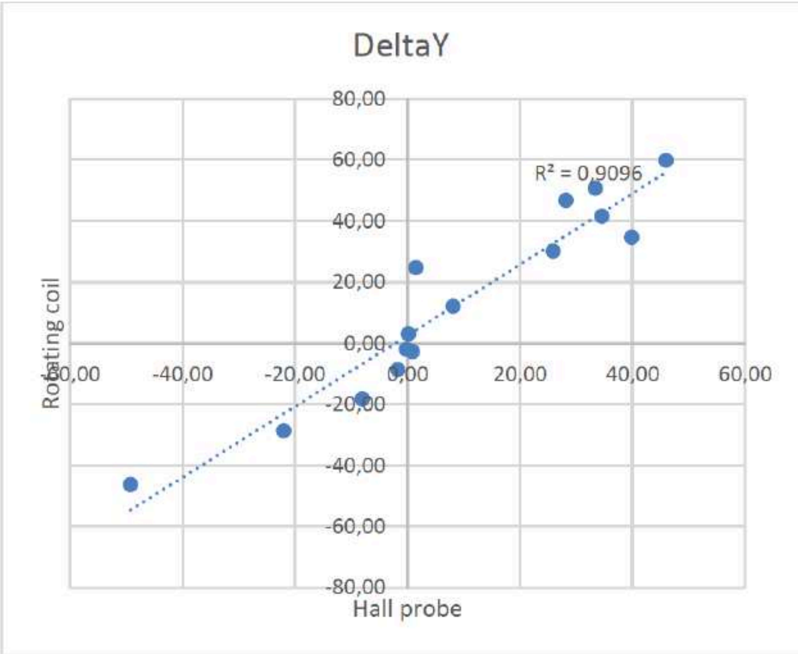

Figure 48: Y axis error comparison

Figure 47 and *Figure 48* show that the rotating coil measurements are correlated to the Hall probe measurements, although the results obtained using the rotating coil have a larger dispersion, which is significantly higher in the horizontal direction *x*.

The reason for this dispersion is thought to be an existing gap between the PMQ and the bench when positioning the PMQ. Therefore, PMQ positioning must be improved. *Elytt Energy* is currently developing an adaptor to reduce this gap between the bench and PMQ.

4.3. ROLL

A roll comparison between Hall probe measurements and rotating coil measurements is shown in *Figure 49* and *Figure 50*. The results of the rotating coil measurements show a good roll agreement with the Hall probe measurements.

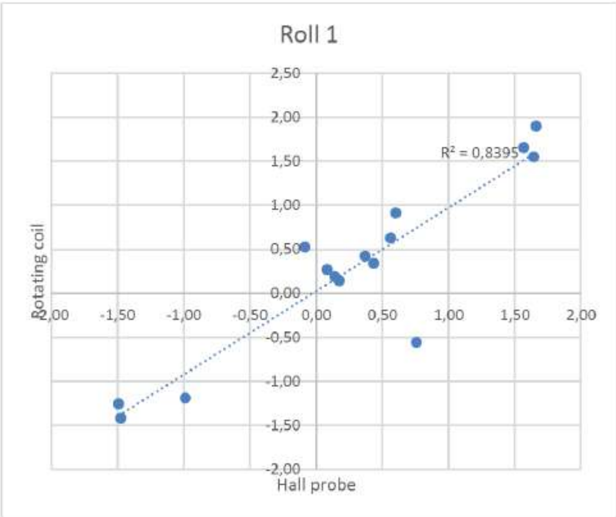

Figure 49: Roll 1 comparison

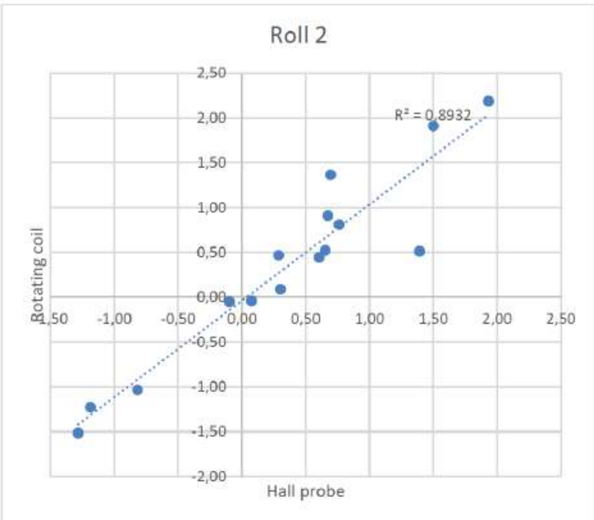

Figure 50: Roll 2 comparison

4.4. HARMONICS COMPARISON

The harmonics have been compared using the PMQ S36, which was initially measured by *BARC*. The results are shown in *Table 2*:

	S36		
Harmonic number	cn BARC Rotating coil	cn Elytt Rotating coil	Difference
3	82	85	3
4	11	15	4
5	24	21	−3
6	58	57	−1
7	17	16	−1
8	16	19	3
9	6	5	−1
10	3	4	1

Table 2: Harmonics comparison between Elytt Energy's rotating coil system and BARC's

Rotating coil harmonics c_3 and c_4 show a good agreement with the ones measured with the Hall probe, as seen in *Figure 51* and *Figure 52*:

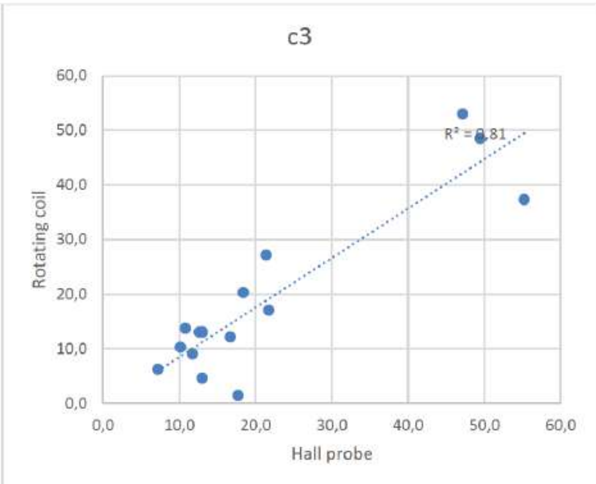

Figure 51: Harmonics (c_3) comparison between rotating coil and Hall probe

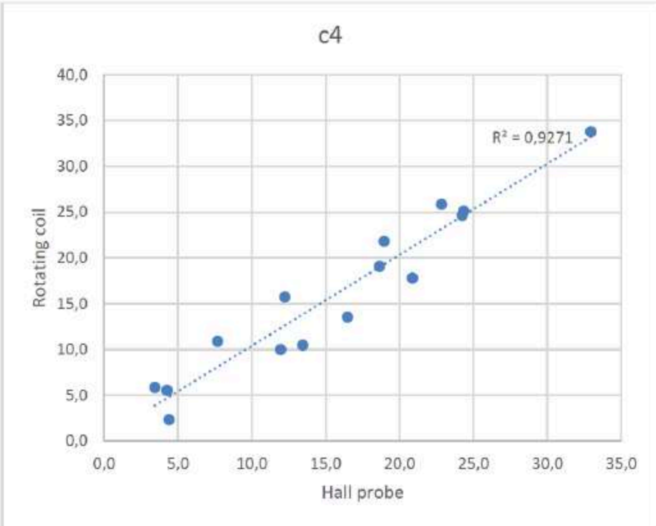

Figure 52: Harmonics (c_4) comparison between rotating coil and Hall probe

4.5. IG TEMPERATURE DEPENDENCE

PMQ 413 was measured (before optimizing magnet positions) at different temperatures to check the temperature dependence. Results are shown in *Table 3*:

Macro	$T = 19°$	$T = 26.1°$	Difference per °C
IG measuring about 70% of the PMQ length	0.9504	0.9473	−0.0454283%
IG measuring 100% of the PMQ length	1.2068	1.2020	−0.0563491%

Table 3: IG temperature dependence

Two different clouds of points where used (one measured about 70% of IG and the other measured the full PMQ). A mean value for temperature dependence shall be selected, i.e. -0.0508887 % / ºC

5. CONCLUSION

The operation of this rotating coil system for measuring PMQs has successfully met all of the requirements and accomplished the main objectives:

- To save time and money by measuring our PMQs at *Elytt Energy's* own facilities with a rotating coil system.

- To be able to accurately map the field harmonics of a PMQ with the smallest possible error.

- To be able to measure 1 PMQ in 1 minute, which is incredibly fast as compared with the previous technology

- To make a completely embedded rotating coil system that can be easily transported

This rotating coil system is currently operating successfully, being used for measuring PMQs in *Elytt Energy's* facility at Bilbao, Spain.

Figure 53: Overview of the rotating coil system

REFERENCES

TEXT REFERENCES

[TURN94] S. Turner, CERN Accelerator School Fifth General Accelerator Physics Course, CERN, Geneva, Switzerland, 26 January 1994

[HOCK10] Kai Hock, Quadrupole Magnet, Report, Cockcroft Institute, Liverpool University, 10 March 2010

Link: http://hep.ph.liv.ac.uk/~hock/Damping_Ring/quadrupole.pdf

[WIKI01] https://en.wikipedia.org/wiki/Quadrupole_magnet

Last Access: 20/04/2019

[WIKI02] https://en.wikipedia.org/wiki/CERN

Last Access: 12/03/2019

[CERN01] https://home.cern/about

Last Access: 02/05/2019

[CERN02] https://home.cern/science/accelerators/linear-accelerator-4

Last Access: 15/03/2019

[ELEC01] https://www.electronics-tutorials.ws/electromagnetism/hall-effect.html

Last Access: 11/04/2019

[HYPE01] http://hyperphysics.phy-astr.gsu.edu/hbase/magnetic/Hall.html
Last Access: 12/04/2019

[LUCA17] Julio Lucas, Design and Manufacturing of Accelerator Components for Use on Linacs, Doctoral Thesis, Universidad del País Vasco, Leioa, July 2017

FIGURE REFERENCES

[F3] K.Wille, Maria Laach lectures, from book S. Turner, CERN Accelerator School Fifth General Accelerator Physics Course, CERN, Geneva, Switzerland, 26 January 1994

[F4] https://en.wikipedia.org/wiki/Quadrupole#/media/File:VFPt_quadrupole_coils_1.svg
Last Access: 20/04/2019

[F5] K.Wille, Maria Laach lectures, from book S. Turner, CERN Accelerator School Fifth General Accelerator Physics Course, CERN, Geneva, Switzerland, 26 January 1994

[F6], [F7], [F8] S. Turner, CERN Accelerator School Fifth General Accelerator Physics Course, CERN, Geneva, Switzerland, 26 January 1994

[F9] Image © Diamond Light Source
https://www2.physics.ox.ac.uk/accelerate/resources/background/particles-and-materials
Last Access: 06/03/2019

[F10] S. Turner, CERN Accelerator School Fifth General Accelerator Physics Course, CERN, Geneva, Switzerland, 26 January 1994

[F11], [F12], [F13]

Kai Hock, Quadrupole Magnet, Report, Cockcroft Institute, Liverpool University, 10 March 2010

Link: http://hep.ph.liv.ac.uk/~hock/Damping_Ring/quadrupole.pdf

[F14]

https://en.wikipedia.org/wiki/Quadrupole_magnet#/media/File:Magnetic_field_of_an_idealized_quadrupole_with_forces.svg
Last Access: 20/04/2019

[F15] Andrew Hara

https://home.cern/news/news/accelerators/linac-4-reached-its-energy-goal
Last Access: 02/05/2019

[F16] https://www.electronics-tutorials.ws/electromagnetism/hall-effect.html
Last Access: 11/04/2019

[F17] [F18] [F46]

Elytt Energy archive

TABLE REFERENCES

[T1] Elytt Energy archive

PART II: ANNEXES

ANNEX I: Octave script for calculating coil parameters

```


  if(n2>1)
    n2=n2-1;
    w=w(n2);
    S1=2*x*n1*(w+(n1-1)*p);
    S2=2*x*n2*(w+2*(n1)*p+(n2-1)*p);

    if((S1<=S2+10^(-9))&&((S1)>= (S2)-10^(-9))&&(w<=wmax)&&(w>=wmin))% nos interesa que S1 y S2 se cancelen conectadas en antiserie, por lo que han de ser
     i++;
      data(i,1)=x;
      data(i,2)=w;
      data(i,3)=n1;
      data(i,4)=n2;
      data(i,5)=S1;
      data(i,6)=S2;
%creamos una matriz data que almacene los datos que cumplan las condiciones requeridas
    end
    w=0;
    n2=0;
  end



  end
end
%IMPORTANTE CONCEPTO:
%1)Nos interesa que S1=S2, para que la sensibilidad del armónico principal de b1 y b2 se cancele cuando estén conectadas en antiserie
  %-Con b1 y b2 conectadas en antiserie no medimos el armónico principal, ya que este será 0 si S1 y S2 se cancelan,
  %  lo que medimos son las tensiones de los armónicos superiores de la antiserie de (b1 y b2) , la ''tensión compensada'', ya que la sensibilidad S_tot (
%2)Nos interesa que S1 y S2 sean máximas cada una de ellas, para poder medir de la mayor forma posible la tensión del armónico principal de cada una de el
  %-Al medir individualmente b1 y b2 lo que nos interesa es medir la tensión del armónico principal (orden 2) de cada una de ellas, ya que S1 y S2 disminu
[res,pos]=max(data(:,5));  %la fila de datos que nos interesa es la que nos proporciona la máxima sensibilidad S1 y S2

results=data(pos,:);       %obtenemos los parámetros que queremos

%Ahora calculamos las sensibilidades de orden n de las bobinas 1 y 2 en cada una de las capas

i=sqrt(-1);
x=results(1);
w=results(2);
n1=results(3);
n2=results(4);




```

```
 b1_pos=[x+w/2:p:x+w/2+p*(n1-1)];                        %espiras positivas de la bobina 1
 b2_pos=[p*(n1-1)+x+w/2+p:p:p*(n1-1)+x+w/2+p+p*(n2-1)]; %espiras positivas de la bobina 2
 b1_neg=[x-w/2:-p:x-w/2-p*(n1-1)];                       %espiras negativas de la bobina 1
 b2_neg=[x-w/2-p*n1:-p:x-w/2-p*n1-p*(n2-1)];             %espiras negativas de la bobina 2


 function S=sensi(vector1, vector2,layer,n,rf) %esta funcion calcula la sensibilidad
 imagina1=ones(1,length(vector1))*layer*i;
 imagina2=ones(1,length(vector2))*layer*i;
 v1=imagina1+vector1;
 v2=imagina2+vector2;

 S=10^(-3)*real(sum(v1.^n)-sum(v2.^n))/(rf^(n-1));
 endfunction

   for n=1:1:1000
     t=0;
     for a=lmax:-dl:lmin
     t++;
     S1(n,t)=sensi(b1_pos,b1_neg,a,n,rf);  %sensibilidad de orden n en la capa a de la bobina 1
     S2(n,t)=sensi(b2_pos, b2_neg,a,n,rf); %sensibilidad de orden n en la capa a de la bobina 2

     end

     S1_tot(n)=sum(S1(n,:));
     S2_tot(n)=sum(S2(n,:));
   end

   S1_tot=transpose(S1_tot); %Sensibilidad total de orden n de la bobiba 1 (cada fila es el orden n)
   S2_tot=transpose(S2_tot); %Sensibilidad total de orden n de la bobiba 2 (cada fila es el orden n)
   %S1: es una matriz en la que cada columnas corresponde a una capa y cada fila n a la sensibilidad de orden n de la bobina 1
   %S2: es una matriz en la que cada columnas corresponde a una capa y cada fila n a la sensibilidad de orden n de la bobina 2
   S_tot_capa=abs(S1-S2); %sensibilidad total de las bobinas 1 y 2 conectadas en antiserie, cada columna es una capa y cada fila n la sensibilidad
   S_tot=(S1_tot-S2_tot); %sensibilidad total de orden n en metros, cada fila es el orden n
  m=0;
  q=0;
  j=0;
  r=0;

  for i=1:1:nc;

     if(rem(i,2)!=0)
       t2=1;
       m++;

       if(i!=1)

```

```
        j++;
        b2i_a(t2,:)=[-pp*j;x];


        else
        b2i_a(t2,:)=[0;0];


        end
        for v=1:1:n2

         t2++;
         b2i_a(t2,:)=[0+p*(v-1);(x+w/2+(n1+n2-1)*p)-p*(v-1)];
         t2++;
         b2i_a(t2,:)=[(n1+n2)*p+ap1+4*di+li+(n1+n2-2)*p+j12-p*(v-1);(x+w/2+(n1+n2-1)*p)-p*(v-1)];
         t2++;
         b2i_a(t2,:)=[(n1+n2)*p+ap1+4*di+li+(n1+n2-2)*p+j12-p*(v-1);(x-w/2-(n1+n2-1)*p)+p*(v-1)];
         t2++;
         b2i_a(t2,:)=[0+p*(v); (x-w/2-(n1+n2-1)*p)+p*(v-1)];


        end
         if(i!=1)
         b2i_a(2,:)=[-pp*j;b2i_a(2,2)];
         end
        b2i_a(t2,:)=[0+p*(v)+pp*m; (x-w/2-(n1+n2-1)*p)+p*(v-1)];
        b2i_a(t2+1,:)=[0+p*(v)+pp*m; x];


        b2i(:,2*m-1)=b2i_a(:,1); %b2i contendrá los puntos de la bobina b2(exterior) en sus capas impares(cada capa serán las columnas tomadas de dos
        b2i(:,2*m)=b2i_a(:,2);
         t1=1;
         if(i!=1)

         b1i_a(t1,:)=[n2*p+ap1-pp*j;x]; %b1i contendrá los puntos de la bobina b1(interior) en sus capas impares(cada capa serán las columnas tomadas


         else
         b1i_a(t1,:)=[n2*p+ap1;0];


         end
```

```
        for v=1:1:n1
          t1++;
          b1i_a(t1,:)=[n2*p+ap1+p*(v-1);x+w/2+(n1-1)*p-p*(v-1)];
          t1++;
          b1i_a(t1,:)= [n2*p+ap1+n1*p+4*di+li+(n1-1)*p-p*(v-1);x+w/2+(n1-1)*p-p*(v-1)];
          t1++;
          b1i_a(t1,:)= [n2*p+ap1+n1*p+4*di+li+(n1-1)*p-p*(v-1); x-w/2-(n1-1)*p+p*(v-1)];
          t1++;
          b1i_a(t1,:)=[n2*p+ap1+p*(v);x-w/2-(n1-1)*p+p*(v-1)];

        end
           if(i!=1)
            b1i_a(2,:)=[n2*p+ap1-pp*j;b1i_a(2,2)];
           end
          b1i_a(t1,:)=[n2*p+ap1+p*(v)+pp*m;x-w/2-(n1-1)*p+p*(v-1)];
          b1i_a(t1+1,:)=[n2*p+ap1+p*(v)+pp*m;x];
          b1i(:,2*m-1)=b1i_a(:,1);
          b1i(:,2*m)=b1i_a(:,2);

      else


       q++;
       b2p_a(1,1)=b2i(t2+1,2*m-1);
       b2p_a(1,2)=b2i(t2+1,2*m);
       k=t2;
       t2=1;

       for v=n2:-1:1
        t2++;
        b2p_a(t2,:)=[0+p*(v);(x+w/2+(n1+n2-1)*p)-p*(v-1)];
        t2++;
        b2p_a(t2,:)=[(n1+n2)*p+ap1+4*di+li+(n1+n2-2)*p+j12-p*(v-1);(x+w/2+(n1+n2-1)*p)-p*(v-1)];
        t2++;
        b2p_a(t2,:)=[(n1+n2)*p+ap1+4*di+li+(n1+n2-2)*p+j12-p*(v-1);(x-w/2-(n1+n2-1)*p)+p*(v-1)];
        t2++;
        b2p_a(t2,:)=[0+p*(v-1); (x-w/2-(n1+n2-1)*p)+p*(v-1)];

       end
       b2p_a(2,:)=[b2p_a(1,1);b2p_a(2,2)];
       if(i!=nc)
       r++;
       b2p_a(t2,:)=[-pp*r;(x-w/2-(n1+n2-1)*p)+p*(v-1)];
       b2p_a(t2+1,:)=[-pp*r;x];
       else
       b2p_a(t2+1,:)=[0;0];
       end
```

```
    b2p(:,2*q-1)=b2p_a(:,1); %b2p contendrá los puntos de la bobina b2(exterior) en sus capas pares(cada capa serán las columnas tomadas de dos en dos, pe
    b2p(:,2*q)=b2p_a(:,2);
    b1p_a(1,1)=b1i(t1+1,2*m-1); %b1p contendrá los puntos de la bobina b1(interior) en sus capas pares(cada capa serán las columnas tomadas de dos en dos,
    b1p_a(1,2)=b1i(t1+1,2*m);
    t1=1;
    for v=n1:-1:1
      t1++;
      b1p_a(t1,:)=[n2*p+ap1+p*(v);x+w/2+(n1-1)*p-p*(v-1)];
      t1++;
      b1p_a(t1,:)=[n2*p+ap1+n1*p+4*di+li+(n1-1)*p-p*(v-1);x+w/2+(n1-1)*p-p*(v-1)];
      t1++;
      b1p_a(t1,:)=[n2*p+ap1+n1*p+4*di+li+(n1-1)*p-p*(v-1);x-w/2-(n1-1)*p+p*(v-1)];
      t1++;
      b1p_a(t1,:)=[n2*p+ap1+p*(v-1);x-w/2-(n1-1)*p+p*(v-1)];



     end
     b1p_a(2,:)=[b1p_a(1,1);b1p_a(2,2)];
     if(i!=nc)
     b1p_a(t1,:)=[n2*p+ap1-r*pp;x-w/2-(n1-1)*p+p*(v-1)];
     b1p_a(t1+1,:)=[n2*p+ap1-r*pp; x];
     else
     b1p_a(t1+1,:)=[n2*p+ap1;0];
     end
     b1p(:,2*q-1)=b1p_a(:,1);
     b1p(:,2*q)=b1p_a(:,2);


   end
 end

 for i=1:1:nc/2
 plot(b2i(:,2*i-1),b2i(:,2*i));
 hold on;
 plot(b2p(:,2*i-1),b2p(:,2*i));
 hold on
 plot(b1i(:,2*i-1),b1i(:,2*i));
 hold on;
 plot(b1p(:,2*i-1),b1p(:,2*i));
 hold on
 end
```

Annex II: TCL script used for controlling the rotation stage and gather data

```
############################################################################
# TCL script created by Administrator on Tue, 02 Jan 2018 09:51:19 GMT #
############################################################################

# Handy function to display an error and close the connection
proc DisplayErrorAndCloseConnection {socketID code APIName} {
    global tcl_argv
    if {$code == -2} {
        set error_message "$APIName ERROR => -2 : TCP timeout"
    } else {
        if {$code == -108} {
            set error_message "$APIName ERROR => -108 : The TCP/IP connection was closed by an administrator"
        } else {
            set code2 [catch "ErrorStringGet $socketID $code strError"]
            if {$code2 != 0} {
                set error_message "$APIName ERROR => $code - ErrorStringGet ERROR => $code2"
            } else {
                set error_message "$APIName $strError"
            }
        }
    }
    puts stdout $error_message
    set tcl_argv(0) $error_message
    catch "TCP_CloseSocket $socketID"
    return
}

####################
# Program entrypoint
set TimeOut 40
set code 0


### variables interesantes

## definir numero de vueltas
set n11 8
set n12 14
set hz 1
set acc 1000

set vel [expr {$hz * 360}]
## definir angulos en funcion de lo anterior
set deg11 [expr {$n11 * (-360)}]
set deg12 [expr {$n12 * 360}]

```

```
## angulos a los que empieza a muestrear
set samp1start -1
set samp2start 1

## max freq 8 kHz, queremos 1 kHz
set samplingPS 8
set samppling NSamples 40000


### operaciones previas (necesarias en general)

## iniciar la comunicación (necesario)
# Open TCP socket
OpenConnection $TimeOut socketID
if {$socketID == -1} {
    puts stdout "OpenConnection failed => -1"
    return
}

## inicializar el grupo (necesario)

# terminar el grupo si no lo estaba
# Run command: GroupKill(Group1)
set code [catch "GroupKill $socketID Group1"]
if {$code != 0} {
    DisplayErrorAndCloseConnection $socketID $code "GroupKill"
    return
}

#iniciar el grupo
# Run command: GroupInitialize(Group1)
set code [catch "GroupInitialize $socketID Group1"]
if {$code != 0} {
    DisplayErrorAndCloseConnection $socketID $code "GroupInitialize"
    return
}

# buscar el 0
# Run command: GroupHomeSearch(Group1)
set code [catch "GroupHomeSearch $socketID Group1"]
if {$code != 0} {
    DisplayErrorAndCloseConnection $socketID $code "GroupHomeSearch"
    return
}

```

```
# habilitar el movimiento
# Run command: GroupMotionEnable(Group1)
# set code [catch "GroupMotionEnable $socketID Group1"]
if {$code != 0} {
    DisplayErrorAndCloseConnection $socketID $code "GroupMotionEnable"
    return
}



# configurar la toma de datos (leer posicion actual, ADC1 y ADC2)
# Run command: GatheringConfigurationSet(Group1.Pos.CurrentPosition,GPIO2.ADC1,GPIO2.ADC2)
#set code [catch "GatheringConfigurationSet $socketID Group1.Pos.CurrentPosition GPIO2.ADC1 GPIO2.ADC2"]
set code [catch "GatheringConfigurationSet $socketID Group1.Pos.CurrentPosition Group1.Pos.CurrentVelocity GPIO2.ADC1 GPIO2.ADC2"]
if {$code != 0} {
    DisplayErrorAndCloseConnection $socketID $code "GatheringConfigurationSet"
    return
}

# definicion de cuando se lanza el trigger
# Run command: EventExtendedConfigurationTriggerSet(Group1.Pos.WaitForPositionLeftToRight,samp1start,0,0,0)
set code [catch "EventExtendedConfigurationTriggerSet $socketID Group1.Pos.WaitForPositionLeftToRight $samp1start 0 0 0"]
if {$code != 0} {
    DisplayErrorAndCloseConnection $socketID $code "EventExtendedConfigurationTriggerSet"
    return
}

# definicion de que ha de hacer el trigger
# Run command: EventExtendedConfigurationActionSet(GatheringRun,sampplingNSamples,samplingPS,0,0)
set code [catch "EventExtendedConfigurationActionSet $socketID GatheringRun $sampplingNSamples $samplingPS 0 0"]
if {$code != 0} {
    DisplayErrorAndCloseConnection $socketID $code "EventExtendedConfigurationActionSet"
    return
}

# iniciar el trigger
# Run command: EventExtendedStart(int *)
set code [catch "EventExtendedStart $socketID arg1"]
if {$code != 0} {
    DisplayErrorAndCloseConnection $socketID $code "EventExtendedStart"
    return
}

# Run command: PositionerSGammaParametersSet(Group1.Pos,vel,1000,0.005,0.05)
set code [catch "PositionerSGammaParametersSet $socketID Group1.Pos $vel  1000 0.005 0.05"]
if {$code != 0} {
    DisplayErrorAndCloseConnection $socketID $code "PositionerSGammaParametersSet"
    return
}
```

```
# movimiento rotatorio previo
# Run command: GroupMoveAbsolute(Group1,deg11)
set code [catch "GroupMoveAbsolute $socketID Group1 $deg11"]
if {$code != 0} {
    DisplayErrorAndCloseConnection $socketID $code "GroupMoveAbsolute"
    return
}

# movimiento rotatorio largo
# Run command: GroupMoveAbsolute(Group1,deg12)
set code [catch "GroupMoveAbsolute $socketID Group1 $deg12"]
if {$code != 0} {
    DisplayErrorAndCloseConnection $socketID $code "GroupMoveAbsolute"
    return
}

# guardar los datos
# Run command: GatheringStopAndSave()
set code [catch "GatheringStopAndSave $socketID"]
if {$code != 0} {
    DisplayErrorAndCloseConnection $socketID $code "GatheringStopAndSave"
    return
}

# renombrar el archivo
# Run command: FileGatheringRename(clockwise.dat)
set code [catch "FileGatheringRename $socketID clockwise.dat"]
if {$code != 0} {
    DisplayErrorAndCloseConnection $socketID $code "FileGatheringRename"
    return
}



# volver a 0
# Run command: GroupMoveAbsolute(Group1,0)
set code [catch "GroupMoveAbsolute $socketID Group1 0"]
if {$code != 0} {
    DisplayErrorAndCloseConnection $socketID $code "GroupMoveAbsolute"
    return
}

# deshabilitar movimiento (opcional)
# Run command: GroupMotionDisable(Group1)
set code [catch "GroupMotionDisable $socketID Group1"]
if {$code != 0} {
    DisplayErrorAndCloseConnection $socketID $code "GroupMotionEnable"
    return
}
```

```

# cerrar la conexion
# Close TCP socket
TCP_CloseSocket $socketID

```

Annex III: Bill of Materials for amplifier and filter circuit

C	D	E	F	G
Reference	**Value**	**Footprint**	**Manufacturer**	**Part number**
C1, C2, C3, C4, C5, C6	1,5u	Capacitors_SMD:C_0603	TDK	C1608X7R1A155K080AC
C7, C8	10n	Capacitors_SMD:C_0402	KEMET	C0402C103K4RACTU
C10, C9	1u	Capacitors_Tantalum_SMD:CP_Tantalum_Case-A_EIA-3216-18_Hand	KEMET	T494A105K020AT
R11	113	Resistors_SMD:R_0603	WALSIN	WR06X1130FTL
R1, R4	10,7	Resistors_SMD:R_0603	PANASONIC	ERJ3EKF10R7V
R10, R13, R2, R3, R5, R6	1,07k	Resistors_SMD:R_0603	MULTICOMP	MCWR06X1071FTL
R7, R8	499	Resistors_SMD:R_0603	TE CONNECTIVITY	CPF0603B499RE1
R12, R9	100	Resistors_SMD:R_0603	BOURNS	CR0603-JW-101ELF
RV1	1k	Potentiometers:Potentiometer_Trimmer_Bourns_3214W	BOURNS	3214W-1-102E
U1	TSV914	Housings_SSOP:TSSOP-14_4.4x5mm_Pitch0.65mm	TEXAS INSTRUMENTS	OPA4209AIPW
p1, p2	puente	puente	HARWIN	S1621-46R

C	D	E	F	G
Reference	**Value**	**Footprint**	**Manufacturer**	**Part number**
R10, R13	2k	Resistors_SMD:R_0603	TE CONNECTIVITY	CPF0603B2K0E1
RV1	100 ohm	Potentiometers:Potentiometer_Trimmer_Bourns_3214W	Bourns	3214W-1-101E

Annex IV: Matlab script used for data processing and calibration

```
clear all
home
clc
more off
close all

pi=-atan(-1)*4;
d2r=pi/180;
mm=0.001;

% Parametros post-proceso
path='';
files={
        'VUELTASCONVELHORARIO2HZ14V_301C2_FP1R1_EJE_20180321_21.dat'
        'VUELTASCONVELHORARIO2HZ14V_301C2_FP1R3_EJE_20180321_21.dat'
        'VUELTASCONVELHORARIO2HZ14V_301C2_FP1R1_ROLL_20180321_21.dat'

        'VUELTASCONVELHORARIO2HZ14V_301C2_FP1R1_ROLL_20180321_21.dat'
        'VUELTASCONVELHORARIO2HZ14V_301C2_FP1R1_ROLL_20180321_21.dat'
        'VUELTASCONVELHORARIO2HZ14V_301C2_FP2R1_ROLL_20180321_21.dat'


        'VUELTASCONVELHORARIO2HZ14V_302C2_FP1R1_EJE_20180321_22.dat'
        'VUELTASCONVELHORARIO2HZ14V_302C2_FP1R3_EJE_20180321_22.dat'
        'VUELTASCONVELHORARIO2HZ14V_302C2_FP1R1_ROLL_20180321_22.dat'

        'VUELTASCONVELHORARIO2HZ14V_302C2_FP1R1_ROLL_20180321_22.dat'
        'VUELTASCONVELHORARIO2HZ14V_302C2_FP1R1_ROLL_20180321_22.dat'
        'VUELTASCONVELHORARIO2HZ14V_302C2_FP2R1_ROLL_20180321_22.dat'

        'VUELTASCONVELHORARIO2HZ14V_303C2_FP1R1_EJE_20180321_22.dat'
        'VUELTASCONVELHORARIO2HZ14V_303C2_FP1R3_EJE_20180321_22.dat'
        'VUELTASCONVELHORARIO2HZ14V_303C2_FP1R1_ROLL_20180321_22.dat'

        'VUELTASCONVELHORARIO2HZ14V_303C2_FP1R1_ROLL_20180321_22.dat'
        'VUELTASCONVELHORARIO2HZ14V_303C2_FP1R1_ROLL_20180321_22.dat'
        'VUELTASCONVELHORARIO2HZ14V_303C2_FP2R1_ROLL_20180321_22.dat'


        'VUELTASCONVELHORARIO2HZ14V_304C2_FP1R1_EJE_20180321_21,5.dat'
        'VUELTASCONVELHORARIO2HZ14V_304C2_FP1R3_EJE_20180321_21,5.dat'
        'VUELTASCONVELHORARIO2HZ14V_304C2_FP1R1_ROLL_20180321_21,5.dat'

        'VUELTASCONVELHORARIO2HZ14V_304C2_FP1R1_ROLL_20180321_21,5.dat'
        'VUELTASCONVELHORARIO2HZ14V_304C2_FP1R1_ROLL_20180321_21,5.dat'
        'VUELTASCONVELHORARIO2HZ14V_304C2_FP2R1_ROLL_20180321_21,5.dat'

        'VUELTASCONVELHORARIO2HZ14V_305C2_FP1R1_EJE_20180321_22.dat'
        'VUELTASCONVELHORARIO2HZ14V_305C2_FP1R3_EJE_20180321_22.dat'
        'VUELTASCONVELHORARIO2HZ14V_305C2_FP1R1_ROLL_20180321_22.dat'

        'VUELTASCONVELHORARIO2HZ14V_305C2_FP1R1_ROLL_20180321_22.dat'
        'VUELTASCONVELHORARIO2HZ14V_305C2_FP1R1_ROLL_20180321_22.dat'
        'VUELTASCONVELHORARIO2HZ14V_305C2_FP2R1_ROLL_20180321_22.dat'


        'VUELTASCONVELHORARIO2HZ14V_306C2_FP1R1_EJE_20180321_22.dat'
        'VUELTASCONVELHORARIO2HZ14V_306C2_FP1R3_EJE_20180321_22.dat'
        'VUELTASCONVELHORARIO2HZ14V_306C2_FP1R1_ROLL_20180321_22.dat'

        'VUELTASCONVELHORARIO2HZ14V_306C2_FP1R1_ROLL_20180321_22.dat'
        'VUELTASCONVELHORARIO2HZ14V_306C2_FP1R1_ROLL_20180321_22.dat'
        'VUELTASCONVELHORARIO2HZ14V_306C2_FP2R1_ROLL_20180321_22.dat'


        'VUELTASCONVELHORARIO2HZ14V_307C2_FP1R1_EJE_20180321_22.dat'
        'VUELTASCONVELHORARIO2HZ14V_307C2_FP1R3_EJE_20180321_22.dat'
        'VUELTASCONVELHORARIO2HZ14V_307C2_FP1R1_ROLL_20180321_22.dat'

        'VUELTASCONVELHORARIO2HZ14V_307C2_FP1R1_ROLL_20180321_22.dat'
        'VUELTASCONVELHORARIO2HZ14V_307C2_FP1R1_ROLL_20180321_22.dat'
        'VUELTASCONVELHORARIO2HZ14V_307C2_FP2R1_ROLL_20180321_22.dat'


        'VUELTASCONVELHORARIO2HZ14V_308C2_FP1R1_EJE_20180321_24,5.dat'
        'VUELTASCONVELHORARIO2HZ14V_308C2_FP1R3_EJE_20180321_24,5.dat'
        'VUELTASCONVELHORARIO2HZ14V_308C2_FP1R1_ROLL_20180321_24,5.dat'

        'VUELTASCONVELHORARIO2HZ14V_308C2_FP1R1_ROLL_20180321_24,5.dat'
        'VUELTASCONVELHORARIO2HZ14V_308C2_FP1R1_ROLL_20180321_24,5.dat'
        'VUELTASCONVELHORARIO2HZ14V_308C2_FP2R1_ROLL_20180321_24,5.dat'

        'VUELTASCONVELHORARIO2HZ14V_309C2_FP1R1_EJE_20180321_22.dat'
        'VUELTASCONVELHORARIO2HZ14V_309C2_FP1R3_EJE_20180321_22.dat'
        'VUELTASCONVELHORARIO2HZ14V_309C2_FP1R1_ROLL_20180321_22.dat'

        'VUELTASCONVELHORARIO2HZ14V_309C2_FP1R1_ROLL_20180321_22.dat'
        'VUELTASCONVELHORARIO2HZ14V_309C2_FP1R1_ROLL_20180321_22.dat'
        'VUELTASCONVELHORARIO2HZ14V_309C2_FP2R1_ROLL_20180321_22.dat'


        'VUELTASCONVELHORARIO2HZ14V_310C2_FP1R1_EJE_20180321_22.dat'
        'VUELTASCONVELHORARIO2HZ14V_310C2_FP1R3_EJE_20180321_22.dat'
        'VUELTASCONVELHORARIO2HZ14V_310C2_FP1R1_ROLL_20180321_22.dat'

```

```
        'VUELTASCONVELHORARIO2HZ14V_310C2_FP1R1_ROLL_20180321_22.dat'
        'VUELTASCONVELHORARIO2HZ14V_310C2_FP1R1_ROLL_20180321_22.dat'
        'VUELTASCONVELHORARIO2HZ14V_310C2_FP2R1_ROLL_20180321_22.dat'


        'VUELTASCONVELHORARIO2HZ14V_311C2_FP1R1_EJE_20180321_22.dat'
        'VUELTASCONVELHORARIO2HZ14V_311C2_FP1R3_EJE_20180321_22.dat'
        'VUELTASCONVELHORARIO2HZ14V_311C2_FP1R1_ROLL_20180321_22.dat'

        'VUELTASCONVELHORARIO2HZ14V_311C2_FP1R1_ROLL_20180321_22.dat'
        'VUELTASCONVELHORARIO2HZ14V_311C2_FP1R1_ROLL_20180321_22.dat'
        'VUELTASCONVELHORARIO2HZ14V_311C2_FP2R1_ROLL_20180321_22.dat'


        'VUELTASCONVELHORARIO2HZ14V_312C2_FP1R1_EJE_20180321_22.dat'
        'VUELTASCONVELHORARIO2HZ14V_312C2_FP1R3_EJE_20180321_22.dat'
        'VUELTASCONVELHORARIO2HZ14V_312C2_FP1R1_ROLL_20180321_22.dat'

        'VUELTASCONVELHORARIO2HZ14V_312C2_FP1R1_ROLL_20180321_22.dat'
        'VUELTASCONVELHORARIO2HZ14V_312C2_FP1R1_ROLL_20180321_22.dat'
        'VUELTASCONVELHORARIO2HZ14V_312C2_FP2R1_ROLL_20180321_22.dat'


        'VUELTASCONVELHORARIO2HZ14V_313C2_FP1R1_EJE_20180321_22.dat'
        'VUELTASCONVELHORARIO2HZ14V_313C2_FP1R3_EJE_20180321_22.dat'
        'VUELTASCONVELHORARIO2HZ14V_313C2_FP1R1_ROLL_20180321_22.dat'

        'VUELTASCONVELHORARIO2HZ14V_313C2_FP1R1_ROLL_20180321_22.dat'
        'VUELTASCONVELHORARIO2HZ14V_313C2_FP1R1_ROLL_20180321_22.dat'
        'VUELTASCONVELHORARIO2HZ14V_313C2_FP2R1_ROLL_20180321_22.dat'

        'VUELTASCONVELHORARIO2HZ14V_314C2_FP1R1_EJE_20180321_23.dat'
        'VUELTASCONVELHORARIO2HZ14V_314C2_FP1R3_EJE_20180321_23.dat'
        'VUELTASCONVELHORARIO2HZ14V_314C2_FP1R1_ROLL_20180321_23.dat'

        'VUELTASCONVELHORARIO2HZ14V_314C2_FP1R1_ROLL_20180321_23.dat'
        'VUELTASCONVELHORARIO2HZ14V_314C2_FP1R1_ROLL_20180321_23.dat'
        'VUELTASCONVELHORARIO2HZ14V_314C2_FP2R1_ROLL_20180321_23.dat'


        'VUELTASCONVELHORARIO2HZ14V_315C2_FP1R1_EJE_20180321_23.dat'
        'VUELTASCONVELHORARIO2HZ14V_315C2_FP1R3_EJE_20180321_23.dat'
        'VUELTASCONVELHORARIO2HZ14V_315C2_FP1R1_ROLL_20180321_23.dat'

        'VUELTASCONVELHORARIO2HZ14V_315C2_FP1R1_ROLL_20180321_23.dat'
        'VUELTASCONVELHORARIO2HZ14V_315C2_FP1R1_ROLL_20180321_23.dat'
        'VUELTASCONVELHORARIO2HZ14V_315C2_FP2R1_ROLL_20180321_23.dat'
%
```

```

        };
n_post=length(files)/3;
n_ciclo=8                       % Numero de ciclos
Ciclo=[504:1:503+500*n_ciclo];  % Seleccion de puntos para 2Hz
%Ciclo=[1005:1:1004+1000*n_ciclo];  % Seleccion de puntos para 1 Hz
PMQS=[301  301  302  302 303  303  304  304  305  305  306  306  307  307  308  308  309  309  310  310  311  311  312  312  313  313  314  314  315  315]
TEMP=[21   21   22   22  22   22   21.5 21.5 22   22   22   22   22   22   24.5 24.5 22   22   22   22   22   22   22   22   22   22   23   23   23   23];
Temp_corr=30                    % Temperatura a la que corrijo
Ft=-0.050889                    % Factor correccion temperatura en %
Fcal=0%(2.14808738246317/2.16218788797306-1)*100            % Factor de calibracion del IG en %
theta_CORR=-1.5239+0.26597-0.021-0.00997+pi/2       % Correccion de angulo theta en rad
coeff_compensada=0.09623228754  % Coeficiente amplificacion compensada

% PARAMETROS MEDIDA
%rref=9.7*mm           % Reference radius
rref=7.5*mm           % Reference radius
n_B=100               % Coefficientes calculados de la bobina
% PARAMETROS PCB
errorX=0*mm            % error al posicionar la espira respecto al PMQ
errorY=0.0*mm            % error al posicionar la espira respecto al PMQ
dist_l=0.5*mm;         % Distancia entre capa y capa (entre su plano medio)
dist_t=0.3*mm;         % Distancia entre turn y turn (entre su plano medio)
espesor=0.15*mm;       % Espesor path
Ampli_B1=100;          % Amplificacion bobina1
Ampli_B2=100;          % Amplificacion bobina2
Ampli_comp=100;        % Amplificacion comp

%%%%%%%%%%%%%%%%%%%%%%%%%%%%%%%%%%%%%%%%%%%%%%%%%%%%%%%%%%%%%%%%%%%%%%%%%%%%%%%%
%%%%%%%%%%%%%%%%%%%%%%%%%%%%%%%%%%%%%%%%%%%%%%%%%%%%%%%%%%%%%%%%%%%%%%%%%%%%%%%%
%%%%%%%%%%%%%%%%%%%%%%%%%%%%%%%%%%%%%%%%%%%%%%%%%%%%%%%%%%%%%%%%%%%%%%%%%%%%%%%%
%%%%%%%%%%%%%%%%%%%%%%%%%%%%%%%%%%%%%%%%%%%%%%%%%%%%%%%%%%%%%%%%%%%%%%%%%%%%%%%%
%% Creacion bobina 1   _B1
% Creo lista de puntos X,Y
nlayers_B1=4;                   % Numero de capas
nturns_B1=12;                   % Numero de vueltas por capa
x0p_B1=4.39*mm;                 % X0 de la primera espira positiva, no considera error
x0n_B1=2.29*mm;                 % X0 de la primera espira negativa, no considera error
Xmean_B1=x0n_B1*0.5+x0p_B1*0.5; % Centro de la bobina


if mod(nlayers_B1,2)==0
  y0_B1=dist_l/2-dist_l*(nlayers_B1/2);  % Y0 de la primera espira mas abajo, no considera error
elseif mod(nlayers_B1,2)==1
  y0_B1=0-dist_l*(nlayers_B1/2-0.5);     % Y0 de la primera espira mas abajo, no considera error
end

XY_B1=[];
for l=1:nlayers_B1
```

```
for t=1:nturns_B1
    XY_B1=[XY_B1
            x0p_B1+(t-1)*dist_t+errorX y0_B1+(l-1)*dist_l+errorY
            x0n_B1-(t-1)*dist_t+errorX y0_B1+(l-1)*dist_l+errorY];
end
end

NTB1=size(XY_B1,1);                              % Numero de puntos en bobina 1
R_B1=(XY_B1(:,1).^2+XY_B1(:,2).^2).^0.5; % Radio en bobina 1 en m
signo_B1=sign(XY_B1(:,1)-Xmean_B1);       % Segun la espira vaya + o vuelva -
phi_B1=atan2(XY_B1(:,2),XY_B1(:,1));      % phi en bobina 1 en rad

%scatter(XY_B1(:,1),XY_B1(:,2))

%%%%%%%%%%%%%%%%%%%%%%%%%%%%%%%%%%%%%%%%%%%%%%%%%%%%%%%%%%%%%%%%%%%%%%%%%%%%%%%%
%%%%%%%%%%%%%%%%%%%%%%%%%%%%%%%%%%%%%%%%%%%%%%%%%%%%%%%%%%%%%%%%%%%%%%%%%%%%%%%%
%%%%%%%%%%%%%%%%%%%%%%%%%%%%%%%%%%%%%%%%%%%%%%%%%%%%%%%%%%%%%%%%%%%%%%%%%%%%%%%%
%%%%%%%%%%%%%%%%%%%%%%%%%%%%%%%%%%%%%%%%%%%%%%%%%%%%%%%%%%%%%%%%%%%%%%%%%%%%%%%%
%% Creacion bobina 2   _B2
%  Creo lista de puntos X,Y
nlayers_B2=4;                    % Numero de capas
nturns_B2=6;                     % Numero de vueltas por capa
x0p_B2=7.99*mm;                  % X0 de la primera espira positiva, no considera error
x0n_B2=-1.31*mm;                 % X0 de la primera espira negativa, no considera error
Xmean_B2=x0n_B1*0.5+x0p_B1*0.5; % Centro de la bobina

if mod(nlayers_B2,2)==0
  y0_B2=dist_l/2-dist_l*(nlayers_B2/2);% Y0 de la primera espira mas abajo, no considera error
elseif mod(nlayers_B2,2)==1
  y0_B2=0-dist_l*(nlayers_B2/2-0.5);      % Y0 de la primera espira mas abajo, no considera error
end

XY_B2=[];
for l=1:nlayers_B2
for t=1:nturns_B2
    XY_B2=[XY_B2
            x0p_B2+(t-1)*dist_t+errorX y0_B2+(l-1)*dist_l+errorY
            x0n_B2-(t-1)*dist_t+errorX y0_B2+(l-1)*dist_l+errorY];
end
end

NTB2=size(XY_B2,1);                               % Numero de puntos en bobina 1
R_B2=(XY_B2(:,1).^2+XY_B2(:,2).^2).^0.5;  % Radio en bobina 1 en m
signo_B2=sign(XY_B2(:,1)-Xmean_B2);        % Segun la espira vaya + o vuelva -
phi_B2=atan2(XY_B2(:,2),XY_B2(:,1));       % phi en bobina 1 en rad

%hold on
%scatter(XY_B2(:,1),XY_B2(:,2))



%%%%%%%%%%%%%%%%%%%%%%%%%%%%%%%%%%%%%%%%%%%%%%%%%%%%%%%%%%%%%%%%%%%%%%%%%%%%%%%%
%%%%%%%%%%%%%%%%%%%%%%%%%%%%%%%%%%%%%%%%%%%%%%%%%%%%%%%%%%%%%%%%%%%%%%%%%%%%%%%%
%%%%%%%%%%%%%%%%%%%%%%%%%%%%%%%%%%%%%%%%%%%%%%%%%%%%%%%%%%%%%%%%%%%%%%%%%%%%%%%%
%%%%%%%%%%%%%%%%%%%%%%%%%%%%%%%%%%%%%%%%%%%%%%%%%%%%%%%%%%%%%%%%%%%%%%%%%%%%%%%%
% DIBUJO LAS DOS BOBINAS
%scatter(XY_B2(:,1),XY_B2(:,2))
%hold on
%scatter(XY_B1(:,1),XY_B1(:,2))


%%%%%%%%%%%%%%%%%%%%%%%%%%%%%%%%%%%%%%%%%%%%%%%%%%%%%%%%%%%%%%%%%%%%%%%%%%%%%%%%
%%%%%%%%%%%%%%%%%%%%%%%%%%%%%%%%%%%%%%%%%%%%%%%%%%%%%%%%%%%%%%%%%%%%%%%%%%%%%%%%
%%%%%%%%%%%%%%%%%%%%%%%%%%%%%%%%%%%%%%%%%%%%%%%%%%%%%%%%%%%%%%%%%%%%%%%%%%%%%%%%
%%%%%%%%%%%%%%%%%%%%%%%%%%%%%%%%%%%%%%%%%%%%%%%%%%%%%%%%%%%%%%%%%%%%%%%%%%%%%%%%


% Calculo coefficientes de cada harmonico de bobina 1
for n=1:n_B
  COSN_B1(n,1)=sum(signo_B1.*cos(n*phi_B1).*((R_B1/rref).^n));
end
for n=1:n_B
  SINN_B1(n,1)=sum(signo_B1.*sin(n*phi_B1).*((R_B1/rref).^n));
end

for n=1:n_B
MN_B1(:,:,n)=[COSN_B1(n) SINN_B1(n)
              SINN_B1(n) -COSN_B1(n)];
end


% Calculo coefficientes de cada harmonico de bobina 2
for n=1:n_B
  COSN_B2(n,1)=sum(signo_B2.*cos(n*phi_B2).*((R_B2/rref).^n));
end
for n=1:n_B
  SINN_B2(n,1)=sum(signo_B2.*sin(n*phi_B2).*((R_B2/rref).^n));
end

for n=1:n_B
MN_B2(:,:,n)=[COSN_B2(n) SINN_B2(n)
              SINN_B2(n) -COSN_B2(n)];
end

```

```
% Calculo matriz compensada
MN_comp=MN_B2-MN_B1;

% Multiplico por amplificadores
MN_B2=MN_B2*Ampli_B2;
MN_B1=MN_B1*Ampli_B1;
MN_comp=MN_comp*Ampli_comp;

%%%%%%%%%%%%%%%%%%%%%%%%%%%%%%%%%%%%%%%%%%%%%%%%%%%%%%%%%%%%%%%%%%%%%%%%%%%%%%%%
%%%%%%%%%%%%%%%%%%%%%%%%%%%%%%%%%%%%%%%%%%%%%%%%%%%%%%%%%%%%%%%%%%%%%%%%%%%%%%%%
%%%%%%%%%%%%%%%%%%%%%%%%%%%%%%%%%%%%%%%%%%%%%%%%%%%%%%%%%%%%%%%%%%%%%%%%%%%%%%%%
%%%%%%%%%%%%%%%%%%%%%%%%%%%%%%%%%%%%%%%%%%%%%%%%%%%%%%%%%%%%%%%%%%%%%%%%%%%%%%%%
%% POST-PROCESO MEDIDAS
for P=1:n_post
for f=1:3
  complete_file1=strcat(path,files{(P-1)*3+f});
  clockwise=dlmread(complete_file1);
  phi_med=clockwise(Ciclo,1)*d2r;
  w_med=clockwise(Ciclo,2)*d2r;
  sig_B2=clockwise(Ciclo,3);
  sig_comp=clockwise(Ciclo,4);
  Npoints=length(phi_med);

  %%%%%%%%%%%%%%%%%%%%%%%%%%%%%%%%%%%%%%%%%%%%%%%%%%%%%%%%%%%%%%%%%%%%%%%%%%%%%%
  % PROCESO BOBINA 2
  %%%%%%%%%%%%%%%%%%%%%%%%%%%%%%%%%%%%%%%%%%%%%%%%%%%%%%%%%%%%%%%%%%%%%%%%%%%%%%
  % DFT
  lambda_sig_B2=fft(sig_B2./w_med);
  lambda_sig_B2(round(Npoints/2)+1:end)=[];
  lambda_sig_B2(1)=[];
  Rn_sig_B2=real(lambda_sig_B2)*2/Npoints;
  Tn_sig_B2=-imag(lambda_sig_B2)*2/Npoints;
  Rn_sig_B2=Rn_sig_B2([n_ciclo:n_ciclo:length(Rn_sig_B2)]);
  Tn_sig_B2=Tn_sig_B2([n_ciclo:n_ciclo:length(Tn_sig_B2)]);

  % Calculo coeficientes Bn, An
  for n=1:n_B
    SOLUCION=inv(MN_B2(:,:,n))*[Tn_sig_B2(n) Rn_sig_B2(n)]'/rref;
    Bn_B2(n,1)=SOLUCION(1);
    An_B2(n,1)=SOLUCION(2);
  end
  Cn_B2=(An_B2.^2+Bn_B2.^2).^0.5;
%  Bmain_B2=An_B2(2)*sin(2*theta_CORR)+Bn_B2(2)*cos(2*theta_CORR);
  Bmain_B2=Cn_B2(2);
  IG(:,f,P)=Bmain_B2/rref;

```

```
  % Calculo coeficientes bn, an, incluyen la correccion de angulo
  numero_harm=[1:1:n_B]';
  bn_B2(:,f,P)=Bn_B2/Bmain_B2*1e4.*cos(numero_harm*theta_CORR)+An_B2/Bmain_B2*1e4.*sin(numero_harm*theta_CORR);
  an_B2(:,f,P)=-Bn_B2/Bmain_B2*1e4.*sin(numero_harm*theta_CORR)+An_B2/Bmain_B2*1e4.*cos(numero_harm*theta_CORR);
  cn_B2(:,f,P)=(an_B2(:,f,P).^2+bn_B2(:,f,P).^2).^0.5;

  % Para que dibujar harmonicos en pantalla
  dibuja=[1:1:18]';
  [dibuja an_B2(dibuja,f,P) bn_B2(dibuja,f,P) cn_B2(dibuja,f,P)];

  %%%%%%%%%%%%%%%%%%%%%%%%%%%%%%%%%%%%%%%%%%%%%%%%%%%%%%%%%%%%%%%%%%%%%%%%%%%%%%
  % PROCESO BOBINA COMPENSADA
  %%%%%%%%%%%%%%%%%%%%%%%%%%%%%%%%%%%%%%%%%%%%%%%%%%%%%%%%%%%%%%%%%%%%%%%%%%%%%%
  % DFT
  lambda_sig_comp=fft(sig_comp./w_med);
  lambda_sig_comp(round(Npoints/2)+1:end)=[];
  lambda_sig_comp(1)=[];
  Rn_sig_comp=real(lambda_sig_comp)*2/Npoints;
  Tn_sig_comp=-imag(lambda_sig_comp)*2/Npoints;
  Rn_sig_comp=Rn_sig_comp([n_ciclo:n_ciclo:length(Rn_sig_comp)]);
  Tn_sig_comp=Tn_sig_comp([n_ciclo:n_ciclo:length(Tn_sig_comp)]);

  % Calculo coeficientes Bn, An
  for n=1:n_B
    SOLUCION=inv(MN_comp(:,:,n))*[Tn_sig_comp(n) Rn_sig_comp(n)]'/rref;
    Bn_comp(n,1)=SOLUCION(1);
    An_comp(n,1)=SOLUCION(2);
  end
  % Calculo coeficientes bn, an, incluyen la correccion de angulo
  Cn_comp=(An_comp.^2+Bn_comp.^2).^0.5;
  % No puedo normalizar con B2 porque esta cancelado aposta
  % Normalizo para obtener el mismo c3 en ambos casos
  numero_harm=[1:1:n_B]';
  coeff_amplificacion=coeff_compensada/Bmain_B2*1e4;
  an_comp(:,f,P)=An_comp*coeff_amplificacion.*cos(numero_harm*theta_CORR)-Bn_comp*coeff_amplificacion.*sin(numero_harm*theta_CORR);
  bn_comp(:,f,P)=An_comp*coeff_amplificacion.*sin(numero_harm*theta_CORR)+Bn_comp*coeff_amplificacion.*cos(numero_harm*theta_CORR);
  cn_comp(:,f,P)=abs(Cn_comp*coeff_amplificacion);

  % Para que dibujar harmonicos en pantalla
  dibuja=[3:1:18]';
  [dibuja an_comp(dibuja,f,P) bn_comp(dibuja,f,P) cn_comp(dibuja,f,P)];

end
  %%%%%%%%%%%%%%%%%%%%%%%%%%%%%%%%%%%%%%%%%%%%%%%%%%%%%%%%%%%%%%%%%%%%%%%%%%%%%%
  %% CALCULO OUTPUT DE DATOS
  %%%%%%%%%%%%%%%%%%%%%%%%%%%%%%%%%%%%%%%%%%%%%%%%%%%%%%%%%%%%%%%%%%%%%%%%%%%%%%

```

```
    %% EJE
    DeltaX_POST(P,:)=-bn_B2(1,:,P)./bn_B2(2,:,P)*rref;
    DeltaY_POST(P,:)=an_B2(1,:,P)./bn_B2(2,:,P)*rref;
    DELTAX_PMQ(P)=(DeltaX_POST(P,1)-DeltaX_POST(P,2))/2;
    DELTAY_PMQ(P)=(DeltaY_POST(P,1)-DeltaY_POST(P,2))/2;
    EJE_PMQ(P)=(DELTAX_PMQ(P)^2+DELTAY_PMQ(P)^2)^0.5;
    %% IG
    Factor_temp=(1+(Temp_corr-TEMP(P))*(Ft)/100);
    Factor_CAL=(1+Fcal/100);
    IG_corrected(P)=Factor_temp*Factor_CAL*IG(1,1,P);
    %% Harmonicos
    bn(:,P)=bn_comp(:,1,P);
    an(:,P)=an_comp(:,1,P);
    cn(:,P)=cn_comp(:,1,P);
    %% ROLL
    theta_1(:,P)=an_B2(2,1,P)/bn_B2(2,1,P)/2;
    theta_2(:,P)=an_B2(2,3,P)/bn_B2(2,3,P)/2;

end

    % VER EJES
    [PMQS(1:n_post)' EJE_PMQ'*1e6]
    [PMQS(1:n_post)' theta_1'*1e3 theta_2'*1e3]

%vectorIG=[2.1481 2.9972 1.5896]
%errorIG=(IG_corrected-vectorIG)./vectorIG*100
%%        101     0.32367     0.52867     0.42617
```

Annex V: Measurement results of Tank 3

Hall probe													
PMQ S/N	Δx (μm)	Δy (μm)	Δθ1 (mrad)	Δθ2 (mrad)	IG (T) at 30°C	Nominal IG at 30°C	Error in IG %	a3	a4	b3	b4	c3	c4
301	-7,07	39,88	0,76	0,70	1,5896	1,5896	0,00	0,0	-4,2	-10,8	-18,1	10,8	18,6
302	2,18	1,50	-0,09	-0,10	1,5156	1,5200	-0,29	-17,7	-7,1	-1,3	2,9	17,7	7,7
303	-5,76	-49,22	0,08	0,29	1,5484	1,5424	0,39	-54,8	-3,0	6,5	-1,7	55,2	3,4
304	-22,72	8,12	0,17	0,08	1,5486	1,5488	-0,01	-0,2	16,4	-7,2	-2,1	7,2	16,5
305	38,85	0,19	-1,47	-1,19	1,5339	1,5344	-0,03	-15,2	-19,0	44,6	-15,3	47,2	24,3
306	17,28	0,86	1,64	1,39	1,5264	1,5216	0,32	7,4	2,4	9,1	-3,7	11,7	4,4
307	2,32	-22,01	0,56	0,76	1,5075	1,5072	0,02	19,8	11,9	-8,9	1,4	21,7	12,0
308	5,01	-1,73	1,57	1,50	1,4957	1,4944	0,09	13,0	-18,4	-0,2	-13,5	13,0	22,8
309	25,40	-0,18	0,37	0,61	1,4793	1,4816	-0,16	-4,2	-18,7	11,9	3,1	12,6	19,0
310	23,88	28,15	0,43	0,66	1,4758	1,4696	0,42	3,2	14,0	12,6	15,5	13,0	20,9
311	-15,46	45,99	0,60	0,68	1,4542	1,4560	-0,12	15,6	-11,2	-9,8	4,8	18,4	12,2
312	-6,96	25,88	-0,99	-0,82	1,4516	1,4456	0,41	19,4	6,4	-9,1	-11,8	21,4	13,5
313	-37,09	33,39	-1,49	-1,28	1,4443	1,4472	-0,20	23,9	-20,8	-43,3	-25,5	49,4	32,9
314	38,59	-8,03	1,66	1,93	1,4479	1,4432	0,33	-4,8	-14,2	8,9	-19,6	10,1	24,2
315	30,38	34,58	0,14	0,30	1,3836	1,3776	0,44	-15,2	4,3	7,0	0,1	16,7	4,3

Rotating coil													
PMQ S/N	Δx (μm)	Δy (μm)	Δθ1 (mrad)	Δθ2 (mrad)	IG (T) at 30°C	Nominal IG at 30°C	Error in IG %	a3	a4	b3	b4	c3	c4
301	14,49	34,68	-0,56	1,36	1,5887	1,5896	-0,06	-3,7	11,0	13,2	15,5	13,7	19,1
302	-4,75	24,82	0,53	-0,05	1,5153	1,5200	-0,31	-1,0	7,4	1,1	-8,0	1,4	10,9
303	13,69	-46,21	0,27	0,47	1,5487	1,5424	0,41	34,2	5,6	-14,9	-1,7	37,3	5,8
304	-11,56	12,17	0,14	-0,04	1,5510	1,5488	0,14	-0,2	-13,4	6,2	1,8	6,2	13,5
305	64,95	3,05	-1,42	-1,23	1,5338	1,5344	-0,04	15,0	23,2	-50,9	9,6	53,1	25,1
306	22,24	-2,72	1,55	0,51	1,5272	1,5216	0,37	-0,7	0,3	-9,0	2,3	9,0	2,3
307	-9,22	-28,62	0,63	0,81	1,5096	1,5072	0,16	-10,1	-10,0	13,7	0,2	17,0	10,0
308	31,05	-8,63	1,66	1,91	1,4951	1,4944	0,05	-4,4	25,2	-1,1	5,9	4,6	25,8
309	19,68	-1,95	0,42	0,44	1,4796	1,4816	-0,13	-2,4	18,5	-12,8	-11,5	13,0	21,8
310	47,13	46,81	0,34	0,52	1,4750	1,4696	0,37	-2,1	-14,0	-12,9	-11,0	13,0	17,8
311	-3,87	59,96	0,91	0,91	1,4573	1,4560	0,09	-16,3	12,6	12,1	-9,4	20,3	15,7
312	2,41	30,21	-1,19	-1,04	1,4519	1,4456	0,44	-21,6	-1,9	16,5	10,3	27,2	10,5
313	-71,10	50,82	-1,25	-1,52	1,4452	1,4472	-0,14	-13,2	29,1	46,7	17,1	48,5	33,8
314	35,69	-18,19	1,90	2,19	1,4477	1,4432	0,31	2,3	20,5	-10,0	13,7	10,2	24,6
315	24,10	41,63	0,19	0,09	1,3838	1,3776	0,45	8,4	-3,4	-8,8	-4,3	12,1	5,5

an with rotating coil								
PMQs	an3	an4	an5	an6	an7	an8	an9	an10
301	-3,65	11,03	-12,15	-3,12	1,57	1,34	1,54	-6,61
302	-0,97	7,41	8,04	0,57	1,62	0,72	1,17	-5,92
303	34,24	5,59	-2,57	-9,85	-0,12	-0,54	2,01	-6,18
304	-0,22	-13,42	-2,42	0,08	-0,79	0,52	1,15	-6,41
305	14,98	23,20	-5,49	0,18	0,93	1,41	1,10	-6,21
306	-0,71	0,26	-1,30	2,33	-0,67	0,76	1,07	-6,13
307	-10,13	-9,99	-0,33	-9,58	-1,59	0,79	2,08	-5,96
308	-4,43	25,15	4,69	-0,69	1,18	0,68	1,45	-5,91
309	-2,35	18,51	0,90	-2,23	0,12	1,38	1,11	-5,65
310	-2,08	-14,02	-11,94	1,79	-0,10	0,26	1,03	-5,69
311	-16,27	12,63	-0,29	2,41	-1,05	1,49	1,02	-5,54
312	-21,57	-1,86	-11,59	-7,08	-1,09	1,22	1,11	-5,41
313	-13,21	29,13	6,06	2,46	0,49	0,05	0,54	-5,44
314	2,28	20,45	0,88	0,16	-0,34	-0,15	1,59	-5,51
315	8,37	-3,40	6,59	3,21	0,81	0,26	0,75	-5,05

bn with rotating coil								
PMQs	bn3	bn4	bn5	bn6	bn7	bn8	bn9	bn10
301	13,19	15,54	-3,06	-6,91	2,55	-0,73	-1,83	-12,51
302	1,06	-7,97	-6,43	-8,63	0,38	-1,72	-1,86	-11,28
303	-14,89	-1,73	-3,27	-6,01	0,60	0,18	-1,66	-11,96
304	6,19	1,81	-0,77	-3,73	0,49	-0,32	-1,80	-11,95
305	-50,90	9,60	-2,74	-9,12	-1,23	-1,24	-1,31	-11,63
306	-8,97	2,32	4,98	-5,26	-0,94	-0,45	-1,69	-11,58
307	13,68	0,16	-1,04	-6,22	2,58	0,07	-2,11	-11,30
308	-1,12	5,88	-4,87	-7,93	-0,13	-0,57	-1,59	-10,99
309	-12,81	-11,53	-2,37	-2,20	-0,20	-0,73	-1,95	-10,88
310	-12,86	-10,98	3,02	-2,30	0,07	-0,49	-1,16	-10,81
311	12,09	-9,37	10,02	-6,00	-0,94	-0,62	-1,66	-10,50
312	16,53	10,30	3,40	-4,04	-0,85	-0,87	-1,43	-10,45
313	46,71	17,13	6,03	-6,64	-0,24	-0,21	-2,08	-10,32
314	-9,98	13,72	4,39	-8,46	-0,83	-0,72	-1,71	-10,37
315	-8,79	-4,33	-3,24	-4,99	-0,46	-0,08	-1,57	-9,40

cn with rotating coil								
PMQs	cn3	cn4	cn5	cn6	cn7	cn8	cn9	cn10
301	13,69	19,05	12,53	7,59	2,99	1,53	2,39	14,15
302	1,44	10,88	10,30	8,65	1,67	1,87	2,20	12,74
303	37,34	5,85	4,16	11,54	0,62	0,57	2,61	13,46
304	6,20	13,54	2,54	3,73	0,94	0,61	2,13	13,56
305	53,06	25,10	6,14	9,12	1,54	1,88	1,71	13,19
306	9,00	2,33	5,15	5,75	1,15	0,88	1,99	13,11
307	17,02	9,99	1,10	11,43	3,04	0,80	2,96	12,78
308	4,57	25,83	6,76	7,96	1,19	0,89	2,15	12,48
309	13,02	21,80	2,53	3,14	0,24	1,56	2,24	12,26
310	13,02	17,81	12,32	2,92	0,12	0,55	1,55	12,22
311	20,27	15,73	10,02	6,47	1,41	1,61	1,95	11,87
312	27,17	10,47	12,08	8,15	1,38	1,50	1,81	11,77
313	48,54	33,79	8,55	7,08	0,54	0,22	2,15	11,67
314	10,24	24,62	4,48	8,46	0,89	0,73	2,33	11,74
315	12,13	5,51	7,34	5,93	0,93	0,27	1,74	10,67

Annex VI: Measurement results of Tank 4

PMQ S/N	Δx (µm)	Δy (µm)	Δθ1 (mrad)	Δθ2 (mrad)	IG (T) at 30°C	Nominal IG at 30°C	Error in IG %	a3	a4	b3	b4	c3	c4
401	43,57	-2,93	-1,44	0,50	1,3725	1,3736	-0,08	4,1	-6,6	44,2	-3,3	44,4	7,4
402	30,04	-20,39	-1,05	-1,02	1,3862	1,3864	-0,02	-10,4	1,1	-0,9	-20,0	10,5	20,0
403	-32,62	29,66	0,40	0,34	1,3878	1,3824	0,39	29,4	25,9	-19,0	-21,2	35,0	33,5
404	43,49	-21,74	-0,62	-0,89	1,3576	1,3584	-0,06	-22,2	-4,8	-3,0	3,2	22,4	5,8
405	6,96	-16,30	0,04	0,33	1,3495	1,348	0,11	-22,5	19,1	0,5	-11,2	22,5	22,1
406	-19,93	31,10	-1,17	-0,34	1,3416	1,3376	0,30	47,8	-8,3	-16,7	-15,2	50,6	17,3
407	-11,49	-8,09	-1,10	-1,04	1,3288	1,328	0,06	-12,3	-3,0	-19,3	-4,5	22,9	5,5
408	-12,65	-19,49	1,23	1,53	1,3160	1,3176	-0,12	-11,1	9,9	-12,1	3,5	16,4	10,5
409	27,49	-29,50	-0,59	-0,02	1,3081	1,308	0,01	-22,3	-1,5	31,7	9,1	38,8	9,3
410	22,39	-36,03	1,46	1,71	1,3000	1,2984	0,12	-11,2	3,4	12,4	11,4	16,7	11,9
411	-30,09	-18,65	0,26	0,19	1,3077	1,3032	0,35	-7,3	-7,9	-15,2	0,8	16,9	8,0
412	-10,82	0,41	-0,70	-1,10	1,3125	1,3096	0,22	11,0	-6,4	-1,8	-16,8	11,1	18,0
413	-25,80	13,09	1,66	1,13	1,2797	1,2824	-0,21	11,9	-12,5	-17,4	-13,5	21,1	18,4

DOCUMENT 2

DIAGRAMS

LIST OF DIAGRAMS

PART I: BEDPLATE DIAGRAMS

PART I: BEDPLATE DIAGRAMS

DIAGRAM 1: BASE

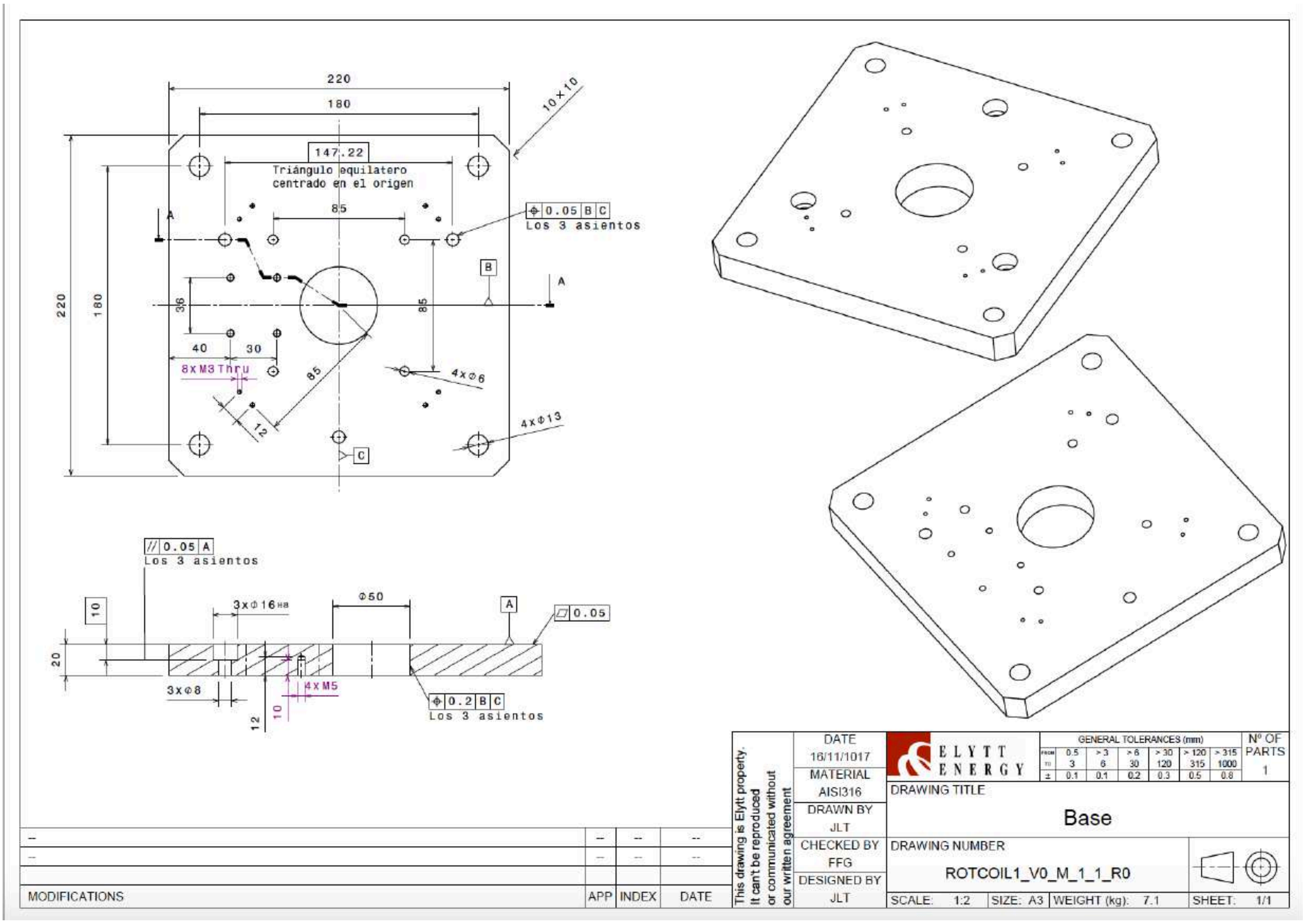

DIAGRAM 2: SUPERIOR PLATE

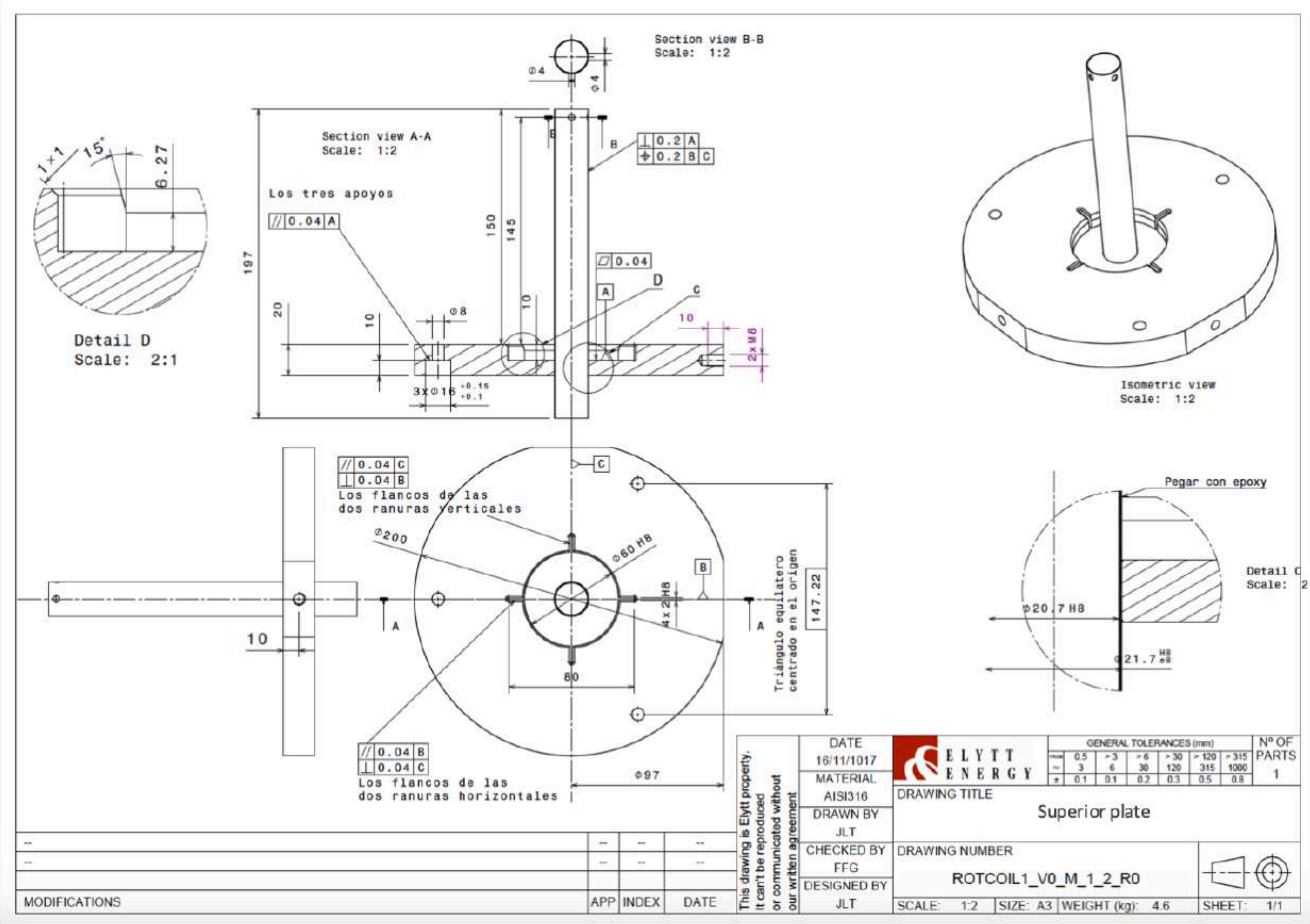

DIAGRAM 3: COLUMN

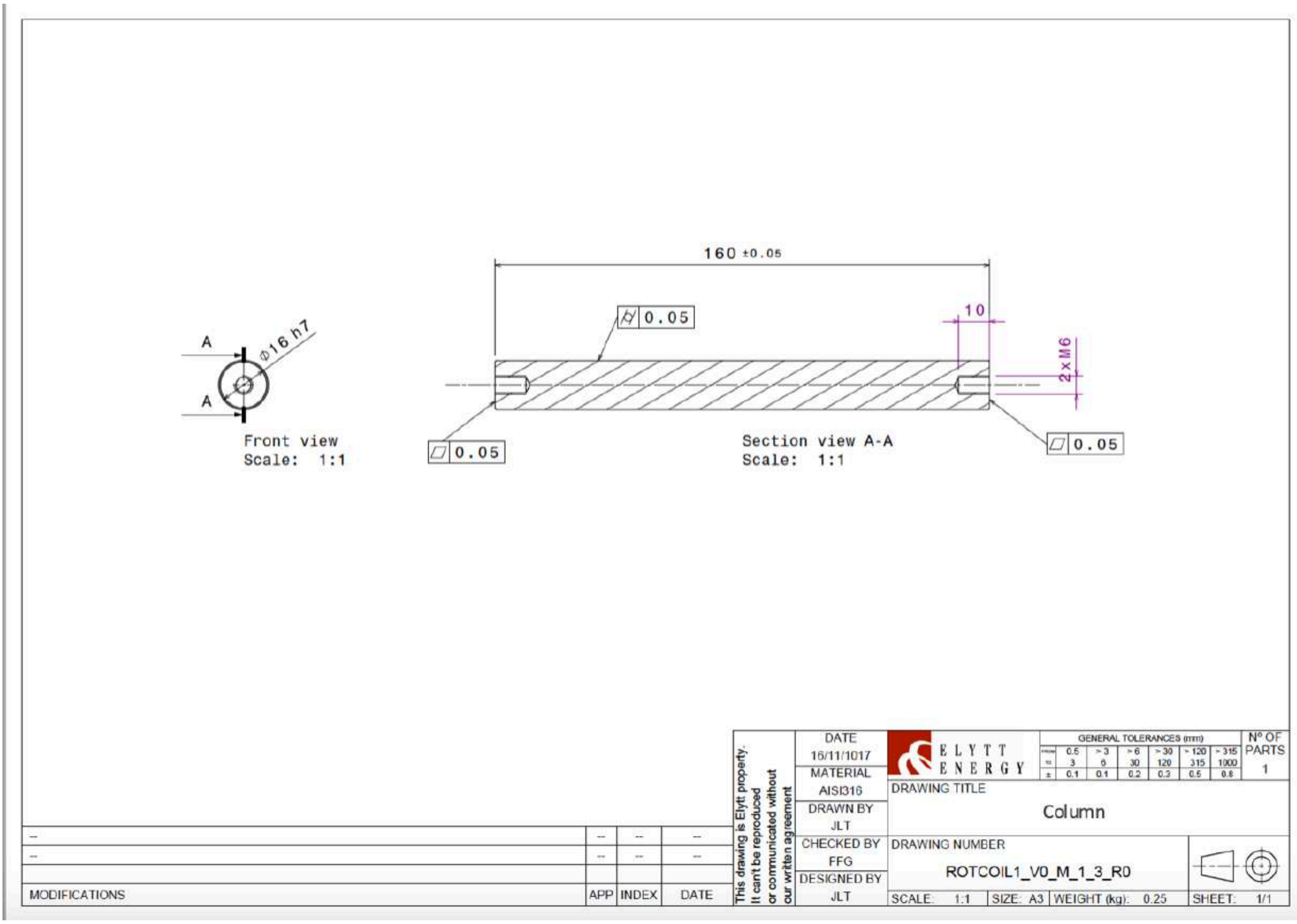

DIAGRAM 4: PUSHER

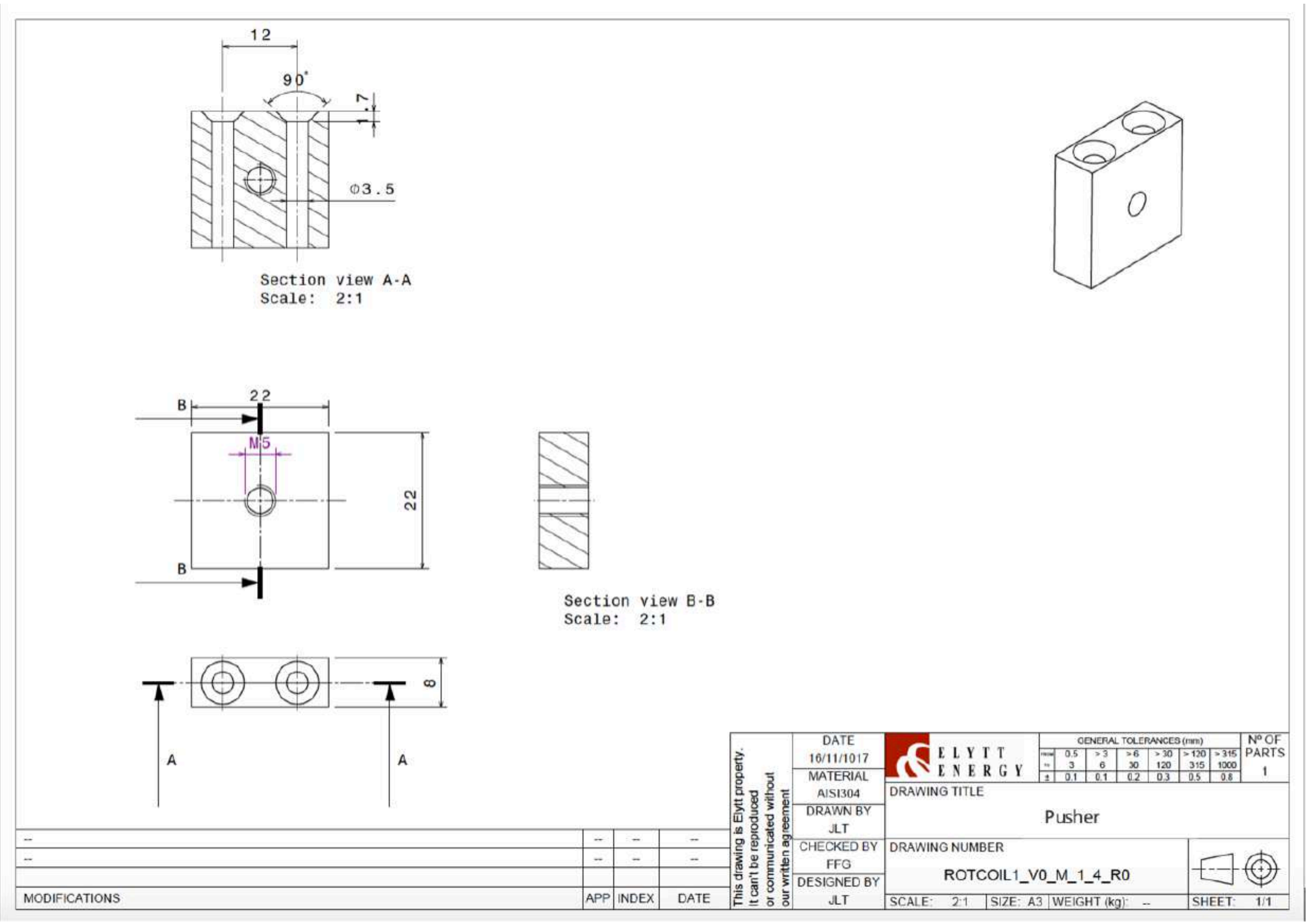

DIAGRAM 5: SLIP RING FIXING

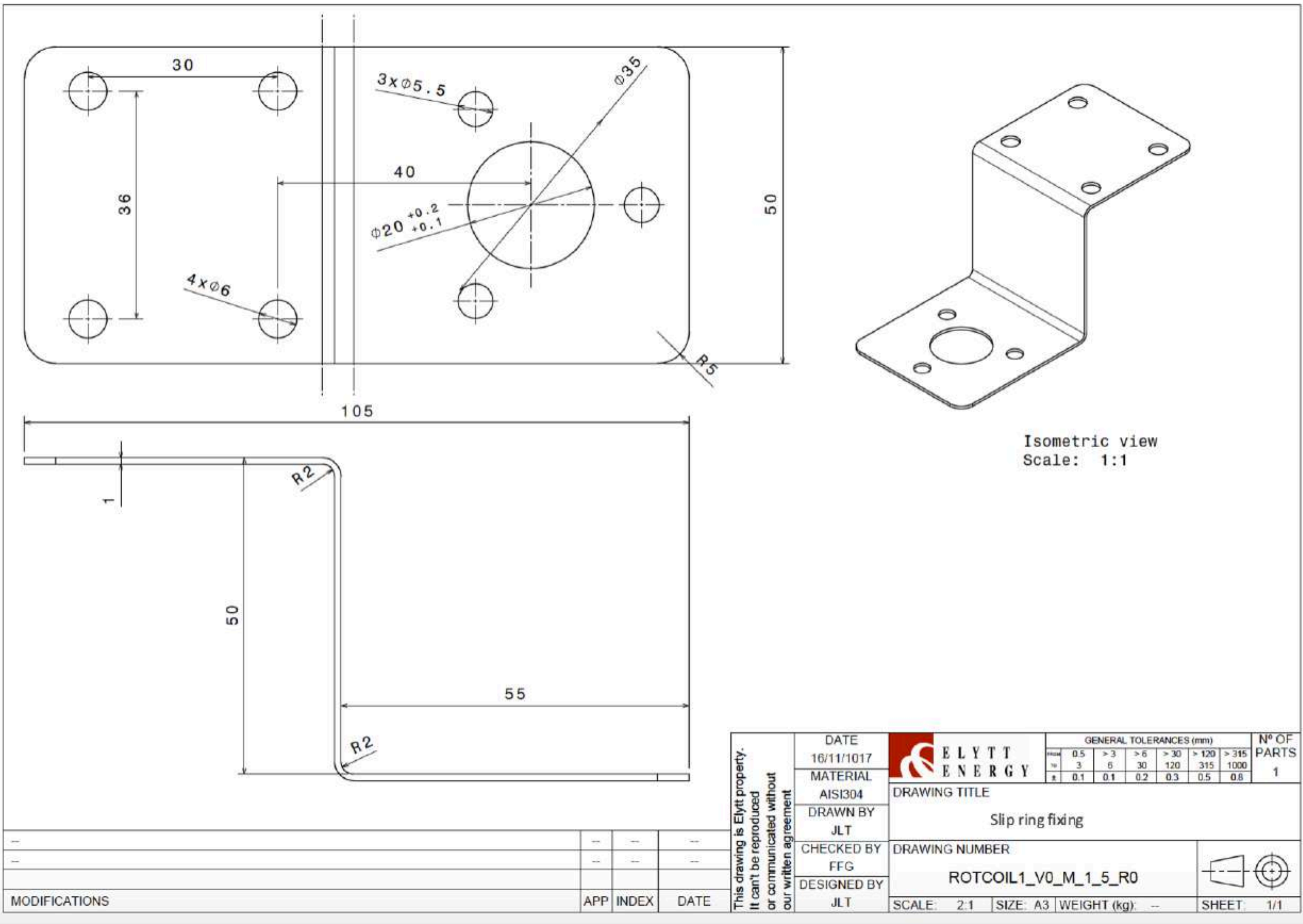

DIAGRAM 6: ADAPTER TO LEHIPA REFERENCE MAGNET

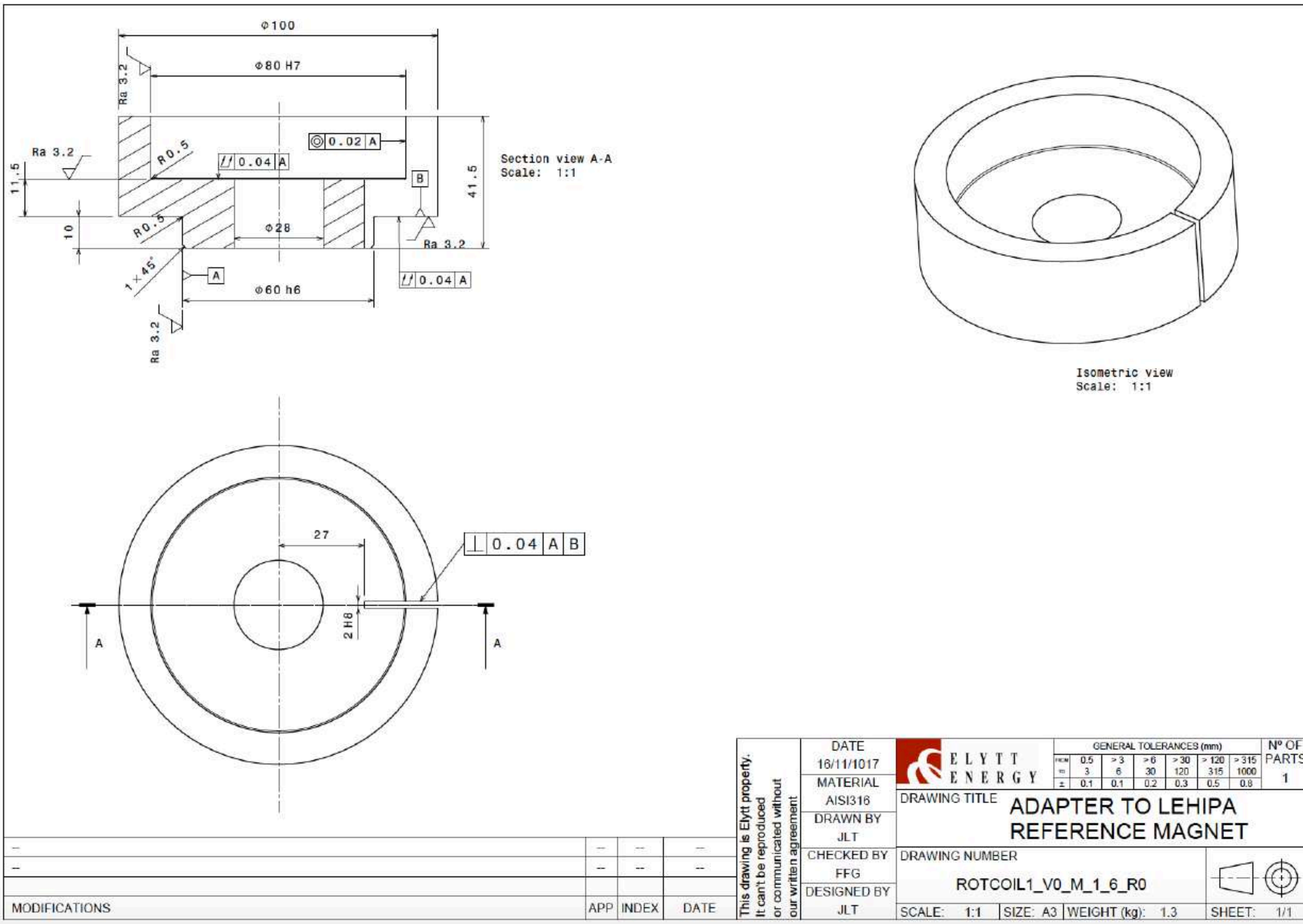

DIAGRAM 7: STATOR

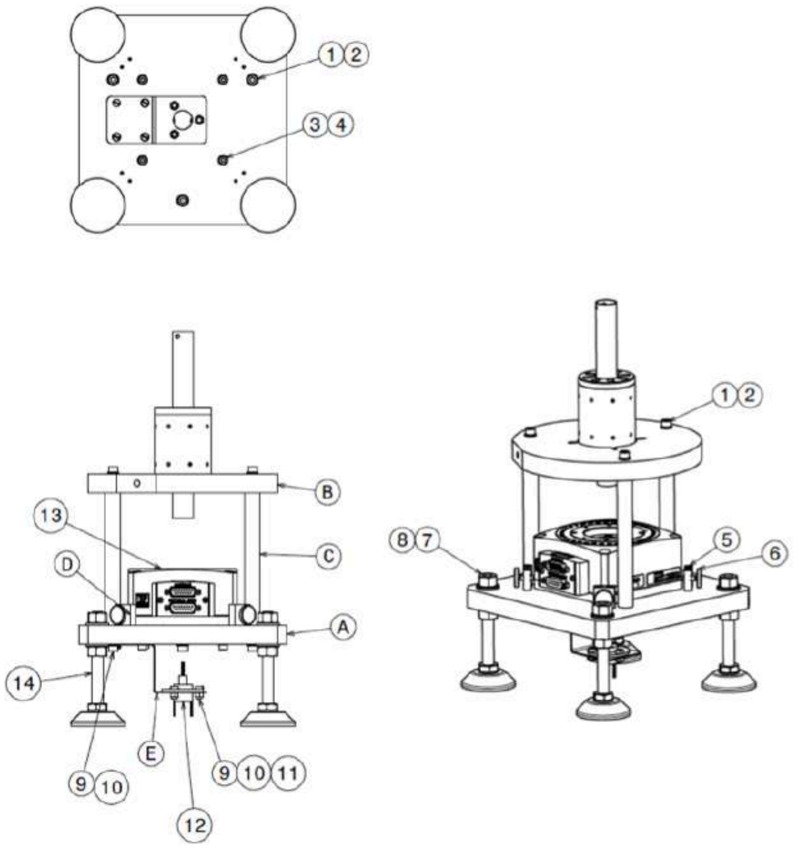

Q	DESCRIPTION	POS.	MAT.	OBSERVATIONS
		15		
4	Pies	14	-	ITEM 0.0.439.23
1	Etapa de giro	13	-	Newport RGV100BL+XPS_RLM
1	Anillos rozantes	12	-	LTN Servotechnik GmbH, SC020, 6 rings, 300mm, 300mm
10	Arandela anillos rozantes	11	A2	ISO7089 5x10
3	Tuerca anillos rozantes	10	A2	ISO4032 M5
7	Tornillo anillos rozantes	9	A2	ISO1207 M5x10
4	Arandela fijación pies	8	A2	ISO7089 12x24
4	Tuerca fijación pies	7	A2	ISO4032 M12
4	Tornillo moleteado	6	A2	DIN653 M5x16
8	Tornillos cónicos	5	A2	ISO10642 M3x30
4	Tornillos Allen	4	A2	ISO4762 M5x25
4	Arandelas	3	A2	ISO7089 5x10
6	Arandelas	2	A4	ISO7089 6x12
6	Tornillo Allen	1	A4	ISO4762 M6x16
	MANUFACTURES			
1	Soporte anillos rozantes	E	AISI304	ROTCOIL1_V0_M_1_5_R0
4	Empujador	D	AISI304	ROTCOIL1_V0_M_1_4_R0
3	Columna	C	AISI316	ROTCOIL1_V0_M_1_3_R0
1	Placa superior	B	AISI316	ROTCOIL1_V0_M_1_2_R0
1	Base	A	AISI316	ROTCOIL1_V0_M_1_1_R0

GENERAL TOLERANCES (mm)

FROM	0.5	> 3	> 6	> 30	> 120	> 315
TO	3	6	30	120	315	1000
±	0.1	0.1	0.2	0.3	0.5	0.8

This drawing is Elytt property. It can't be reproduced or communicated without our written agreement

ELYTT ENERGY

DATE	16/11/1017
MATERIAL	XXXX
DRAWN BY	JLT
CHECKED BY	FFG
DESIGNED BY	JLT
Nº OF PARTS	1
DRAWING TITLE	STATOR
DRAWING NUMBER	ROTCOIL1_V0_M_1C_R0
SCALE	1:1
SIZE	A3
WEIGHT (kg)	-
SHEET	1/1

MODIFICATIONS	APP	INDEX	DATE
--	--	--	--
--	--	--	--

DIAGRAM 8: MOLE

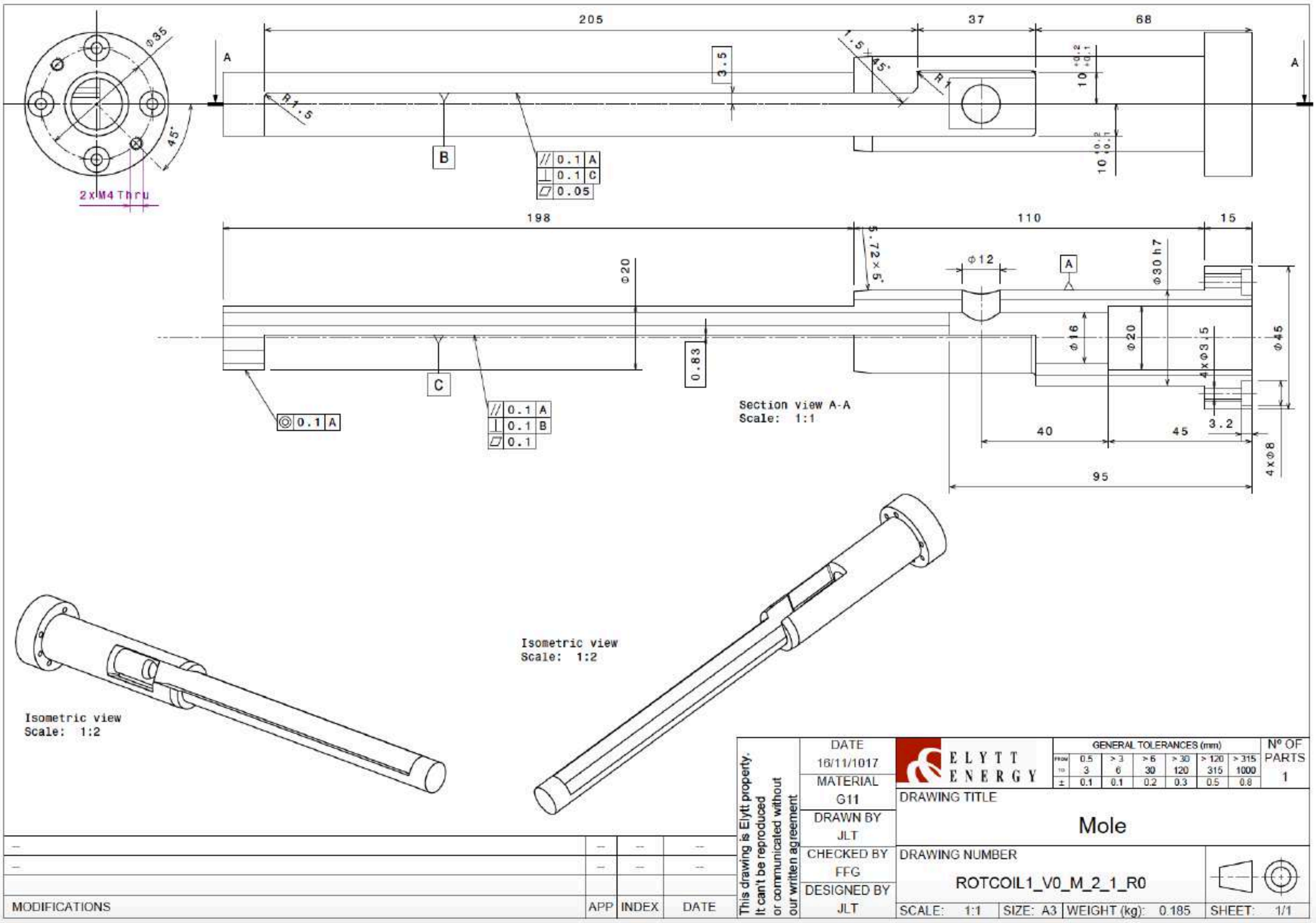

DIAGRAM 9: CONNECTION FRAME

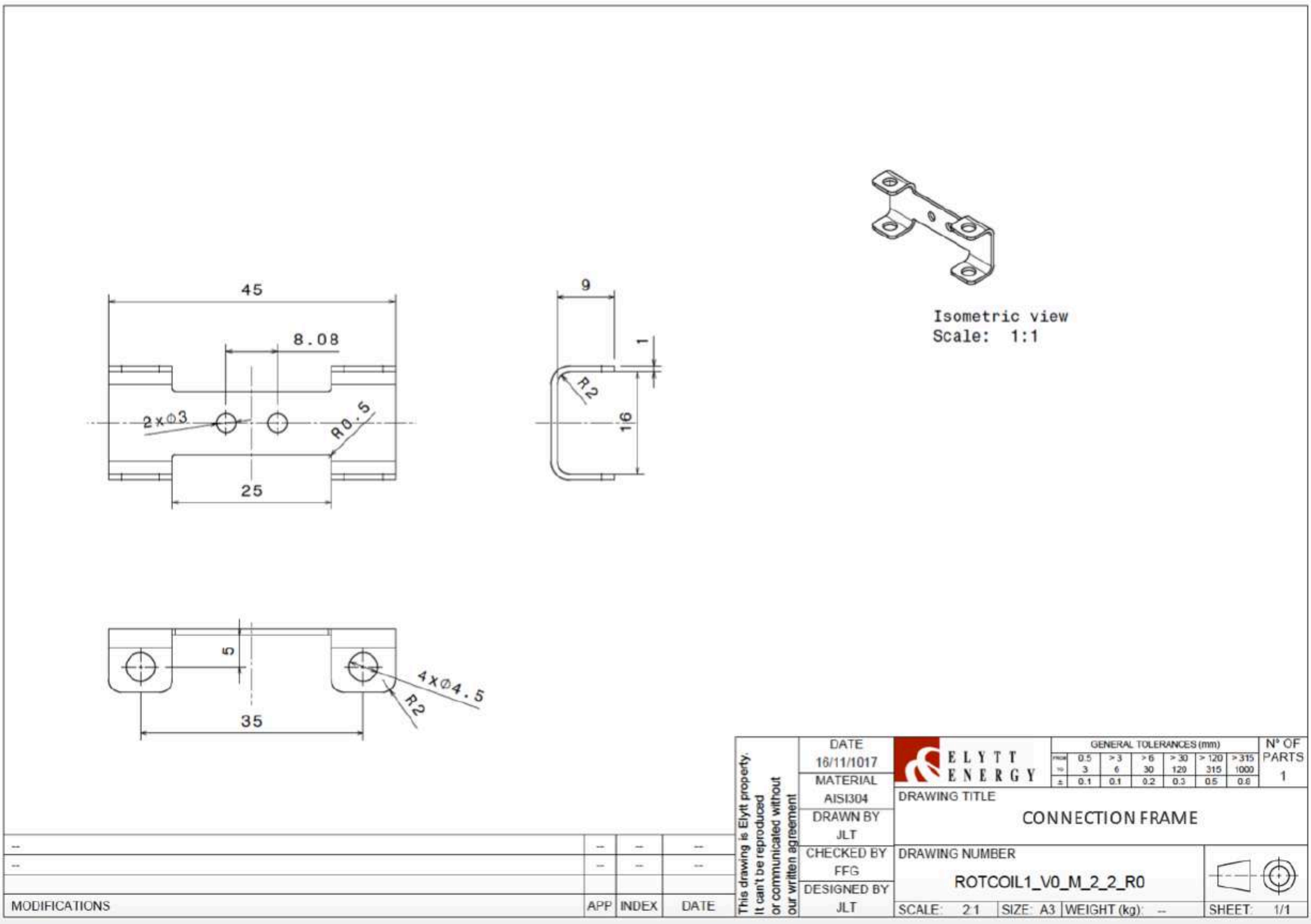

DIAGRAM 10: ROTOR

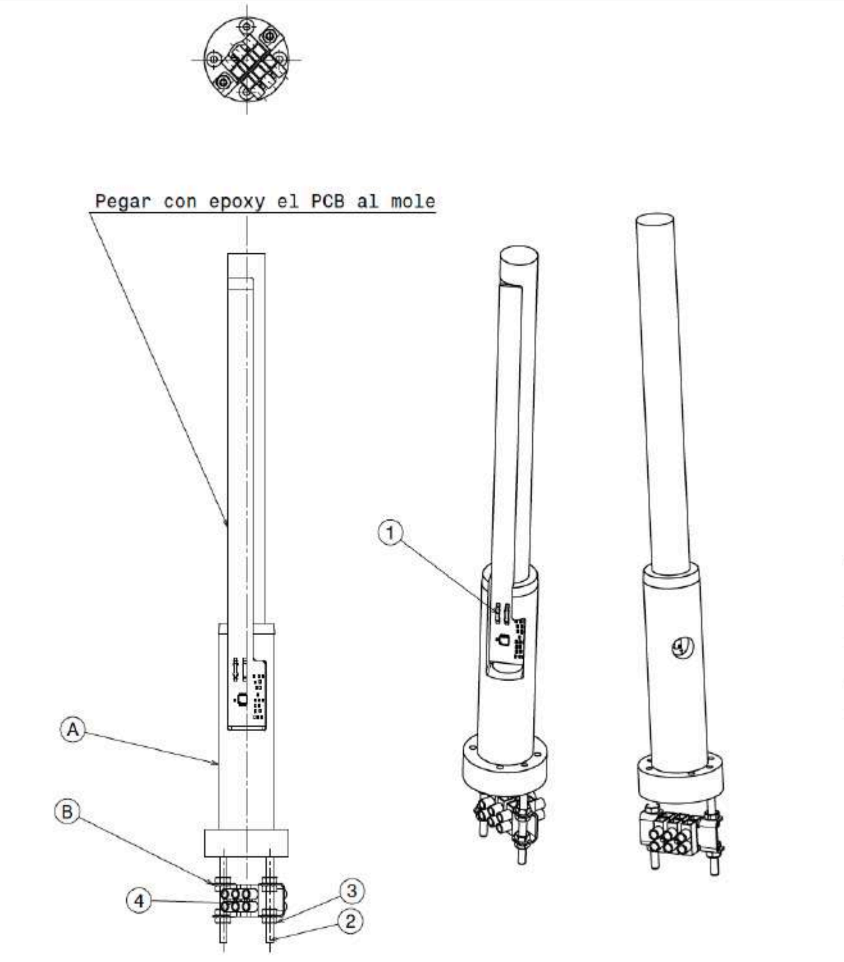

Q	DESCRIPTION	POS.	MAT.	OBSERVATIONS
2	Clemas	4	A2	Paso 8.08, cable 2,5 mm², 3 tomas
4	Tuercas	3	A2	ISO4032 M4
2	Varillas roscadas	2	A2	M4 x 60
1	PCB	1	-	Eurocircuits+montador
	MANUFACTURES			
1	Soporte conexiones	B	AISI304	ROTCOIL1_V0_M_2_2_R0
1	Mole	A	G11	ROTCOIL1_V0_M_2_1_R0

MODIFICATIONS	APP	INDEX	DATE
--	--	--	--
--	--	--	--

DATE 16/11/1017
MATERIAL XXXX
DRAWN BY JLT
CHECKED BY FFG
DESIGNED BY JLT

ELYTT ENERGY

GENERAL TOLERANCES (mm)							
FROM	0.5	> 3	> 6	> 30	> 120	> 315
TO	3	6	30	120	315	1000
±	0.1	0.1	0.2	0.3	0.5	0.8

Nº OF PARTS: 1

DRAWING TITLE: ROTOR

DRAWING NUMBER: ROTCOIL1_V0_M_2C_R0

SCALE: 1:1 | SIZE: A3 | WEIGHT (kg): - | SHEET: 1/1

DIAGRAM 11: SLIP-RING FLANGE

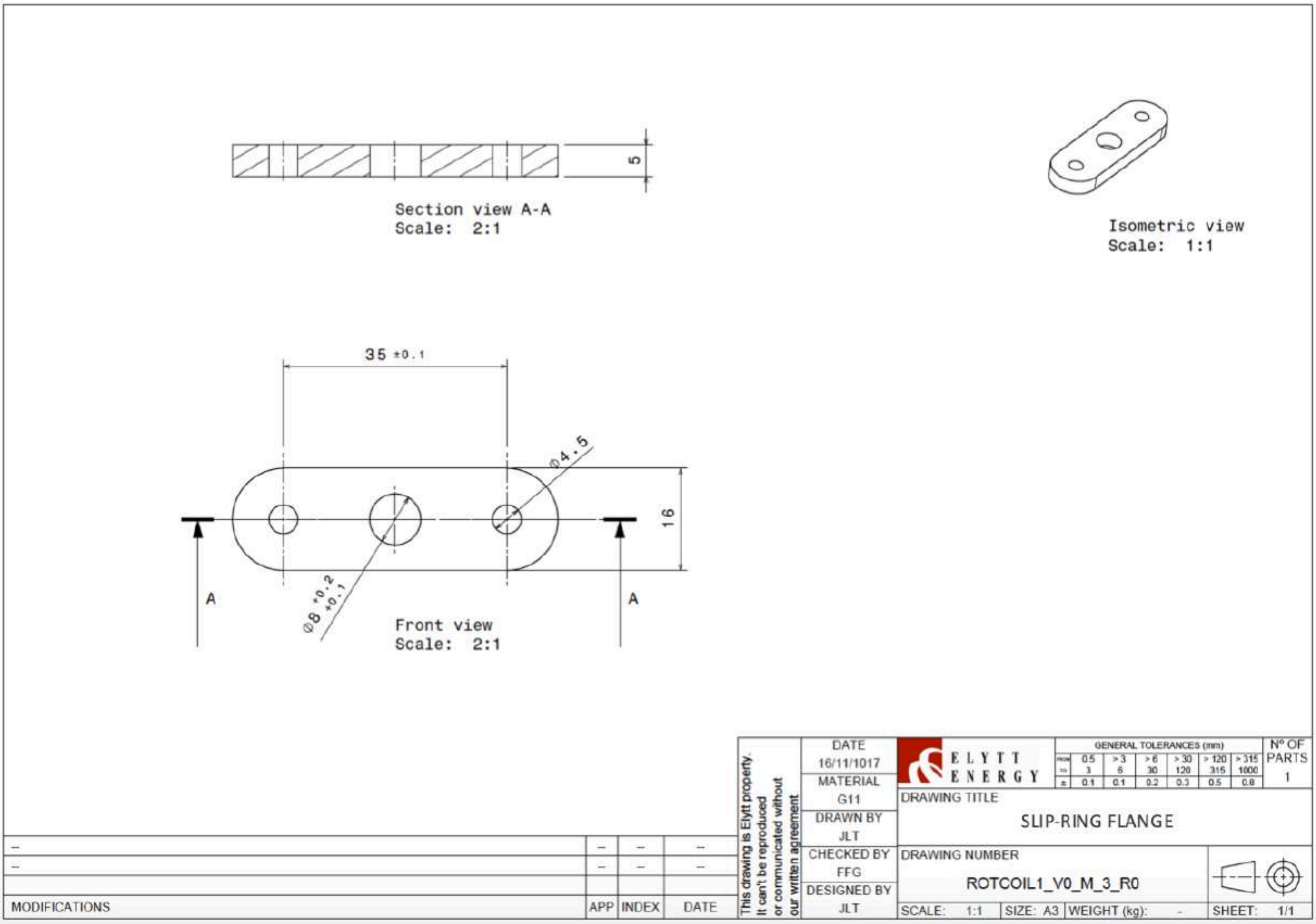

DIAGRAM 12: PMQ ROTATING COIL SYSTEM